



**Centro de Investigación en Alimentación  
y Desarrollo, A.C.**

**FORMACIÓN Y CARACTERIZACIÓN DE  
NANOPARTÍCULAS DE LA FRACCIÓN DE ALBÚMINAS  
DE SALVADO DE TRIGO POR EL MÉTODO DE  
DESOLVATACIÓN**

---

Por:

**Jesús Guadalupe Luna Valdez**

TESIS APROBADA POR LA COORDINACIÓN DE

TECNOLOGÍA DE ALIMENTOS DE ORIGEN VEGETAL

Como requisito parcial para obtener el grado de

**DOCTOR EN CIENCIAS**

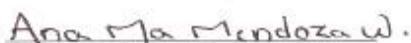
## APROBACIÓN

Los miembros del comité designado para la revisión de la tesis de Jesús Guadalupe Luna Valdez, la han encontrado satisfactoria y recomiendan que sea aceptada como requisito parcial para obtener el grado de Doctor en Ciencias.



---

Dr. René Renato Balandrán Quintana  
Director de Tesis



---

Dra. Ana María Mendoza Wilson  
Asesor



---

Dra. Gabriela Ramos Clamont Montfort  
Asesor



---

Dr. Agustín Rascón Chu  
Asesor



---

Dr. José Antonio Azamar Barrios  
Asesor



---

Dr. Tomás Jesús Madera Santana  
Asesor

## DECLARACIÓN INSTITUCIONAL

La información generada en esta tesis es propiedad intelectual del Centro de Investigación en Alimentación y Desarrollo, A.C. (CIAD). Se permiten y agradecen las citas breves del material contenido en esta tesis sin permiso especial del autor, siempre y cuando se dé crédito correspondiente. Para la reproducción parcial o total de la tesis con fines académicos, se deberá contar con la autorización escrita del Director General del CIAD.

La publicación en comunicaciones científicas o de divulgación popular de los datos contenidos en esta tesis requiere la autorización escrita, del manuscrito en cuestión, del director o directora de tesis. En estos casos siempre se deberá dar los créditos al CIAD.



---

Dr. Pablo Wong González  
Director General

## AGRADECIMIENTOS

Al Consejo Nacional de Ciencia y Tecnología (CONACYT, México), por el apoyo económico brindado para cubrir los gastos durante mis estudios de doctorado.

Al Centro de Investigación en Alimentación y Desarrollo (CIAD, AC), por brindarme la oportunidad de realizar mis estudios de doctorado en dicha institución.

Al Consejo Nacional de Ciencia y Tecnología (CONACYT, México), por el financiamiento del proyecto CB-2011/169839 a cargo del Dr. René Balandrán, para la ejecución y desarrollo de esta tesis.

A Dios y a la Virgen María, por guiarme siempre por el buen camino.

A mi director de tesis, el Dr. René Renato Balandrán Quintana por darme la oportunidad de formar parte de su equipo de investigación. Además, por la buena disposición que mostró siempre para atender las dudas, comentarios e imprevistos que surgían en su momento y sobretodo, agradezco el gran profesionalismo que siempre tuvo y con el que trató todos los asuntos académicos, de investigación y personal con un servidor.

A mi comité de tesis por compartir sus conocimientos en cada semestre que se le solicitó, los cuales contribuyeron en gran medida a la investigación realizada, así como a mi formación académica. A todos ustedes gracias, Dr. René Renato Balandrán Quintana, Dra. Ana María Mendoza Wilson, Dra. Gabriela Ramos Clamont Montfort, Dr. Agustín Rascón Chu, Dr. José Antonio Azamar Barrios y al Dr. Tomás Jesús Madera Santana. Además, agradezco a la Dra. Gabriela Ramos por la facilidad de usar los equipos del Laboratorio de Bioquímica de Proteínas y Glicanos de la Coordinación de Ciencia de los Alimentos y también al Dr. José Antonio Azamar por las facilidades brindadas en los laboratorios de CINVESTAV—Unidad Mérida, Yucatán.

Un agradecimiento muy especial a la M.C. Dora A. Huerta Quintanilla y a la Biol. Ana Ruth Cristobal Ramos, por los análisis de SEM-EDX, JSM-7600F. También, al M.C. Daniel Aguilar Treviño por su asistencia técnica en los análisis de difracción de rayos X, todos ellos personal técnico del CINVESTAV—Unidad Mérida, Yucatán.

A la Coordinación de Programas Académicos de CIAD, por su apoyo técnico, en especial a su personal: Argelia Marín, Verónica Araiza, Laura García, Aurora Vidal y Héctor Galindo.

A todos los investigadores que de alguna u otra manera fueron parte y contribuyeron a este trabajo de investigación. A los miembros de la Coordinación de Alimentos de Origen Vegetal (CTAOV) dirigida por la Dra. Alma Rosa Islas, investigadores y compañeros de área. A los maestros que me impartieron clases durante mi doctorado, los doctores Alma Rosa Islas, Ana María Calderón de la Barca, Dra. Herlinda Soto, Dra. Gabriela Ramos, Dra. Elizabeth Carvajal, Dra. Tere Gollas, Dr. René Balandrán, Dr. Tomás Madera, Dr. Miguel Ángel Martínez, Dr. Mario Camberos, Dr. Jaime Lizardi, Dr. Agustín Rascón, Dr. Alberto González. Además de un agradecimiento muy especial al Dr. Ángel Huerta de la Plataforma Analítica Institucional del CIAD por su apoyo en asesoría sobre los protocolos de preparación, obtención y disección de geles SDS-PAGE para la identificación de proteínas mediante espectrometría de masas.

Al M.C. Jorge Mercado por el gran apoyo técnico y académico que recibí de su parte desde el primer día en que le conocí. También por sus buenos consejos, tanto académicos como personales.

A Lupita Chaquilla, con quien compartí los logros y fracasos que tuvimos durante todo el tiempo que estuvimos trabajando en equipo. Además, por esa gran amistad que me brindó desde el primer momento en que la conocí, la cual se fortaleció en el día a día el trabajo de laboratorio. Gracias también, por todo ese cariño y aprecio que compartió con mi familia, su familia.

A mis compañeros de laboratorio: Lupita, Javier Carmelo, Iván Torres, Jorge Zavala, con quienes pasé momentos muy gratos durante todo el tiempo que estuve compartiendo el laboratorio con ustedes.

Al Ing. Francisco Javier Noriega Muñoz, quien desde el principio me impulsó a emprender esta aventura. Gracias por todo.

## DEDICATORIA

*A Dios, por guiarme día a día en el buen camino y por todas sus bendiciones otorgadas.*

*A mis padres, **Guadalupe Luna Meza** y **Ana María Valdez Ruelas** por su apoyo tanto económico como moral, el cual lo realizaron incondicionalmente durante toda mi formación profesional.*

*A mi esposa Jazmín e hijos (José, Luna y Lupita) por su comprensión, apoyo y paciencia durante este largo camino, el cual, estuvo lleno de aventuras.*

*A mi abuela, Elvira Ruelas Alcaraz, porque fue parte fundamental desde el primer momento que salí en busca de la superación académica.*

*A mis hermanas Ana María e Irlanda por su apoyo en todos los aspectos y por todas las alegrías que hemos pasado juntos.*

*A mi tía Ramona Reina y mi tío Alejandro Bermúdez por su grato recibimiento a mi llegada a Hermosillo y por todas las atenciones recibidas de su parte.*

*A mi cuñado Arturo (el muñe) por su apoyo brindado.*

El presente trabajo fue realizado en la Coordinación de Tecnología de Alimentos de Origen Vegetal del Centro de Investigación en Alimentación y Desarrollo, A.C. (CIAD), bajo la dirección del Dr. René Renato Balandrán Quintana. Se contó con el apoyo económico del Consejo Nacional de Ciencia y Tecnología (CONACYT) para el proyecto CB-2011/169839: “Autoensamblaje de estructuras supramoleculares a partir de péptidos liberados de la fracción de albúminas de salvado de trigo mediante proteólisis” a cargo del Dr. René Renato Balandrán Quintana. Se reconoce la participación del Laboratorio de Química de Materiales CINVESTAV-IPN Unidad Mérida Yucatán, y de los laboratorios LANNBIO, proyectos FOMIX-YUCATAN 2008-108160 y CONACYT LAB-2009-01 No. 123913, así como de la Plataforma Analítica Institucional del CIAD.

## CONTENIDO

<b>APROBACIÓN</b> .....	2
<b>DECLARACIÓN INSTITUCIONAL</b> .....	3
<b>AGRADECIMIENTOS</b> .....	4
<b>DEDICATORIA</b> .....	6
<b>CONTENIDO</b> .....	8
<b>RESUMEN</b> .....	9
<b>ABSTRACT</b> .....	11
<b>SINOPSIS</b> .....	13
<b>BIBLIOGRAFÍA</b> .....	26
<b>1. Structural and physiochemical characterization of nanoparticles synthesized from an aqueous extract of wheat bran by a cold-set gelation/desolvation approach</b> .....	32
<b>2. Nanoparticle formation after mild thermal conditioning of proteins in a wheat bran extract fractionated by size exclusion chromatography</b> .....	42
<b>3. FTIR analysis of thermally-induced nanoparticles from a fraction of water soluble wheat bran proteins, to elucidate the formation mechanism</b> .....	76



## RESUMEN

Se evaluó la factibilidad de sintetizar nanopartículas a partir del extracto acuoso de salvado de trigo (EAST) mediante la técnica de desolvatación/gelación en frío. Para ello se aplicó un pre-tratamiento térmico de 68.5 °C al EAST en solución, seguido de la adición de CaCl<sub>2</sub> y liofilización. Las micrografías de microscopía electrónica de barrido (MEB) mostraron nanopartículas esféricas. El análisis químico y de espectroscopía infrarroja indicó la naturaleza proteica de las nanoesferas, además de estar estabilizadas por interacciones electrostáticas proteína-calcio e inmersas en una matriz de polisacáridos. Para corroborarlo, las proteínas del EAST se purificaron parcialmente mediante cromatografía de exclusión por tamaños (SEC), obteniéndose 6 fracciones con masas moleculares 0.4–94 kDa. El análisis de proteína disuelta y de espectroscopía UV e IR mostró la presencia de carbohidratos en las fracciones, y que dos de ellas estaban compuestas por proteína, dos por una mezcla proteína-ácido ferúlico, otra por proteína más otros compuestos no identificados y la última por ácido ferúlico libre. Cada fracción SEC se sometió a desolvatación/gelación en frío. El análisis de MEB y la electroforesis SDS-PAGE, mostraron que la fracción proteica 20–43 kDa es responsable de la formación de nanoesferas con diámetros entre 190–250 nm. Estas últimas también se observaron en la muestra control, a la que no le fue añadido Ca<sup>2+</sup>, por lo que se asumió que el calcio no intervino en su formación sino que se produjeron por efecto del tratamiento térmico. La ausencia de Ca<sup>2+</sup> en las nanoesferas se verificó por espectrometría de energía dispersiva de rayos x. Los resultados también mostraron que las nanopartículas se formaron por la integración de nanoesferas de 30 nm de diámetro, visibles después de un tratamiento ultrasónico. El análisis de la banda Amida I (1700-1600 cm<sup>-1</sup>) del espectro infrarrojo de las nanopartículas mostró una disminución del 46% de hojas β y un incremento del 33% en la formación de agregados, lo que indicó agregación intermolecular a través de hojas β en las nanopartículas. Con base en los resultados y el alto contenido del aminoácido cisteína reportado en las proteínas identificadas en la fracción 20–43 kDa, se propuso el siguiente mecanismo de formación de las nanoesferas. El tratamiento térmico indujo la formación de agregados a través de enlaces disulfuro e interacciones moleculares tipo hoja beta, creciendo hasta

alcanzar un diámetro de 30 nm. Posteriormente se integraron mediante interacciones físicas (hidrofóbicas, van der Waals, electrostáticas) hasta formar los agregados esféricos de mayor tamaño.

**Palabras clave:** nanopartículas, salvado de trigo, cromatografía preparativa, tecnología de cereales, espectroscopía infrarroja, nanotecnología de proteínas.

## ABSTRACT

The feasibility of synthesizing nanoparticles from the wheat bran aqueous extract (EAST) was evaluated by the desolvation /cold gelation technique. For this, a thermal pretreatment of 68.5 ° C was applied to the EAST in solution, followed by the addition of CaCl<sub>2</sub> and lyophilization. Scanning electron microscopy (SEM) micrographs showed spherical nanoparticles. The chemical analysis and infrared spectroscopy indicated the protein nature of nanospheres, in addition to being stabilized by protein-calcium interactions and immersed in a polysaccharide matrix. To corroborate it, the EAST proteins were partially purified by size exclusion chromatography (SEC), obtaining 6 fractions with molecular masses 0.4–94 kDa. The analysis of dissolved protein and UV and IR spectroscopies showed the presence of carbohydrates in the fractions and that two of them were composed of protein; two for a protein-ferulic acid mixture; another for protein plus other unidentified compounds and the last one by free ferulic acid. Each SEC fraction was subjected to desolvation /cold gelation. SEM analysis and SDS-PAGE electrophoresis showed that the 20–43 kDa protein fraction is responsible for the formation of nanospheres with diameters between 190–250 nm. The latter were also observed in the control sample, to which Ca<sup>2+</sup> was not added, so it was assumed that calcium did not intervene in its formation but that they were produced by the effect of the heat treatment. The absence of Ca<sup>2+</sup> in the nanospheres was verified by x-ray dispersive energy spectroscopy. The results also showed that the nanoparticles were formed by the integration of nanospheres of 30 nm diameter, visible after an ultrasonic treatment. The analysis of the Amide I band (1700–1600 cm<sup>-1</sup>) of the infrared spectrum of the nanoparticles showed a decrease of 46% of β-sheets and a 33% increase in aggregate formation, which indicated intermolecular aggregation through β-sheets in the nanoparticles. Based on the results and the high content of the amino acid cysteine reported in the proteins identified in the 20–43 kDa fraction, the following mechanism of nanosphere formation was proposed. The heat treatment induced the formation of aggregates through disulfide bonds and β-sheet molecular interactions, growing to a diameter of 30 nm. Subsequently they were integrated by physical interactions (hydrophobic, van der Waals, electrostatic) to form the larger spherical aggregates.

**Keywords:** nanoparticles, wheat bran, preparative chromatography, infrared spectroscopy, cereal technology, protein nanotechnology.

## SINOPSIS

El salvado de trigo es un subproducto de la industria molinera (Beaugrand et al., 2004) que actualmente es subutilizado, aún y cuando contiene entre 15 y 22% de proteína (Zhang et al., 2011). En el salvado, las proteínas se encuentran localizadas principalmente en las células de la capa aleurona, protegidas por la pared celular (Jerkovic, 2010), por lo que no son fácilmente digeribles, incluso por los animales. Las albúminas y globulinas representan entre el 15-20% de la proteína total del grano de trigo (Singh y Skerritt, 2001), de las cuales el 25% de las proteínas solubles en agua (albúminas) se encuentran en la capa más externa, una de las siete capas principales que conforman el salvado de trigo (Jerkovic, 2010), lo que significa que no es necesario de un procedimiento complejo de extracción en el que se requiera el empleo de reactivos, sino solo de agua. Es decir, las albúminas del salvado de trigo representan una fuente importante de proteínas de bajo costo, a las cuales se les puede dar un valor agregado. La composición química y la diversidad estructural de las albúminas de salvado de trigo las hace candidatas para aplicaciones nanotecnológicas en las industrias alimentaria y farmacéutica (Balandrán-Quintana et al., 2015).

Actualmente se elaboran nanopartículas a partir de fuente animal y vegetal, así como de suero humano, las cuales tienen propiedades para encapsular y transportar fármacos y compuestos bioactivos (Gülseren et al., 2012; Zhang et al., 2012; Mehravar et al., 2009). Para la elaboración de dichos nanotransportadores se emplean proteínas con grados de pureza de al menos 90%, lo cual puede aumentar los costos de producción, debido que se requieren de una mayor cantidad de operaciones unitarias para su obtención. Por otro lado, también son escasos los esfuerzos para desarrollar nanopartículas a partir de proteínas origen vegetal, a pesar de que en algunos casos estas proteínas son más asequibles en el sentido de que forman parte de la composición de residuos agroindustriales, además de ser más aceptables para el consumidor. Entre los pocos ejemplos se encuentran los aislados de proteína de soya (Zhang et al., 2012), las gliadinas de trigo (Arangoa et al., 2001; Joye et al., 2015) y las zeínas del maíz (Gomez-Estaca et al., 2012). Por otro lado, no existen reportes sobre la elaboración de nanopartículas a partir de proteínas que no hayan sido aisladas o purificadas. En ese

sentido, existen fuentes proteicas de origen vegetal que no han sido consideradas, como las albúminas del salvado de trigo, a pesar tener propiedades funcionales aceptables para su uso en la industria de los alimentos (Idris et al., 2003). La fracción de albúminas del salvado de trigo se caracteriza por un contenido importante de aminoácidos ácidos, como el aspártico y el glutámico (Shewry et al., 2009), cuyos grupos carboxílicos laterales desarrollan una carga negativa a pH mayor a 7.0. Esta característica imparte las propiedades de solubilidad en agua de las albúminas en el estado nativo (Pace et al., 2004), así como la susceptibilidad de formar nanopartículas a través de un enfoque de desolvatación/gelación en frío y las posibilidades de adsorción de otras moléculas. Además, las albúminas de salvado de trigo presentan una alta capacidad de enlaces reversibles con moléculas hidrofóbicas, todo lo cual se considera ventajoso para la elaboración de nanopartículas (Yedomon et al., 2013).

En el ARTÍCULO 1 de esta tesis se describe la formación de nanopartículas a partir de extractos acuosos de salvado de trigo (EAST), mediante un enfoque de gelación/desolvatación en frío. Este método consiste en precalentar una solución proteica, seguida de un enfriamiento hasta temperatura ambiente y ajuste de pH a básico; finalmente, se adicionan iones divalentes como el  $\text{Ca}^{2+}$  (Zhang et al., 2012). Dicho proceso se considera como desolvatación, ya que los iones calcio compiten por las moléculas de agua. Esto resulta en la eliminación de la capa de hidratación de las proteínas y consecuentemente, la carga de estas se vuelve negativa debido a la presencia en exceso de iones calcio, favoreciendo las interacciones electrostáticas proteína-calcio. El empleo de calcio como agente de desolvatación y entrecruzante a la vez, evita el uso de sustancias tóxicas, tales como solventes orgánicos (acetona y etanol) y glutaraldehído para la elaboración de nanopartículas (Konan et al., 2002; Langer et al., 2003; Gülseren et al., 2012; Yedomon et al., 2013).

En una etapa preliminar de la investigación se aplicó un tratamiento térmico de 68.5 °C al EAST y se evaluó el efecto de diferentes concentraciones de  $\text{CaCl}_2$  y el pH sobre el tamaño de partícula y el potencial-z de las estructuras resultantes, determinados mediante dispersión dinámica de luz. Se determinó que la concentración de  $\text{CaCl}_2$  en el intervalo 0.25, 0.5, 0.75, 1.0 y 1.5 M y un pH de 8, eran las condiciones más adecuadas

para la obtención de nanopartículas. En este experimento, al agregar el  $\text{CaCl}_2$  se obtuvieron dos fases, sobrenadante y precipitado. El contenido proteico siempre fue mayor en los precipitados, lo cual sugirió que la agregación de proteínas fue inducida por la desolvatación. El tamaño de los aglomerados precipitados fue directamente proporcional a la concentración de  $\text{CaCl}_2$  en el rango 0-0.5 M, mientras que el potencial-z se comportó de manera inversa; un efecto contrario se obtuvo en los sobrenadantes. En un intervalo superior de concentraciones de  $\text{CaCl}_2$  (1.0-1.5 M) se obtuvieron aglomerados hasta tres veces más grandes que las partículas de la muestra control. Esto último probablemente se debió a una disminución en la repulsión entre partículas, y con ello que la proximidad entre estas fuera mayor, lo que favoreció el entrecruzamiento proteína- $\text{Ca}^{2+}$ .

La similitud del tamaño de partícula en la muestra control, tanto en el sobrenadante como en el precipitado, demostró que la adición de  $\text{CaCl}_2$  favoreció la aglomeración y que el pre-acondicionamiento no tuvo un efecto sobre la misma. Por otro lado, el diámetro de partícula se mantuvo constante en el rango 0.25-1.0 M de  $\text{CaCl}_2$  y aumentó significativamente en 1.5 M, lo cual pudo deberse a la mayor concentración de  $\text{Ca}^{2+}$  que consecuentemente favoreció las interacciones intermoleculares. Por otro lado, la disminución progresiva del potencial-z con respecto al aumento de la concentración del  $\text{CaCl}_2$ , corresponde con lo discutido anteriormente para el rango de concentración de 0.25-1.0 M de  $\text{CaCl}_2$  en ambas fases. No obstante, la carga en las dos fases (sobrenadante y precipitado) a la máxima concentración evaluada, fue mayor, por lo que no puede ser explicado en los términos antes discutidos, debido a que a tal concentración, el número de cargas negativas restantes debería ser más baja, así que el potencial-z tendría que ser menos negativo. Es posible que este efecto haya sido ocasionado por un evento desconocido que inhibió a los iones calcio para formar interacciones con proteínas, pero resultó en partículas grandes.

Después de analizar el tamaño de partícula y el potencial-z de las muestras en fresco mediante dispersión dinámica de luz, las dos fases de cada muestra fueron congeladas y posteriormente liofilizadas para su respectiva caracterización. Los polvos liofilizados fueron analizados mediante microscopía electrónica de barrido (MEB), observándose la presencia de nanopartículas de forma esférica con diámetros  $<100$  nm en todo el rango

de concentraciones de  $\text{CaCl}_2$  evaluado. Estas nanoestructuras se observaron inmersas en una matriz compuesta principalmente por polisacáridos, de acuerdo con el análisis químico. El diámetro de las esferas fue prácticamente el mismo dentro del rango 0.25-1.0 M de  $\text{CaCl}_2$ . Sin embargo, a la máxima concentración de  $\text{CaCl}_2$  evaluada, el diámetro de partícula fue significativamente mayor debido a que se favoreció un mayor número de interacciones intermoleculares. Estos resultados fueron similares a los reportados por Zhang et al. (2012) quienes evaluaron el efecto del  $\text{CaCl}_2$  sobre la formación de nanopartículas de aislados de proteína de soya; los autores encontraron que cuanto mayor es la concentración de  $\text{CaCl}_2$  mayor es el tamaño de las partículas y la cantidad de precipitado resultante, independientemente del pH y la concentración de proteína. También, Gülseren et al. (2012) reportaron que un aumento de la concentración del agente de desolvatación produjo nanopartículas de mayor tamaño.

Con el fin de analizar la estructura interna de las esferas formadas, el polvo liofilizado de la muestra adicionada con  $\text{CaCl}_2$  0.25 M fue resuspendido en agua y sonificado durante 5 min con la intención de disgregar la matriz de polisacáridos (Czechowska-Biskup et al., 2005). Posteriormente, la muestra fue visualizada mediante MEB en modo de transmisión. Si bien no fue posible observar la estructura interna de las esferas, este análisis permitió ver las nanopartículas de forma individual, las cuales formaron estructuras con arreglo de tipo collar.

La presencia de minerales en el EAST tuvo un efecto negativo sobre la resolución de las imágenes MEB, el cual fue mayor a la concentración 1.0 M. Este efecto pudo deberse a la luminosidad producida por los electrones retrodispersados del Ca y otros minerales como el P, K y Mg (Talbot y White, 2013), lo que indica que estos pudieran formar parte de las nanoestructuras.

Debido a que a la concentración máxima de  $\text{CaCl}_2$  (1.5 M) se observó mediante MEB la formación de lo que parecían ser cristales minerales, se realizó un análisis de difracción de rayos-X en tres muestras seleccionadas (EAST,  $\text{CaCl}_2$  0.5 M y  $\text{CaCl}_2$  1.5 M). La muestra EAST resultó amorfa, mientras que en la muestra  $\text{CaCl}_2$  0.5 M se detectó, por indexación, la presencia de  $\text{Na}_2\text{CO}_3 \cdot \text{H}_2\text{O}$ , el cual probablemente se generó al reaccionar el sodio presente en la muestra con el  $\text{CO}_2$  atmosférico. A la concentración 1.5 M de  $\text{CaCl}_2$  se encontró la formación de cristales tales como sylvita (KCl), brushita



( $\text{CaHPO}_4 \cdot 2\text{H}_2\text{O}$ ), weddellita ( $\text{CaC}_2\text{O}_4 \cdot 2\text{H}_2\text{O}$ ) y fosfato de magnesio sódico [ $\text{Na}_{6.13}\text{Mg}_{1.44}(\text{PO}_4)_3$ ]. Lo anterior indica que a este nivel de concentración de  $\text{CaCl}_2$  la nucleación y crecimiento de cristales prevaleció sobre el ensamblaje que conduce a la formación de nanopartículas. El crecimiento de cristales es probablemente la explicación de por qué se detectó una menor presencia de algunos minerales (Mg, P, K y Ca) en el análisis de la composición elemental realizado mediante espectroscopía de energía dispersiva de rayos X (EED) y la explicación de por qué el valor del potencial-z a esta concentración de sal se volvió más negativo. Es posible que los minerales presentes estuvieran más disponibles para el crecimiento de cristales que para el establecimiento de las interacciones que llevan a la formación de nanopartículas, lo que resultó en un menor número de cargas negativas neutralizadas sobre la superficie de las proteínas y así en un potencial-z más negativo. Por lo tanto, el incremento en el tamaño de partícula se debió a la formación de cristales y no a la aglomeración de la matriz que contenía las nanopartículas.

Los resultados obtenidos en esta etapa de la investigación no solo permitieron establecer los límites de concentración de  $\text{CaCl}_2$  para la obtención de nanopartículas sino mostrar el potencial que tienen los EAST como plataformas para la mineralización inducida de una variedad de minerales.

ARTÍCULO 2. En el artículo 1 se describió la obtención de nanopartículas a partir del EAST mediante el método de desolvatación/gelación en frío, las cuales fueron aparentemente estabilizadas mediante interacciones electrostáticas calcio-proteína. En este artículo, se muestra nueva evidencia que indica que los iones calcio no participaron en la formación de las nanopartículas, demostrando que éstas se formaron antes de la adición de  $\text{CaCl}_2$  y que incluso no todas las proteínas que conforman el EAST estuvieron involucradas en la formación de dichas nanoestructuras.

Se realizaron experimentos de desolvatación/gelación en frío con seis fracciones resultantes de la separación de los extractos de salvado de trigo mediante cromatografía de exclusión por tamaño (SEC). Cada fracción fue identificada de acuerdo al orden de elución como pk-1, pk-Int, pk-2, pk-3, pk-4 y pk-5. Cabe destacar que la fracción pk-Int no fue obtenida como un pico definido en el cromatograma, pero fue considerado como

una fracción debido a la cantidad importante de proteína que contenía. Las masas moleculares relativas de las fracciones SEC resultaron entre 0.4-94 kDa. Estas fracciones fueron liofilizadas y se les determinó el perfil de masas moleculares por SDS-PAGE (electroforesis en gel de poliacrilamida con dodecilsulfato sódico). El rango de masas moleculares (5-94 kDa) obtenida mediante electroforesis coincidió con el encontrado en SEC. Rangos de masas moleculares similares ya han sido previamente reportados en estudios con salvado de trigo (Jerkovic et al., 2010).

Previo a los experimentos de desolvatación/gelación en frío, a cada fracción SEC se le determinó el contenido de proteína soluble (disueltas al 4%, peso-volumen) con el fin de reproducir la relación calcio:proteína que resultó en la formación de nanopartículas en los experimentos descritos en el artículo 1. La concentración de proteína osciló entre 0.04-12.6 mg/mL. Cabe destacar que la concentración de proteína en pk-4 fue muy baja y en pk-5 no fue detectada. Es decir, la alta absorbancia registrada en el cromatograma de SEC (Abs 280 nm) para estas dos fracciones, se debió principalmente a compuestos fenólicos (Hromádková et al., 2013), ya que el contenido de éstos es alto en el salvado de trigo (De Brier et al., 2015). La presencia de dichos compuestos también fue confirmada por los barridos espectrofotométricos realizados a cada fracción en el rango 200-800 nm. De acuerdo con la evidencia obtenida, pk-Int y pk-2 resultaron estar compuestas principalmente de proteína, pk-1 y pk-4 por una mezcla de proteína-ácido ferúlico, pk-3 por proteína y otros compuestos no identificados, y pk-5 corresponde a ácido ferúlico libre (Saulnier et al., 2008).

Posterior a la obtención y caracterización de las fracciones se procedió a realizar el experimento de desolvatación/gelación en frío mediante la adición de  $\text{CaCl}_2$  bajo las mismas condiciones empleadas en el experimento de desolvatación con EAST.

El pre-acondicionamiento térmico de las muestras SEC generó un cambio de apariencia en pk-2 y pk-3 en los primeros dos minutos de exposición. En ambas fracciones se formó un precipitado gelatinoso de color blanco, siendo mucho más visible en pk-2. La gran cantidad de precipitado en pk-2 resultó interesante de analizar, por lo que se sometió una nueva muestra (pk-2) a tratamiento térmico y el precipitado formado fue separado mediante centrifugación. El sobrenadante fue recuperado, identificado como pk-2CS (2) y desolvatado con  $\text{CaCl}_2$  al igual que el resto de las fracciones. La apariencia

del resto de las muestras no fue alterada por efecto del tratamiento térmico. Después de la adición de  $\text{CaCl}_2$ , dos fases fueron rápidamente detectadas en pk-2 y pk-3. En pk-1 y pk-Int se obtuvo un pequeño precipitado, no así en pk-4 y pk-5. Las dos fases fueron separadas mediante centrifugación y posteriormente liofilizadas. Todas las fracciones desolvatadas fueron caracterizadas mediante espectroscopia infrarroja con transformada de Fourier (FTIR), EED, SDS-PAGE y MEB.

Los espectros FTIR mostraron las bandas características de polisacáridos (región  $1200\text{-}800\text{ cm}^{-1}$ ) en todas las fracciones. También se encontraron las bandas más comúnmente citadas en estudios estructurales de proteína (Pelton y McLean, 2000), es decir las bandas Amida I ( $1600\text{-}1700\text{ cm}^{-1}$ ), Amida II ( $1600\text{-}1500\text{ cm}^{-1}$ ) y Amida III ( $1200\text{-}1300\text{ cm}^{-1}$ ) (Haris y Severcan, 1999; Barth, 2007). Además, se encontró una banda de gran amplitud en la región de  $3000\text{-}3600\text{ cm}^{-1}$ , la cual corresponde a los estiramientos del enlace O-H (Elisa et al., 2006)

En general, tanto en los sobrenadantes como en los precipitados, se encontraron las mismas bandas. Sin embargo, en los precipitados se observó un cambio en la forma y un ligero desplazamiento ( $1050\text{ a }1017\text{ cm}^{-1}$ ) de la banda asignada a carbohidratos después de la adición de  $\text{CaCl}_2$ . Existe la posibilidad de que los arabinosilanos, ácido ferúlico y proteínas en cada una de las fracciones se encontraran formando complejos carbohidrato-proteína mediante interacciones intermoleculares o entrecruzamientos a través de sustituyentes de ácido ferúlico (Lapierre et al., 2001).

De forma particular, se obtuvieron los espectros IR del sobrenadante y el precipitado de la muestra control de pk-2. Al igual que el resto de las fracciones, ambas presentaron una banda en  $1050\text{ cm}^{-1}$ , la cual puede ser asignada a arabinosilanos (Robert et al., 2005). Además, dos bandas, una en  $988$  y la otra en  $946\text{ cm}^{-1}$ , están relacionadas con el grado de sustitución de arabinosilanos (Robert et al., 2005), mismas que confirman la presencia de este polisacárido. También se encontró en el espectro correspondiente a las nanopartículas (precipitado de la muestra control de pk-2), que las bandas Amida I y Amida II fueron más intensas y definidas en comparación con el resto de las fracciones. También, en este mismo espectro se observó una disminución importante en la intensidad de la banda asignada a polisacáridos, lo que sugirió que las nanopartículas están compuestas principalmente de proteínas, a diferencia de las nanopartículas

obtenidas en el precipitado de la muestra desolvatada de pk-2, en la cual se obtuvo una banda muy intensa asignada a carbohidratos. Esto sugirió que los polisacáridos presentes en esta fracción no estaban fuertemente unidos a la fracción de proteínas involucradas en la formación de nanopartículas, ya que estos no precipitaron con las nanoestructuras formadas.

El análisis de composición elemental reveló la presencia de C, O, N, Na, P, S, Cl y Ca en las fracciones. C y O fueron los elementos más abundantes debido a los altos niveles de materia orgánica. La detección de N confirmó la presencia de proteína en las fracciones, especialmente en las nanopartículas formadas, ya que en estas fue mayor. Este elemento no tuvo mucha variación entre los sobrenadantes y precipitados de pk-1, pk-Int o pk-3, lo que sugiere que las proteínas en esas fracciones no están involucradas en la formación de nanopartículas, como fue evidente en las imágenes obtenidas en MEB para estas tres fracciones. La presencia de Na y P probablemente se debió, en parte, a residuos del bufer usado en la separación por SEC, mientras que el P también podría provenir de fitatos presentes en el salvado de trigo (De Brier et al., 2015). El S puede corresponder a residuos de aminoácidos azufrados, tal como la cisteína. En tanto, la presencia de Cl en los sobrenadantes y precipitados proviene seguramente del agente de desolvatación. El predominio del Ca en los precipitados de todas las fracciones, así como la ausencia de éste en sobrenadantes, confirmó que el calcio estuvo involucrado en los precipitados formados después de la desolvatación en esas fracciones.

Al comparar la composición de los precipitados de la muestra control de pk-2 y del precipitado de la muestra desolvatada de pk-2, se observaron diferencias importantes con respecto al contenido de Na, P, Cl y Ca. Es decir, las nanopartículas vistas en el precipitado de la muestra control de pk-2 están formadas principalmente por proteínas, a diferencia de las nanopartículas obtenidas en el precipitado desolvatado de pk-2, en el cual se observó la presencia de estructuras coraloides, además de las nanopartículas. El aumento en el porcentaje de S en el precipitado de la muestra control de pk-2 soporta la presencia de proteínas, mientras que la ausencia de Ca en esta corrobora que el Ca no participó en la formación de nanopartículas.

La morfología de las dos fases resultantes de cada fracción fue contrastada con su muestra control. Los análisis de MEB mostraron que la muestra control de pk-1 tuvo una

superficie rugosa, mientras que la superficie del sobrenadante fue liso y el precipitado presentó una morfología coraloide. En el sobrenadante y precipitado de pk-Int y pk-3, se encontró una morfología similar a los de pk-1. Sin embargo, en la muestra control de pk-3, se observó la presencia de estructuras esféricas y ovoides con tamaños entre 210 y 470 nm, respectivamente. Estas estructuras esféricas y ovoides, pudieron ser resultado de la presencia de proteínas de masa molecular entre 20-31 kDa (SDS-PAGE), proteínas de la misma masa están presentes en la muestra pk-2CP, las cuales formaron las nanopartículas vistas en MEB. La forma de estas nanoestructuras puede deberse a la baja concentración de estas proteínas (Ge et al., 2011).

Por otro lado, en el sobrenadante de la muestra desolvatada de pk-2, se obtuvo la formación de partículas rocosas con diámetros entre 51-500 nm, mientras que en el precipitado de esta misma muestra, se encontró la formación de estructuras esféricas con diámetros entre 190-250 nm acompañadas de estructuras coraloideas. Sin embargo, la muestra control de pk-2, resultó positiva, ya que también se obtuvo la formación de nanopartículas idénticas a las formadas en la muestra desolvatada (pk-2) con  $\text{CaCl}_2$  (precipitado). No obstante, en estas esferas no se observó la presencia de estructuras coraloideas como las vistas en el precipitado de pk-2. Debido a que en la muestra control de pk-2 no se añadió  $\text{CaCl}_2$ , la evidencia sugiere que las nanopartículas se formaron antes de la adición de  $\text{CaCl}_2$  y que el acondicionamiento térmico fue el responsable de su formación. Esto último se corroboró con las nuevas fases obtenidas luego de la desolvatación de pk-2CS (2). En la imagen (MEB) del precipitado de esta muestra (pk-2P2), se observó una morfología de tipo coral muy similar a la observada en los precipitados de todas las fracciones evaluadas con excepción del control pk-2. Esto significa que el calcio no está involucrado en la formación de nanopartículas, sino más bien en la precipitación de estructuras coraloideas, que de hecho podrían ser cristales (Luna-Valdez et al., 2017).

En el ARTÍCULO 3 se analizaron los cambios conformacionales de las proteínas involucradas en la formación de nanopartículas, generados por efecto de la temperatura. Las nanopartículas se obtuvieron mediante un tratamiento térmico de proteínas (albúminas) de bajo peso molecular (25-44 kDa) derivadas del salvado de trigo, las

cuales fueron liofilizadas y analizadas por MEB. Se obtuvieron nanopartículas de forma esférica con diámetros entre 190-250 nm. A su vez, una porción de polvo de estas nanopartículas fueron resuspendidas en agua deionizada y sonicadas durante 5 min, las cuales posteriormente se analizaron por MEB en modo de transmisión. Esto permitió distinguir que las nanoesferas están conformadas por nanopartículas de menor tamaño (30 nm de diámetro). De acuerdo a lo reportado en la literatura, existen diferencias importantes con respecto a los agregados proteicos por efecto de la temperatura (albúmina de suero de bovino,  $\beta$ -lactoglobulina y aislados de proteína de suero) (Doi, 1993; Aymard et al., 1996; Ikeda y Morris, 2002; Lovedey, et al., 2010; Oboroceanu et al., 2010; Lovedey et al, 2012; Borzova et al., 2016), ya que para lograr dichos agregados se requiere del empleo de sales (Na o  $\text{CaCl}_2$ ) y de tiempos de inducción térmica muy prolongados (20 h) a temperaturas de al menos 80 °C. A diferencia de las condiciones empleadas para la obtención de las nanopartículas del presente trabajo, donde solo fueron necesarias 3 h de inducción térmica a 68.5 °C sin el empleo de sales. Se empleó la espectroscopía infrarroja de transformada de Fourier (FTIR) para el análisis de la región Amida I de las proteínas (1700-1600  $\text{cm}^{-1}$ ), ya que con esta técnica es posible monitorear cambios sutiles en la conformación de la cadena polipeptídica debido a que es muy sensible a cambios en los enlaces de hidrógeno (van Stokkum et al., 1995; Natalello et al., 2005) y, por lo tanto, es útil para analizar modificaciones en la estructura secundaria causadas por efecto de la temperatura o el pH (Vicent et al., 1984). El análisis de la región Amida I permitió realizar una estimación cuantitativa de las diferentes estructuras secundarias (hélices- $\alpha$ , hojas- $\beta$ , vueltas y al azar) de las proteínas. Dicho análisis se realizó aplicando la segunda derivada en la región 1700-1600  $\text{cm}^{-1}$  del espectro infrarrojo para resolver la banda en cuestión en dos o más señales que no son visibles en el espectro original y poder así, identificar cada uno de los componentes de las diferentes estructuras secundarias (Dong et al., 1992; Carbonaro y Nucara, 2010). Para realizar lo anterior se asumió que la suma de las áreas de las conformaciones de la Amida I, están relacionadas al total de la proteína dada (Byler y Susi, 1986; Kong y Yu, 2007). De dicho análisis resultó que las proteínas en forma nativa están compuestas principalmente de conformaciones hojas- $\beta$  con un 46%. El 18% son de giros- $\beta$  y un 14%

a hélices- $\alpha$ , mientras que 16% corresponde a conformaciones aleatorias y el 5% restante a agregados.

El cambio en la estructura secundaria de las proteínas involucradas en la formación de nanopartículas por efecto del tratamiento térmico fue evidente, ya que la conformación hojas- $\beta$  disminuyó hasta 20% de la estructura secundaria. Estos resultados concuerdan con lo reportado por Natalello et al. (2005), quienes reportaron una disminución del 50% en las conformaciones hojas- $\beta$  después de someter la proteína a una temperatura de 64 °C así como una disminución simultánea en hélices- $\alpha$ . En nuestro caso, las hélices- $\alpha$  permanecieron constantes.

Por otro lado, las conformaciones de giro- $\beta$  representaron el 11%, lo que significó una disminución con respecto a las proteínas nativas. Las conformaciones aleatorias se mantuvieron sin cambios. Además, el cambio conformacional de la estructura secundaria fue acompañada por una banda de gran amplitud e intensidad en  $1619\text{ cm}^{-1}$ , que representó el 38% y se debió a la formación de agregados intermoleculares por hojas- $\beta$  de proteínas, inducidos por el tratamiento térmico (Haris y Severcan 1999, Seshadri et al., 1999, Yan et al., 2004, Natalello et al., 2005).

La formación de agregados por hojas- $\beta$  intermoleculares puede deberse al hecho de que el experimento se realizó a pH 8. Es decir, cuando se emplea un  $\text{pH} > \text{pI}$  de las proteínas, la agregación procede a través de la formación de agregados ordenados relativamente pequeños (oligómeros), los cuales se caracterizan por una cantidad considerable de hojas- $\beta$  intermoleculares, como se reveló por espectroscopia FTIR para BSA (Militello et al., 2004).

Durante la estimación cuantitativa de las estructuras secundarias de las proteínas, se tuvo en cuenta que los cambios conformacionales en las proteínas no solamente pueden ser debidos al efecto de la temperatura, sino también a la pérdida de la capa de hidratación después de la liofilización. Es decir, durante este proceso pueden producirse alteraciones inducidas por la deshidratación en las bandas características del enlace amida. Sin embargo, esto no excluye el uso de la espectroscopia FTIR para realizar dicha estimación (van de Weert et al., 2001). Incluso, los posibles cambios que pudieron haberse generado en la estructura de las proteínas por efecto de la liofilización debieron

haber sido mínimos ya que la morfología no fue afectada, de acuerdo a lo visto en las imágenes de obtenidas en MEB (Griebenow y Klibanov, 1995).

Con base en los resultados obtenidos, además de información en la literatura, existe la posibilidad de que las nanopartículas hayan sido formadas por enlaces disulfuro, debido a la aparición de una banda de gran amplitud a  $560\text{ cm}^{-1}$  vista en el espectro infrarrojo, la cual puede ser asignada a la formación de enlaces disulfuro (Sadeghi et al., 2014). Para soportar esto, las proteínas (20-43 kDa) que estuvieron involucradas en la formación de nanopartículas son ricas en cisteína (Tabla 1, anexos), aminoácido que puede formar este tipo de enlaces entre residuos vecinos (Doi, 1993). Dichas proteínas (albúminas del salvado de trigo) han sido previamente identificadas mediante espectrometría de masas por Chaquilla-Quilca et al. (2017) utilizando el método reportado por Huerta-Ocampo et al. (2014). Es decir, durante el proceso de agregación térmica, las proteínas experimentan un desdoblamiento parcial de su estructura nativa, la cual genera cambios en la estructura tridimensional debido a la ruptura de enlaces de hidrógeno y grupos hidrófobos no polares, lo cual causa que los grupos hidrofóbicos y los grupos SH libres se vuelvan más expuestos y puedan formar enlaces disulfuro intermoleculares e interacciones hidrofóbicas entre las cadenas proteicas desplegadas, resultando así en la formación de agregados (Shimada et al., 1989; Vetri, Librizzi, Leone, & Militello, 2007).

Es probable que el mecanismo de agregación de las nanoestructuras obtenidas en este trabajo sea el mismo que el propuesto por Aymard et al. (1996). Dicho mecanismo consiste de agregación en dos etapas. En la primera se forman agregados de pequeñas partículas (glóbulos) mediante intercambio disulfuro, el cual surge de monómeros desnaturalizados que consecuentemente se asocian en dímeros. En la segunda etapa, los glóbulos resultantes se agregan para formar estructuras fractales. De acuerdo a lo antes mencionado, es posible considerar dicho mecanismo, ya que aparentemente las nanoesferas están formadas por agregados más pequeños (30 nm de diámetro), que podrían haberse formado por enlaces disulfuro (glóbulos), los cuales a su vez forman agregados de mayor tamaño por interacciones físicas tales como las fuerzas de van der Waals, enlaces de hidrógeno e interacciones hidrofóbicas o electrostáticas (Le Bon et al., 1999)



La presencia de nanoesferas de 30 nm vistas en MEB, luego de resuspender las nanopartículas en agua y sonicarlas durante 5 min, inclinan a considerar que las interacciones agregado-agregado corresponden efectivamente a interacciones físicas, ya que una parte de estas se desagregaron de las nanopartículas de mayor tamaño por efecto del ultrasonido (Hu et al., 2013) a diferencia de las nanopartículas que no fueron expuestas a este.

## BIBLIOGRAFÍA

- Arangoa M.A., Campanero M.A, Renedo M.J, Ponchel G. and Irache J.M. 2001. Gliadin nanoparticles as carriers for the oral administration of lipophilic drugs. Relationships between bioadhesion and pharmacokinetics. *Pharmaceutical Research*. 18(11):1521–1527.
- Aymard P., Gimel JC., Nicolai T. and Durand D. 1996. Experimental evidence for a two-step process in the aggregation of  $\beta$ -lactoglobulin at pH 7. *Journal de Chimie Physique*. 93:987-997.
- Balandrán-Quintana R.R., Mercado-Ruiz J.N. and Mendoza-Wilson A.M. 2015. Wheat bran proteins: A review of their uses and potential. *Food Reviews International*. 31:279-293.
- Barth A. 2007. Infrared spectroscopy of proteins. *Biochimica et Biophysica Acta*. 1767(9):1073–1101.
- Beaugrand J., Crónier D., Thiebeau P., Schreiber L., Debeire P. and Chabbert B. 2004. Structural, chemical composition and xylanase degradation of external layers isolated from developing wheat grain. *Journal of Agricultural and Food Chemistry*. 52:7108-7117.
- Borzova V.A., Markossian K.A., Chebotareva N.A. and Kleymenov S.Y. 2016. Kinetics of Thermal Denaturation and Aggregation of Bovine Serum Albumin. *PLoS ONE*. 11(4): 1-29.
- Byler D. M., and Susi H. 1986. Examination of the Secondary Structure of Proteins by Deconvolved FTIR Spectra. *Biopolymers*. 25:469-487.
- Carbonaro M. and Nucara A. 2010. Secondary structure of food proteins by Fourier transform spectroscopy in the mid-infrared region. *Amino Acids*. 38:679-690.
- Chaquilla-Quilca G., Balandrán-Quintana R.R., Huerta-Ocampo J.G. Ramos-Clamont Montfort G. and Luna-Valdez J.G. 2017. Identification of proteins contained in aqueous extracts of wheat bran through a proteomic approach. *Journal of Cereal Science*. (En revision).

- Czechowska-Biskup R., Rokita B., Lotfy S., Ulanski P. and Rosiak J.M. 2005. Degradation of chitosan and starch by 360-kHz ultrasound. *Carbohydrate Polymers*. 60(2):175-184.
- De Brier N., Gomand S.V., Donner E., Paterson D., Delcour J.A., Lombi E. and Smolders E. 2015. Distribution of minerals in wheat grains (*Triticum aestivum* L.) and in roller milling fractions affected by pearling. *Journal of Agricultural and Food Chemistry*. 63:1276-1285.
- Doi E. 1993. Gels and Gelling of globular proteins. *Trends in Food Science & Technology*. 4:1-5.
- Dong A., Caughey B., Caughey WS., Bhat KS. and Coe JE. 1992. Secondary structure of the pentraxin female protein in water determined by infrared spectroscopy: Effects of calcium and phosphorylcholine. *Biochemistry*. 31:9364–9370.
- Elissa A.S., Puhl C., Kadla J.F. and Khan S.A. 2006. Enzymatic cross-linking of  $\beta$ -lactoglobulin: conformational properties using FTIR spectroscopy. *Biomacromolecules*. 7:1707-1713.
- Ge J., Lei J. and Zare R.N. 2011. Bovine Serum Albumin Poly(methyl methacrylate) Nanoparticles: An Example of Frustrated Phase Separation. *Nano Letters*. 11:2551-2554.
- Gomez-Estaca J, Balaguer M.P, Gavara R. and Hernandez-Munoz P. 2012. Formation of zein nanoparticles by electrohydrodynamic atomization: Effect of the main processing variables and suitability for encapsulating the food coloring and active ingredient curcumin. *Food Hydrocolloids*. 28:82-91.
- Griebenow K. and Klibanov A.M. 1995. Lyophilization-induced reversible changes in the secondary structure of proteins. *Proceedings of the National Academy of Sciences*. 92:10969-10976
- Gülseren I., Fang Y. and Correding M. 2012. Whey protein nanoparticles prepared with desolvation with ethanol: characterization, thermal stability and interfacial behaviour. *Food Hydrocolloids*. 29:258-264.
- Haris P.I. and Severcan F. 1999. FTIR spectroscopic characterization of protein structure in aqueous and non-aqueous media. *Journal of Molecular Catalysis B: Enzymatic*. 7:207–221.

- Hromádková Z., Paulsen B.S., Polovka M., Košťálová Z. and Ebringerová A. 2013. Structural features of two heteroxylan polysaccharide fractions from wheat bran with anti-complementary and antioxidant activities. *Carbohydrate Polymers*. 93: 22-30.
- Hu H., Wu J., Li-Chan E.C.Y., Zhu L., Zhang F., Xu X., Fan G., Wang L., Huang X. and Pan S. 2013. Effects of ultrasound on structural and physical properties of soy protein isolate (SPI) dispersions. *Food Hydrocolloids*. 30:647-655.
- Huerta-Ocampo J.A., Barrera-Pacheco A., Mendoza-Hernández C.S., Espitia-Rangel E., Mock H.P., and Barba de la Rosa A.P. 2014. Salt stress-induced alterations in the root proteome of *Amaranthus cruentus* L. *Journal of Proteome Research*. 13(8):3607-3627.
- Idris W.H, Babiker E.E, and Tinay A.H. 2003. Fractionation, solubility and functional properties of wheat bran proteins as influenced by pH and/or salt concentration. *Nahrung/Food*. 47:425-429.
- Ikeda S. and Morris V.J. 2002. Fine-stranded and particulate aggregates of heat-denatured whey proteins visualized by atomic force microscopy. *Biomacromolecules*. 3:382-389.
- Jerkovic A., Kriegel A., Bradner J., Atwell B., Roberts T. and Willows R. 2010. Strategic distribution of protective proteins within bran layers of wheat protects the nutrient-rich endosperm. *Plant Physiology*. 152:1459-1470.
- Joye I.J, Nelis V.A, and McClements D.J. 2015. Gliadin-based nanoparticles: Fabrication and stability of food-grade colloidal delivery systems. *Food Hydrocolloids*. 44:86-93
- Konan Y.N., Gurny R. and Allémann E. 2002. Preparation and characterization of sterile and freeze-dried sub-200 nm nanoparticles. *International Journal of Pharmaceutics*. 233:239-252.
- Kong J. and Yu S. 2007. Fourier transform infrared spectroscopic analysis of protein secondary structures. *Acta Biochimica et Biophysica Sinica*. 39 (8):549-559.
- Langer K., Balthasar S., Vogel V., Dinauer N., Von Briesen H. and Shubert D. 2003. Optimization of the preparation process for human serum albumin (HAS) nanoparticles. *International Journal of Pharmaceutical*. 257:169-180.

- Lapierre C., Pollet B., Ralet M.-C. and Saulnier L. 2001. The phenolic fraction of maize bran: evidence for lignin-heteroxylan association. *Phytochemistry*. 57:765-772.
- Le Bon C., Nicolai T. and Durand D. 1999. Kinetics of aggregation and gelation of globular proteins after heat-induced denaturation. *Macromolecules*. 32:6120-6127.
- Loveday S.M., Su J., Rao M.A., Anema S.G. and Singh H. 2012. Whey protein nanofibrils: the environment-morphology-functionality relationship in lyophilization, rehydration, and seeding. *Journal of Agricultural and Food Chemistry*. 60:5229-5236.
- Loveday S.M., Wang X.L., Rao M.A., Anema S.G., Creamer L.K. and Singh H. 2010. Tuning the properties of  $\beta$ -lactoglobulin nanofibrils with pH, NaCl and CaCl<sub>2</sub>. *International Dairy Journal*. 20:571-579.
- Luna-Valdez J.G., Balandrán-Quintana R.R., Azamar-Barrios J.A., Clamont-Montfort G.R., Mendoza-Wilson A.M., Mercado-Ruiz J.N., Madera-Santana T.J., Rascón-Chu A. and Chaquilla-Quilca G. 2017. Structural and physicochemical characterization of nanoparticles synthesized from an aqueous extract of wheat bran by a cold-set gelation/desolvation approach. *Food Hydrocolloids*. 62:165-173.
- Mehravar R, Jahanshahi M, and Saghatoleslami N. 2009. Production of biological nanoparticles from  $\alpha$ -lactalbumin for drug delivery and foods science application. *African Journal of Biotechnology*. 8:6822-6827.
- Militello V., Casarino C., Emanuele A., Giostra A., Pullara F. and Leone M. 2004. Aggregation kinetics of bovine serum albumin studied by FTIR spectroscopy and light scattering. *Biophysical Chemistry*. 107:175-187.
- Natalello A., Ami D., Brocca S., Lotti M., and Doglia S.M. 2005. Secondary structure, conformational stability and glycosylation of a recombinant *Candida rugosa* lipase studied by Fourier-transform infrared spectroscopy. *Biochemical Journal*. 385: 511-517.
- Oboroceanu D., Wang L., Brodkorb A., Magner E., and Auty M.A.E. 2010. Characterization of  $\beta$ -lactoglobulin fibrillary assembly using atomic force microscopy, polyacrylamide gel

- electrophoresis, and in situ Fourier transform infrared spectroscopy. *Journal of Agricultural and Food Chemistry*. 58:3667-3673.
- Pace C.N., Treviño S., Prabhakaran E. and Scholtz J.M. 2004. Protein structure, stability and solubility in water and other solvents. *Philosophical Transactions of the Royal Society B: Biological Sciences*. 359(1448):1225-1235.
- Pelton J.T. and McLean L.R. 2000. Spectroscopic methods for analysis of protein secondary structure. *Analytical Biochemistry*. 277:167-176.
- Robert P., Marquis M., Barron C., Guillon F. and Saulnier L. 2005. FT-IR investigation of cell wall polysaccharides from cereal grains. Arabinoxylan infrared assignment. *Journal of Agricultural and Food Chemistry*. 53(18):7014-7018.
- Sadeghi, S., Madadlou, A., Yarmand, M. 2014. Microemulsification-cold of date palm pit extract. *Food Hydrocolloids*. 35:590-596.
- Saulnier L., Marot C., Elgottiaga M., Bonnin E. and Thibault J.F. 2008. Thermal and enzymatic treatments for the release of free ferulic acid from maize bran. *Carbohydrate Polymers*. 45:269–275.
- Seshadri S., Khurana R. and Fink A.L. 1999. Fourier transform infrared spectroscopy in analysis of protein deposits. *Methods in Enzymology*. 309:559–576.
- Shewry P.R., D'Ovidio R., Lafiandra D., Jenkins J.A., Mills E.N.C. and Békés F. 2009. Wheat grain proteins. In K. Khan, and P.R. Shewry (Eds.), *Wheat: Chemistry and technology* (4th ed., pp. 223-298). St. Paul Minnesota: AACC International, Inc.
- Shimada K. and Cheftel J.C. 1989. Sulfhydryl group/disulfide bond interchange reactions during heat-induced gelation of whey protein isolate. *Journal Agricultural Food Chemistry*. 37:161-168.
- Singh J. and Skerritt J.H. 2001. Chromosomal control of albumins and globulins in wheat grain assessed using different fractionation procedures. *Journal Cereal Science*. 33:163-181.
- Talbot M.J. and White R.G. 2013. Cell surface and cell outline imaging in plant tissues using the backscattered electron detector in a variable pressure scanning electron microscope. *Plant Methods*. 9(40):1-16.

- van de Weert M., Haris P.I. Hennink W.E. and Crommelin D.J.A. 2001. Fourier transform infrared spectrometric analysis of protein conformation: effect of sampling method and stress factors. *Analytical Biochemistry*. 297:160–169
- van Stokkum I.H.M., Linsdell H., Hadden J.M., Haris P.I., Chapman D. and Bloemenda M. 1995. Temperature-induced changes in protein structures studied by fourier transform infrared spectroscopy and global analysis. *Biochemistry*. 34:10508-10518.
- Vicent J.S., Steer C.J. and Levin I.W. 1984. Infrared spectroscopic study of the pH-dependent secondary structure of Brain Clathrin. *Biochemistry*. 23:625-631.
- Yan Y., Wang Q., He H. and Zhou H. 2004. Protein thermal aggregation involves distinct regions: sequential events in the heat-induced unfolding and aggregation of hemoglobin. *Biophysical Journal*. 86:1682-1690.
- Yedomon B., Fessi H. and Charcosset C. 2013. Preparation of bovine serum albumin (BSA) nanoparticles by desolvation using a membrane contactor: A new tool for large scale production. *European Journal of Pharmaceutics and Biopharmaceutics*. 85:398-405.
- Yedomon B., Fessi H. and Charcosset C. 2013. Preparation of Bovine Serum Albumin (BSA) nanoparticles by desolvation using a membrane contactor: A new tool for large scale production. *European Journal of Pharmaceutics and Biopharmaceutics*. 85:398-405.
- Zhang J, Liang L, Tian Z, Chen L and Subidare M. 2012. Preparation and vitro evaluation of calcium-induced soy protein isolate nanoparticles and their formation mechanism study. *Food Chemistry*. 133:390-399.
- Zhang Y, Pitkänen I, Douglade J, Tenkanen M, and Remond C. 2011. Wheat bran arabinoxylans: Chemical structure and film properties of three isolated fractions. *Carbohydrate Polymers*. 86:852-859

## ARTÍCULO 1

### **Structural and physicochemical characterization of nanoparticles synthesized from an aqueous extract of wheat bran by a cold-set gelation/desolvation approach**

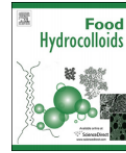
J.G. Luna-Valdez, R.R. Balandrán-Quintana, J.A. Azamar-Barrios, G. Ramos-Clamont Montfort, A.M. Mendoza-Wilson, J.N. Mercado-Ruiz, T.J. Madera-Santana, A. Rascón-Chu, G. Chaquilla-Quilca.

(2017)

Artículo publicado en

Food Hydrocolloids, 62:165-163





## Structural and physicochemical characterization of nanoparticles synthesized from an aqueous extract of wheat bran by a cold-set gelation/desolvation approach

J.G. Luna-Valdez <sup>a</sup>, R.R. Balandrán-Quintana <sup>a,\*</sup>, J.A. Azamar-Barríos <sup>b</sup>,  
G. Ramos Clamont-Montfort <sup>c</sup>, A.M. Mendoza-Wilson <sup>a</sup>, J.N. Mercado-Ruiz <sup>a</sup>,  
T.J. Madera-Santana <sup>a</sup>, A. Rascon-Chu <sup>a</sup>, G. Chaquilla-Quilca <sup>a</sup>

<sup>a</sup> Centro de Investigación en Alimentación y Desarrollo, A.C. Coordinación de Tecnología de Alimentos de Origen Vegetal, Carretera a La Victoria km 0.6, 83304, Hermosillo, Sonora, México

<sup>b</sup> Centro de Investigación y de Estudios Avanzados del IPN, Unidad Mérida. Departamento de Física Aplicada, Carretera antigua a Progreso Km. 6, 97310, Mérida, Yucatán, Mexico

<sup>c</sup> Centro de Investigación en Alimentación y Desarrollo, A.C. Coordinación de Ciencias de los Alimentos, Carretera a La Victoria km 0.6, 83304, Hermosillo, Sonora, Mexico

### ARTICLE INFO

#### Article history:

Received 9 January 2016

Received in revised form

10 June 2016

Accepted 27 July 2016

Available online 1 August 2016

#### Keywords:

Protein nanoparticles

Agroindustrial byproducts

Wheat bran proteins

Cold set gelation

Protein desolvation

### ABSTRACT

The aqueous extracts of wheat bran are rich in carbohydrates and contain water soluble proteins with a high content of Asp and Glu, which could enable the fabrication of nanoparticles through the cold-set gelation/desolvation of the proteins, while carbohydrates would act as the matrix on which the nanoparticles are formed. In order to test this hypothesis, in this work it was assayed the desolvation of the wheat bran aqueous extracts using CaCl<sub>2</sub> as desolvation agent. Aggregates between 3 and 5 μm were formed immediately after addition of a range of CaCl<sub>2</sub> concentrations, as detected by dynamic light scattering. Scanning electron microscopy showed that such aggregates consisted of spherical nanoparticles with diameters between 20 and 100 nm, immersed into a matrix composed mainly by polysaccharides. This matrix was disrupted by ultra-sonication and individual nanoparticles, arranged in a necklace fashion, were visible by scanning electron microscopy in transmission mode. This is the first report on the formation of nanoparticles from an aqueous extract of wheat bran by a cold-set gelation/desolvation approach.

© 2016 Elsevier Ltd. All rights reserved.

### 1. Introduction

An interesting application of food nanotechnology is the nanoencapsulation of molecules sensitive to surroundings (Khare & Vasisht, 2014). Proteins are perhaps the most important biopolymers for producing nanoparticles intended to nanoencapsulation, not only because are biocompatible and biodegradable but also because of a great chemical diversity that permits a variety of non-covalent interactions, inter- and intramolecular, which enables the design of different types of

nanostructures (Foegeding & Davis, 2011; Kratz, 2014; Rohiwal et al., 2015; Sağlam, Venema, van der Linden, & de Vries, 2014).

There are two main methods for preparing protein nanoparticles: coacervation/desolvation and emulsification. Coacervation is based on the conformational changes of the proteins when exposed to desolvation agents, such as ethanol or acetone, which leads to precipitation and concomitant formation of nanoparticles; these nanoparticles can be stabilized by the addition of a crosslinking agent, more commonly glutaraldehyde. In the emulsification method the protein is emulsified in oil and the nanoparticles are formed at the w/o interface; surfactants and crosslinking agents are used to stabilize the emulsion and the nanoparticles, respectively, whereas the oil phase has to be removed with organic solvents (Arroyo-Maya, Hernández-Sánchez, Jiménez-Cruz, Camarillo-

\* Corresponding author.

E-mail address: [rbalandran@ciad.mx](mailto:rbalandran@ciad.mx) (R.R. Balandrán-Quintana).

Cadena, & Hernández-Arana, 2014; Lohcharoenkal, Wang, Chen, & Rojanasakul, 2014).

A third strategy, although not extensively reported, consists in adaptations to the cold-set protein gelation process. In this method a protein solution is first preheated, then is cooled out to room temperature, followed by adjustment of pH to basicity and, finally, by addition of a divalent ion (for example  $\text{Ca}^{2+}$ ). In a strict sense, the cold-set gelation process for preparing protein nanoparticles is also a desolvation one since the net charge of the protein becomes negative due to the basic pH, permitting the calcium ions be electrostatically attached by replacement of the solvation layer of water that surrounds the protein surfaces. Under such condition,  $\text{Ca}^{2+}$  act as bridge between two protein molecules, eliminating the repulsive forces. Although in the cold gelation the result is a bulky gel, it is also possible to obtain nanoparticles through a precise control of the process variables. One advantage of this method is that avoids the use of glutaraldehyde (toxic) and organic solvents (Hongprabhas & Barbut, 1997; Ju & Kilara, 1998; Sadeghi, Madadlou, & Yarmand, 2014; Zhang, Liang, Tian, Chen, & Subirade, 2012).

Proteins from animal origin are by far the most studied to prepare nanoparticles, however there are a few reports about producing nanoparticles from plant proteins (Duclairon, Orecchioni, Depraetere, Osterstock, & Nakache, 2003; Joye, Nelis, & McClements, 2015; Zhang et al., 2012). In this context, the proteins contained in agroindustrial byproducts of vegetable origin are interesting because of potential add value. Wheat bran (WB), i.e. the outer set of layers of the wheat kernel obtained as byproduct after milling, contains 14–20% (w/w) of total protein (Grundas & Wrigley, 2004; Shewry et al., 2009; USDA, 2014). WB is almost entirely used for animal feed but the proteins are not assimilated at all (Donangelo & Eggum, 1985; Saunders, 1978) so these biomolecules are underutilized.

The water soluble protein fraction of WB, i.e. the albumin fraction, is mainly localized in the outer layers (Jerkovic et al., 2010; Shewry et al., 2009). Although its extraction is simple (Idris, Babiker, & El Tinay, 2003; Jerkovic et al., 2010), the protein concentration in the powdered extracts is not high enough because of the presence of carbohydrates, mainly dietary fiber (Chaquilla-Quilca et al., 2016). Since a further purification would lead to low yields, an innovative approach for using the extracts as a whole is to take advantage of the coexistence of proteins and carbohydrates, having these latter the role of scaffolds on which protein assemblies could be formed. This concept has already been addressed in the supramolecular assembly of peptides and/or proteins (Brown, Aksay, Saville, & Hecht, 2002; Chaquilla-Quilca et al., 2016; Thakur, Prashanthi, & Thundat, 2013).

In general, albumins are proteins characterized by a significant content of the acidic amino acids Asp and Glu, whose carboxylate side groups develop a negative charge at pH greater than 7.0. This feature imparts the water solubility properties of albumins in the native state (Pace, Treviño, Prabhakaran, & Scholtz, 2004) as well as the susceptibility to form nanoparticles through a cold gelation approach and the possibilities of electrostatic adsorption of other molecules. In sight of their amino acid profile (Shewry et al., 2009), the WB albumins could exhibit all these properties besides a high capacity of reversible binding to hydrophobic molecules, all of which is considered advantageous for the preparation of nanoparticles (Yedomon, Fessi, & Charcosset, 2013).

To the best of our knowledge, there are no reports dealing with the preparation of nanoparticles from the proteins contained in aqueous extracts of WB by desolvation and/or adaptations to the cold gelation process. Thus, the objective of this investigation is to synthesize nanoparticles from the aqueous WB extracts by the cold gelation/desolvation method.

## 2. Materials and methods

### 2.1. Materials

Wheat bran (*Triticum aestivum* L.) was purchased in a commercial mill of Hermosillo, Sonora, Mexico. The proximate composition, amino acid profile and neutral sugar composition were analyzed according to the methods outlined in sections 2.3.1–2.3.3. All the reagents, unless otherwise specified, were purchased from Sigma-Aldrich (St. Louis, MO, USA). Washing of WB and extraction, as well as the preparation of solutions and reagents, were performed with deionized water (18 M $\Omega$ ) obtained with a Milli-Q system (Bedford, MA, USA).

### 2.2. Aqueous extraction of the wheat bran

Before the aqueous extraction, WB was sieved through a 40 mesh, washed by immersion in cold water and then dried at 40 °C, as described in Campas-Ríos et al. (2012). The extraction was performed by mixing WB and cold water in a 1:10 ratio, w/v, into 50 mL conical tubes which were placed on a rotary wheel for 3 h at 4 °C. After this period, the aqueous extracts were filtered through organza cloth in order to separate the larger particles; then the extracts were collected and centrifuged for 20 min at 5,500g. The supernatants were recovered, frozen at –40 °C and lyophilized on a Labconco lyophilizer (Labconco®, MO, USA). The lyophilized powder, labeled as the aqueous extract of wheat bran (AEWB), was stored at –40 °C for subsequent treatments or analysis.

### 2.3. Characterization of the AEWB

#### 2.3.1. Proximate analysis and soluble protein

Total protein (Nx5.75), moisture, fat, dietary fiber and ash, were quantified by methods 2001.11, 950.02, 920.39C, 985.29 and 942.05 of the AOAC (1990), respectively; the total carbohydrate content was estimated by difference. The soluble protein was analyzed by the Bradford method (Bradford, 1976).

#### 2.3.2. Amino acid profile and molecular mass of AEWB proteins

The amino acid profile was determined by hydrolysis of samples at 110 °C with 6 N HCl, derivatization with o-ftalaldehyde and injection in a HPLC chromatograph Varian 910 (Varian instrument group, Walnut Creek, CA), equipped with a reverse phase column C-18 (Rainin Instruments LLC, CA) and using a standard amino acid kit, 0.1 mol/mL, from H Thermo Scientific (Rockford, IL), according to Vázquez-Ortiz, Caire, Higuera-Ciapara, and Hernández (1995). SDS-PAGE under non-reducing conditions was run to determine the molecular mass profile of the AEWB proteins. Both, AEWB and hydrolysates were dissolved in buffer pH 8 and subjected to SDS-PAGE, 12% polyacrilamide, in a Mini Protean Tetra Cell (Bio-Rad Laboratories Inc., Hercules, CA) at 80 mV for 3 h. All the chemicals for the SDS-PAGE, including the standard molecular mass markers and Coomassie blue for staining were from Bio-Rad. Gels were documented in a Gel Doc™ XR + System, also from Bio-Rad.

#### 2.3.3. Neutral sugar composition

For the neutral sugar analysis the AEWB was hydrolyzed with 1 M HCl at 100 °C for 150 min, followed by cleaning and filtering through Sep-pak C18 cartridges (Waters Corp., USA) and GH Polypro membranes, 0.45  $\mu\text{m}$  (Pall Corp., USA), respectively. After filtering, the samples were dried under air flux and reconstituted with HPLC grade water; this process was repeated twice to ensure remove any remaining acid. The dry samples were reconstituted with HPLC grade water in appropriate concentrations and filtered through Acrodisc syringe filters, 0.45  $\mu\text{m}$  (Pall Corp., USA). Aliquots

were analyzed by HPAEC-PAD (Dionex, Sunnyvale, CA). The elution times of samples were compared with those of standard sugars (Sigma-Aldrich) and concentration was calculated from the peak areas.

#### 2.3.4. Elemental composition of the AEWB

The elemental composition of AEWB was analyzed by energy dispersive X-ray spectrometry (EDS) on a JEOL JSM-7600F electron microscope (JEOL Ltd., Tokyo, Japan), equipped with a low angle backscattered electron detector. Measurements were made within 80 s and the scanned average areas were of 1540  $\mu\text{m}^2$  for the desolvated samples, 4465  $\mu\text{m}^2$  for the AEWB and 42,120  $\mu\text{m}^2$  for the control, respectively. Data are reported as % atom.

#### 2.3.5. Analysis of functional groups in AEWB

The analysis of functional groups was made by FTIR spectroscopy at 25 °C on a ThermoNicolet Nexus 670 FT-IR spectrometer (ThermoNicolet Analytical Instruments, Madison, WI) in pellets of KBr containing the AEWB samples. Data were collected in the range of 4000–400  $\text{cm}^{-1}$  with a resolution of 4  $\text{cm}^{-1}$  and each spectrum was the result of 64 scans.

#### 2.3.6. Morphology and particle size

The morphology and particle size of the AEWB was visualized by scanning electron microscopy (SEM). Samples were placed on SEM grids and coated with gold palladium on a pumped-rotary sputter coater Q150R ES (Quorum Technologies Ltd., USA). SEM was carried out on a JEOL JSM-7600F electron microscope (JEOL Ltd., Tokyo, Japan) at 2.0 kV.

### 2.4. Desolvation of the AEWB with $\text{CaCl}_2$

#### 2.4.1. Preparation and pre-conditioning of an AEWB stock solution

The AEWB powder was dispersed in water in a w/v ratio that ensured a protein concentration of 8 mg/mL in the resulting final stock solution. This dispersion was sonicated for 20 min at room temperature. In the preliminaries, the pH adjustment to 8.0 of a stock solution resulted in a white precipitate, which could interfere with the further pre-conditioning and desolvation steps. Because of this, a slight modification to the conventional procedure was made: the adjustment of pH to 8.0 (with 1.0 M NaOH) was done before the thermal pre-conditioning and the precipitate was removed by centrifugation. Then, the dispersion was centrifuged at 6,000g, 20 min, 10 °C. The supernatant, considered the stock solution, was recovered and conditioned to 68.5 °C in water bath for 3 h in order to facilitate the unfolding of the proteins; finally, it was cooled out to 25 °C with running water and was analyzed for its content of soluble protein.

#### 2.4.2. Desolvation treatments with $\text{CaCl}_2$

Desolvation of the pre-conditioned AEWB stock solution was carried out into a series of 2 mL aliquots, adding to each one 200  $\mu\text{L}$  of 0.25, 0.5, 1.0 or 1.5 M  $\text{CaCl}_2$ , with no stirring. An aliquot containing the protein solution, with no addition of  $\text{CaCl}_2$ , was evaluated as control. After the addition of  $\text{CaCl}_2$  the physical changes at first sight were recorded immediately, each hour for 3 h and at 24 h. When phase separation occurred, samples of the supernatants and precipitates were analyzed for soluble protein, dynamic light scattering and z potential (described in section 2.5.1). Finally, the precipitates constituting the desolvated phases of each treatment were recovered, frozen and lyophilized for their subsequent characterization.

### 2.5. Characterization of the desolvated and lyophilized AEWB

#### 2.5.1. Particle size distribution, z potential and soluble protein

The samples of supernatants and precipitates obtained after desolvation (section 2.4.2), were diluted to a protein concentration of 1 mg/mL, pH 8.0, in order to measure the particle size distribution by dynamic light scattering (DLS) as well as the z potential. The measurements were made at 25 °C in a Zetasizer Nano ZS90 (Malvern Instruments Ltd., Malvern, UK). Soluble protein was determined by Bradford.

#### 2.5.2. Electron microscopy, SEM and STEM

The morphology and size of particles of the desolvated AEWB corresponding to each treatment, were visualized by SEM in the same way as described in section 2.3.6. In addition, samples of the treatment 0.25 M  $\text{CaCl}_2$  were analyzed by scanning transmission electron microscopy (STEM). For this, 50 mg of powder were re-suspended in 1 mL of water and sonicated for 5 min at 25 °C. Then, 15  $\mu\text{L}$  of this suspension were placed on a 200 mesh copper grid, diameter 3 mm, coated with formvar. After air drying at room temperature, the analysis was run in the STEM instrument at 30 kV.

#### 2.5.3. Elemental composition

The elemental composition of the samples corresponding to each treatment was analyzed by EDS as described in section 2.3.4.

#### 2.5.4. Functional groups (FTIR)

Functional groups of the desolvated phases were analyzed by FTIR spectroscopy as described in section 2.3.5.

#### 2.5.5. X-ray diffraction

Because crystal-like structures were detected by SEM in the treatment 1.5 M  $\text{CaCl}_2$ , samples of this treatment as well as 0.5 M  $\text{CaCl}_2$  and AEWB were subjected to X-ray diffraction in order to corroborate their amorphous or crystalline nature. The analysis was made in a SIEMENS D5000 X-ray diffractometer. Measurements were made in samples of 0.02 g, wavelength 1.54 Å,  $2\theta$  values from 3 to 70° and a time step of 12 s.

#### 2.5.6. Statistical analysis

Experiments were performed by triplicate and the results displayed on tables represent the mean value  $\pm$  standard error. Means analysis was performed by the Tukey's test ( $p < 0.05$ ) in the NCSS software (Number Cruncher Statistical Systems, Kaysville, Utah, USA).

## 3. Results and discussion

### 3.1. Aqueous extraction of WB

Sieving and washing of WB by immersion in cold water are important steps to remove starch granules and adherent endosperm protein. SEM micrographs of representative samples show that starch granules were mostly removed from WB after washing (Fig. 1) as well as the polymeric glutenins, one of the two representative groups of proteins of the endosperm with MW > 100 kDa (Hurkman & Tanaka, 2007; Shewry et al., 2009) as seen in the SDS-PAGE gel (Fig. 2). It is assumed that gliadins, the other group of predominant endosperm proteins, as well as globulins and albumins from endosperm, were removed, but this is difficult to assert because their MW profile is similar to that of the WB albumins (Jerkovic et al., 2010).

After aqueous extraction and lyophilization, a straw-colored powder was obtained, yielding 7 g/100 g of WB. Because neither isolation nor partial purification of the proteins was performed, it

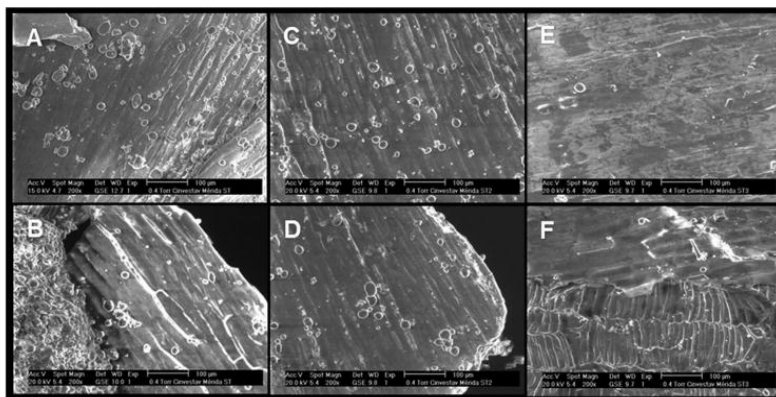


Fig. 1. SEM micrographs of wheat bran, before and after preparation for aqueous extraction. (A–B) before sieving and washing; (C–D) after sieving through 40 mesh; (E–F) after washing and drying at 40 °C.

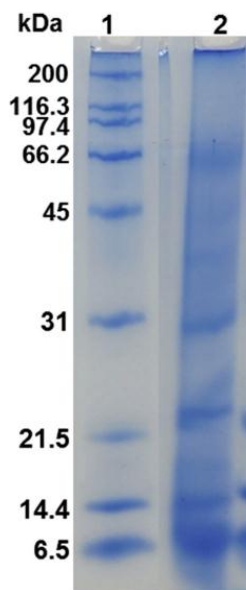


Fig. 2. SDS-PAGE of the aqueous extract of wheat bran (AEWB). Electrophoresis was run under non-reducing conditions in a 12% gel, at 80 mV. Line 1, MW standard; line 2, AEWB.

would be inappropriate to speak of albumins, so it was labeled AEWB.

### 3.1.1. Proximate analysis, amino acid profile and neutral sugar composition of WB and AEWB

Table 1 shows the proximate composition and amino acid profile of both WB and AEWB. The values found for WB are very similar to the average values reported in the literature (Saunders, 1978; USDA, 2014) but it was not possible to compare the AEWB because of the lack of references. However, it is reported that the

Table 1  
Proximate analysis, amino acid profile and neutral sugar composition of WB and AEWB.

	Proximate analysis (g/100 g)		Amino acid content (g/100 g protein)		
	WB	AEWB	WB	AEWB	
Water	3.7 ± 0.0	8.8 ± 0.19	Asp	2.91 ± 0.2	4.6 ± 0.4
Protein (Nx5.7)	13.6 ± 0.84	22.8 ± 0.59	Glu	15.80 ± 0.6	13.2 ± 0.5
Fat	8.4 ± 0.32	6.30 ± 0.17	Ser	3.15 ± 0.2	3.15 ± 0.1
Ash	5.14 ± 0.02	19.4 ± 0.09	His	8.72 ± 0.5	6.9 ± 0.3
Total fiber	51.5 ± 0.29	6.29 ± 0.48	Gly	9.71 ± 0.6	9.6 ± 0.6
Total carbohydrates <sup>a</sup>	17.8	36.4	Arg	3.12 ± 0.2	3.91 ± 0.4
Neutral sugars (μg/mg)			Ala	3.50 ± 0.1	5.75 ± 0.3
Ara	1.38 ± 0.07	0.68 ± 0.04	Tyr	6.89 ± 0.6	5.34 ± 0.4
Gal	0.84 ± 0.01	0.90 ± 0.01	Met	3.43 ± 0.4	2.28 ± 0.2
Glc	4.23 ± 0.18	3.14 ± 0.08	Val	4.66 ± 0.2	4.24 ± 0.3
Xyl	5.1 ± 0.33	0.42 ± 0.01	Phe	4.20 ± 0.2	3.13 ± 0.4
Ara/Xyl	0.3	1.6	Ile	3.71 ± 0.2	3.36 ± 0.3
			Leu	7.10 ± 0.4	5.99 ± 0.4
			Lys	1.52 ± 0.1	1.92 ± 0.2

<sup>a</sup> Calculated by difference to 100.

content of albumins in the WB is about 20% relative to total protein (Idris, et al., 2003; Jones & Gersdorff, 1923), so we can estimate a protein extraction yield of 52%. The high content of ash and carbohydrates in the AEWB are due to the co-extraction of minerals and soluble fiber, both present in the WB in significant quantities (USDA, 2014).

Regarding the amino acid profile, Asp and Glu were present in high concentrations in WB, especially Glu, which also has been reported by other authors (Shewry et al., 2009). As expected, the same was observed for AEWB since it is known that albumins have major proportions of acidic amino acids, which favor the water solubility (Pace et al., 2004). These amino acids could facilitate protein-protein interactions by cross-linking through divalent cations like  $Ca^{2+}$ , because of the negative charges developed by the side carboxylate groups at pH greater than 7.0 (Nelson & Cox, 2008).

Also in Table 1 is shown the composition of neutral sugars. Because of differences in extraction methods and degree of purification, is not appropriate to compare the percentage of each sugar with data in literature. However, the important data is the Ara/Xyl ratio since this value indicates the substitution degree of the xylan

**Table 2**  
Elemental composition (% atom) of AEWB and samples subjected to treatments with CaCl<sub>2</sub>.

Element	AEWB	CaCl <sub>2</sub> concentration (M)				
		0 (control)	0.25	0.5	1.0	1.5
<b>C</b>	40.42	42.77	46.35	42.11	42.99	40.62
<b>N</b>	5.3	3.61	nd	nd	nd	nd
<b>O</b>	43.39	49.38	35.25	34.98	27.35	40.18
<b>Na</b>	nd <sup>a</sup>	1.05	1.38	2.09	1.42	1.67
<b>Mg</b>	0.77	0.14	0.5	0.53	1.29	0.23
<b>P</b>	3.54	0.68	5.28	6.22	7.62	4.17
<b>S</b>	0.27	0.08	0.55	0.47	0.38	0.31
<b>Cl</b>	0.26	0.16	1.33	2.81	5.23	4.54
<b>K</b>	6.06	2.12	4.27	4.42	5.07	2.4
<b>Ca</b>	nd	nd	5.08	6.36	8.65	5.87

<sup>a</sup> nd = No detected.

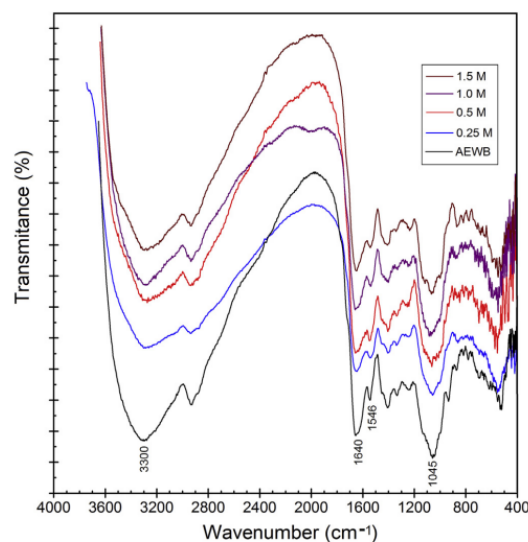
backbone with Ara residues, which in turn depends on the anatomical part of the wheat grain. The average value of the Ara/Xyl ratio in the water extractable arabinoxylans of wheat endosperm is 0.5 (Saulnier, Sado, Branlard, Charmet, & Guillon, 2007) and this ratio is very similar to that of the whole bran (0.6) as can be calculated from the data reported by Maes and Delcour (2002). Among the different layers of the bran, however, the Ara/Xyl ratio is higher in the pericarp than in both the intermediate and aleurone layers; the values for the latter are around 0.37 whereas in the pericarp the ratio is 1.14 (Antoine et al., 2003). The high Ara/Xyl ratio of 1.6 in AEWB indicates the presence of arabinoxylans coming from the outer pericarp. The high content of glucose in AEWB is surely due to the presence of  $\beta$ -glucans and starch that were into the pericarp layers.

### 3.1.2. Elemental composition

The elemental composition of the AEWB indicates the elements in WB that were extracted with water (Table 2), the most abundant of which are C and O because of the high levels of organic material. Mineral reserves in WB are in the globoid portion of the protein bodies of the innermost layer or aleurone, mainly in the form of phytin, the cationic salt of hexametaphosphoric acid (phytic acid). The globoids contain P, K and Mg, but not Ca (Lott & Spitzer, 1980); the latter, as well as Mn, Si and Sr, are in the outermost layers of pericarp (Brier et al., 2015). It seems difficult that aleurone globoids had been extracted by diffusion; however, it is possible that these were released from cells which were broken during milling, explaining thus the relatively high contents of P, K and Mg. The absence of Ca in the AEWB indicates that this could form very stable complexes with other components of the pericarp (Anglani, 1998) so it was not removed.

**Table 3**  
Soluble protein, average particle size and z potential, in the supernatants and precipitates of a dispersion of AEWB after desolvation with CaCl<sub>2</sub>.

CaCl <sub>2</sub> (M)	Soluble protein (mg/mL)	Average particle diameter (nm)	Z potential (mV)
<b>Supernatants</b>			
0	8.0 ± 0.2 <sup>a</sup>	914 ± 3.8 <sup>a</sup>	-11.6 ± 0.9 <sup>a</sup>
0.25	6.7 ± 0.9 <sup>b</sup>	875 ± 53.2 <sup>b</sup>	-10.83 ± 0.5 <sup>b</sup>
0.5	4.7 ± 1.9 <sup>c</sup>	740 ± 27.5 <sup>c</sup>	-7.7 ± 0.9 <sup>c</sup>
1.0	1.4 ± 0.1 <sup>d</sup>	1025 ± 31.6 <sup>d</sup>	-3.99 ± 0.5 <sup>d</sup>
1.5	1.3 ± 0.03 <sup>d</sup>	3278 ± 8.5 <sup>e</sup>	-4.34 ± 0.8 <sup>d</sup>
<b>Precipitates</b>			
0	—	1098 ± 32 <sup>f</sup>	-12.7 ± 0.4 <sup>e</sup>
0.25	19.7 ± 0.7 <sup>e</sup>	3498 ± 173 <sup>e</sup>	-11.7 ± 0.65 <sup>a</sup>
0.5	20.6 ± 0.9 <sup>e</sup>	3528 ± 613 <sup>e</sup>	-11.15 ± 0.64 <sup>a</sup>
1.0	17.3 ± 1.9 <sup>f</sup>	3327 ± 385 <sup>e</sup>	-7.0 ± 1.0 <sup>c</sup>
1.5	17.4 ± 0.9 <sup>f</sup>	5351 ± 413 <sup>g</sup>	-10.0 ± 0.17 <sup>f</sup>

<sup>a</sup>Superscripts in a same column indicate significant differences.**Fig. 3.** FTIR spectra of the aqueous extract of wheat bran (AEWB), before and after cold gelation/desolvation with 0.25, 0.5, 1.0 or 1.5 M CaCl<sub>2</sub>.

Due to system complexity, it is difficult to predict a certain pattern on the elemental composition of the samples in response to the treatments; however there are some aspects that draw attention in the context of the nanoparticle formation. One of them is that no nitrogen was detected in any of the samples subjected to desolvation, which is strange since the protein content in all of them is high, as can be seen in Table 3. Possibly this is because the proteins are in the center of the matrix, covered by a layer of polysaccharides and/or other components, so that the X-rays were not able to reach the amino acid residues and excite the electrons of nitrogen. This idea is plausible because it has been reported that the matrix has significant effects on the detection of nitrogen by SEM-EDS (Gazulla, Rodrigo, Blasco, & Orduña, 2013); further studies are needed in this regard.

Another interesting fact is the higher content of all the minerals in the desolvated samples with respect to the control (i.e., the suspension of AEWB which was subjected to the heat treatment but not to desolvation), suggesting that these were co-precipitated and form part of the complex in which the nanoparticles are embedded, or even are part of the nanoparticles themselves. It is also

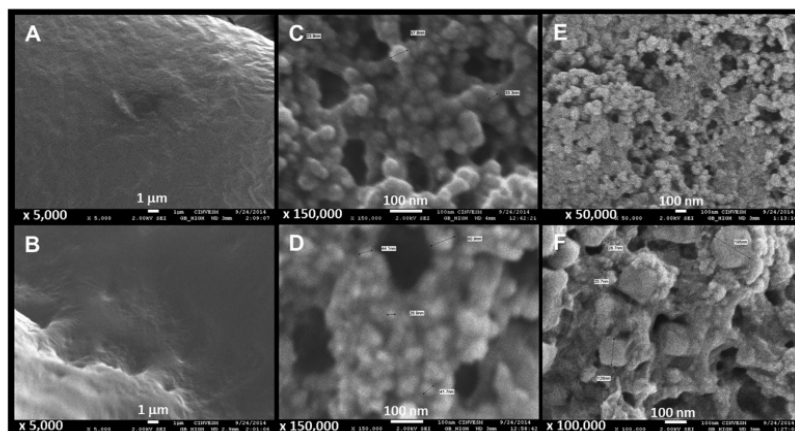


Fig. 4. SEM images of the particles obtained after subjecting the aqueous extract of wheat bran (AEWB) to cold gelation/desolvation with a range of  $\text{CaCl}_2$  concentrations.

noteworthy the highest content of Mg, P, K and Ca in the treatment 1.0 M  $\text{CaCl}_2$  (Table 3) and the abrupt decrease at 1.5 M. This is probably due to that, in the former case, most of the minerals were used in the nanoparticle formation; however, at the light of these results there is no explanation for the decrease at 1.5 M.

### 3.1.3. Functional groups by FTIR

In Fig. 3 are observed the IR spectra of the AEWB subjected to desolvation in the whole range of  $\text{CaCl}_2$  concentrations. Spectra show the characteristic bands of proteins and polysaccharides, which are the major components of AEWB. The region between 800 and  $1200\text{ cm}^{-1}$  corresponds to polysaccharides (Robert, Marquis, Barron, Guillon, & Saulnier, 2005) whereas those at  $1200\text{--}1400$  (amide III);  $1500$  (amide II);  $1600$  (amide I), and  $3300\text{ cm}^{-1}$  (amide A) are representative of proteins (Barth, 2007). The broad band in the  $3000\text{--}3600\text{ cm}^{-1}$  region is assigned to the OH groups (Sweeting, 1998).

### 3.2. Desolvation of the AEWB

After adding  $\text{CaCl}_2$  in the whole range of concentrations, samples quickly changed from opaque amber to a cloudy appearance and two phases were discernible: a precipitate and a turbid supernatant. The higher the concentration of  $\text{CaCl}_2$  added, the denser the precipitate and the less turbid the supernatant. Within the following 3 h the two phases were better defined. At the end of the 24 h period the precipitates were beige, while the supernatants looked clear yellow.

### 3.3. Characterization of the desolvated AEWB samples

#### 3.3.1. Particle size and z potential

In Table 3 are presented the protein content, the average size of particles and the zeta potential of the precipitates and supernatants resulting from the desolvation with  $\text{CaCl}_2$  (before lyophilization). As can be seen, the protein content was much higher in the precipitates than in the supernatants, a clear demonstration that protein aggregation was induced by desolvation. Regarding the particle size, there was a step-down decrease in the average size of the particles that remained in the supernatants in the range of  $0\text{--}0.5\text{ mM CaCl}_2$ , whereas beyond this point the inverse occurred.

The rationale for this is as follows.

According to the zeta potential, the supernatant particles with the most net negative charge are those of the control (Table 3), so that there is some electrostatic repulsion, although this is not enough to avoid formation of agglomerates due to the establishment of no electrostatic interactions such as hydrophobic, van der Waals, etc. The calcium ions that remained in supernatants (after the addition of increasing concentrations of  $\text{CaCl}_2$  to the AEWB) neutralized the negative charges to some degree but the net charge was still negative so that repulsion prevailed. Since the system would be more thermodynamically favorable because of the increase in entropy (Fiorucci & Zacharias, 2010), the agglomerates formed by non-electrostatic attractions were taken apart to allow a greater exposed surface and, consequently, the average particle size decreased slightly; this effect became more pronounced at a concentration of  $0.5\text{ M CaCl}_2$ . However, at 1.0 and  $1.5\text{ M CaCl}_2$ , the concentration of the remaining calcium ions was so high that the net charge became significantly less negative, as indicated by the zeta potential; in such conditions, the minor repulsion between particles allowed a closer proximity and the formation of cross linking with  $\text{Ca}^{2+}$ , resulting in agglomerates up to three times larger than the particles of the control.

The almost equal particle size of both supernatant and precipitate from control (Table 3), corroborates that the addition of  $\text{CaCl}_2$  triggered the agglomeration and that the pre-conditioning had a no significant effect on it. The diameter of particles was maintained constant in the range  $0.25\text{--}1.0\text{ M CaCl}_2$  and raised significantly at  $1.5\text{ M}$ , which could be due to the higher concentration of  $\text{Ca}^{2+}$  that favored the intermolecular interactions. These results are similar to those of Zhang et al. (2012), who evaluated the effect of the  $\text{CaCl}_2$  on the formation of nanoparticles from isolated soy protein; the authors found that the higher the concentration of  $\text{CaCl}_2$  the larger the particles and the precipitates, regardless the pH and protein concentration. Also Gülseren, Fang, and Corredig (2012) reported that increasing concentrations of the desolvation agent (ethanol in that study) resulted in increasing sizes of nanoparticles.

The decreasing z potential (less negative) in the present study corresponds well with this reasoning in the range  $0.25\text{--}1.0\text{ M CaCl}_2$ , but the abrupt rise at  $1.5\text{ M}$  (more negative) is not explained in these terms because at such concentration the number of remaining negative charges would be lower, so the z potential must

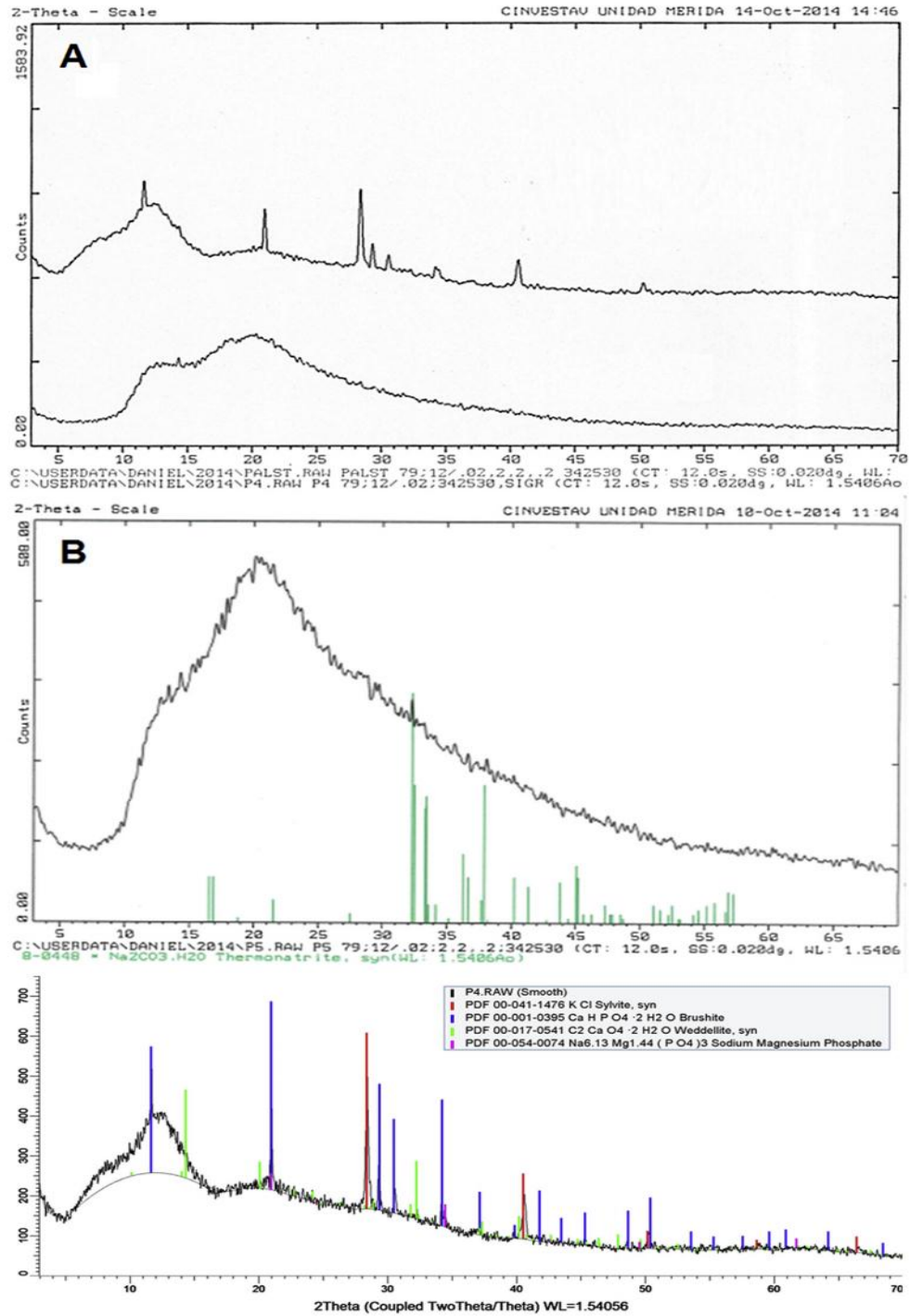


Fig. 5. X-ray diffraction pattern of (A) aqueous extract of wheat bran (AEWB); (B) treatment with 0.5 M CaCl<sub>2</sub>, (C) treatment with 1.5 M CaCl<sub>2</sub>.

be less negative. An unknown event took place at this concentration, which inhibited the  $\text{Ca}^{2+}$  to form interactions with proteins but resulted in large particles.

### 3.3.2. Morphology of the particles in the desolvated AEWB

Particles of the AEWB powder (Fig. 4A) and the control treatment (Fig. 4B) had a smooth surface. Because of this, the highest possible resolution was achieved at a 5,000 $\times$  magnification and it was not possible to see their internal structure. However, it is observed that the addition of  $\text{CaCl}_2$  had a noticeable effect on the microstructure, because even at the lowest concentration of 0.25 M, particles approximately spherical with diameters between 20 and 100 nm were formed; these are bound together or embedded in what appears to be a matrix (Fig. 4C). Something very similar is observed at the 0.5 M concentration but with a lower resolution at the same magnification (150,000 $\times$ ) (Fig. 4D). This blurring may be due to the bright produced by backscattered electrons of Ca and other minerals like P, K and Mg (Talbot & White, 2013) and indicates that these could form part of the nanostructures. Such effect was greater at 1.0 M, since the image with highest resolution was obtained at a magnification 3 times lower, i.e. 50,000 $\times$  (Fig. 4E). Here, agglomerates of particles are also observed, however the definition of these is not as clear as in 0.25 M besides prevailing the matrix phase.

At an even higher concentration of  $\text{CaCl}_2$ , 1.5 M, some structures in the micrographs were observed, which seem to be mineral crystals (Fig. 4F) and could indicate that at such concentration of salt the nucleation and crystal growth prevails over the assembly that leads to the nanoparticle formation. The X ray diffraction analysis showed that the AEWB was amorphous (Fig. 5A), whereas in the sample 0.5 M it was detected by indexation some  $\text{Na}_2\text{CO}_3 \cdot \text{H}_2\text{O}$  (Fig. 5B) which probably came from the reaction of the sodium present in the sample, with atmospheric  $\text{CO}_2$ . By the other hand, in the sample 1.5 M there were found crystal formations of sylvite (KCl), brushite  $\text{CaHPO}_4 \cdot 2\text{H}_2\text{O}$ , weddellite ( $\text{CaC}_2\text{O}_4 \cdot 2\text{H}_2\text{O}$ ), and sodium magnesium phosphate [ $\text{Na}_{6.13}\text{Mg}_{1.44}(\text{PO}_4)_3$ ] (Fig. 5C).

The crystal growth is a probably explanation for the abrupt decrease in the content of Mg, P, K and Ca at 1.5 M after the maximum reached at 1.0 M as well as for the corresponding more negative z potential at this concentration (Table 3). The rationale is that minerals were more available for crystal growth than for the establishment of the molecular interactions that leads to nanoparticle formation, resulting in a minor number of neutralized

negative charges on the protein surface and so in a more negative z potential. By the other hand, the increase in the particle size was surely due to the crystal formation rather than to agglomeration of the matrix that contains the nanoparticles. We consider this result very interesting because not only permits to establish the threshold of  $\text{CaCl}_2$  but shows the potential of the AEWB as scaffolds for the induced mineralization of a variety of minerals, a subject which we have already begun to investigate in the laboratory.

When a sample of the desolvated phase corresponding to the 0.25 M  $\text{CaCl}_2$  treatment was analyzed by STEM, spherical nanoparticles with diameter <100 nm were visualized, arranged in like pearl necklaces segments (Fig. 6). This is an evidence that the nanoparticles were imbibed in a polysaccharide matrix, since has been reported the effect of the ultrasound in the degradation of polysaccharides such as starch and chitosan (Czechowska-Biskup, Rokita, Lotfy, Ulanski, & Rosiak, 2005), as well as of glucuronarabinoxylans from WB (Hollmann, Elbegzaya, Pawelzik, & Lindhauer, 2009). Interactions between particles of different segments are observed, establishing more complex associations. This is interesting because it indicates the possibility of formation of three-dimensional networks. Because of the nanometer size of individual particles, such three-dimensional structures may be transparent, which is a desirable feature in the manufacturing of food products and/or pharmaceuticals.

## 4. Conclusions

Spherical nanoparticles with sizes between 20 and 100 nm were obtained by subjecting the aqueous extracts of wheat bran to desolvation with  $\text{CaCl}_2$ , through the adaptation of a cold gelation/desolvation process. The nanoparticles appeared embedded in a matrix, which was disturbed by ultrasound exposing thus individual nanoparticles; these were observed to form interactions leading to necklace like structures. At 1.5 M  $\text{CaCl}_2$ , the growth of several kinds of crystals prevailed over the nanoparticle formation.

## Acknowledgments

To Consejo Nacional de Ciencia y Tecnología (CONACYT), México, for financing the project CB2011-169839 and the scholarship for the doctoral studies of the author Luna-Valdez. It is acknowledged the participation of the staff of the different departments of CIAD. Thanks to the Laboratorio de Química de Materiales CINVESTAV-IPN Unidad Mérida Yucatán and the Laboratorio Nacional de Nano y Biomateriales (LANNBIO), projects FOMIX-YUCATAN 2008-108160 and CONACYT LAB-2009-01 N° 123913, specially to Dra. Patricia Quintana for allowing accessibility to LANNBIO and Dora Huerta-Quintana, Ana Ruth Cristobal Ramos and M.C. Daniel Aguilar Treviño from CINVESTAV, for their technical assistance in the STEM, SEM-EDX and X-ray diffraction analysis, respectively.

## References

- Anglani, C. (1998). Wheat minerals—a review. *Plant Foods for Human Nutrition*, 52(2), 177–186.
- Antoine, C., Peyron, S., Mabilhe, F., Lapiere, C., Bouchet, B., Abecassis, J., et al. (2003). Individual contribution of grain outer layers and their cell wall structure to the mechanical properties of wheat bran. *Journal of Agricultural and Food Chemistry*, 51, 2026–2033.
- AOAC. (1990). *Official methods of analysis of the AOAC* (Vol. 2). Arlington: Association of Official Analytical Chemists Inc.
- Arroyo-Maya, I. J., Hernández-Sánchez, H., Jiménez-Cruz, E., Camarillo-Cadena, M., & Hernández-Arana, A. (2014).  $\alpha$ -Lactalbumin nanoparticles prepared by desolvation and cross-linking: Structure and stability of the assembled protein. *Biophysical Chemistry*, 193–194, 27–34.
- Barth, A. (2007). Infrared spectroscopy of proteins. *Biochimica et Biophysica Acta*, 1767(9), 1073–1101.

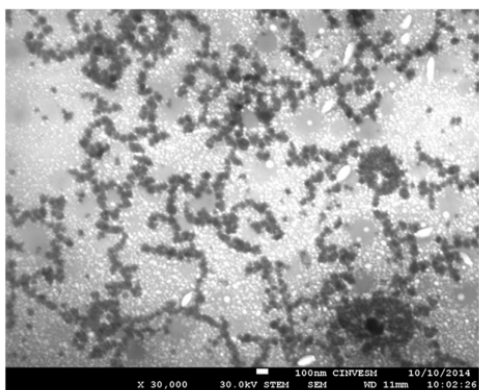


Fig. 6. STEM image of the aqueous extract of wheat bran (AEWB) subjected to cold gelation/desolvation with 0.25 M  $\text{CaCl}_2$ .



- Bradford, M. M. (1976). A rapid and sensitive method for the quantitation of microgram quantities of protein utilizing the principle of protein-dye binding. *Analytical Biochemistry*, 72, 248–254.
- Brier, N., Gomand, S. V., Donner, E., Paterson, D., Delcour, J. A., Lombi, E., et al. (2015). Distribution of minerals in wheat grains (*Triticum aestivum* L.) and in roller milling fractions affected by pearling. *Journal of Agricultural and Food Chemistry*, 63(4), 1276–1285.
- Brown, C. L., Aksay, I. A., Saville, D. A., & Hecht, M. H. (2010). Template-directed assembly of a *de novo* designed protein. *Journal of the American Chemical Society*, 124, 6846–6848.
- Campas-Ríos, M., Mercado-Ruiz, J., Valdéz-Covarrubias, M., Islas-Rubio, A., Mendoza-Wilson, A., & Balandrán-Quintana, R. (2012). Hydrolysates from wheat bran albumin as color-adding agents and inhibitors of apple polyphenol oxidase. *Journal of Food Biochemistry*, 36(4), 470–478.
- Chaquilla-Quilca, G., Balandrán-Quintana, R. R., Azamar-Barrios, J. A., Ramos-Clamont Montfort, G., Mendoza-Wilson, A. M., Mercado-Ruiz, J. N., et al. (2016). Synthesis of tubular nanostructures from wheat bran albumins during proteolysis with V8 protease in the presence of calcium ions. *Food Chemistry*, 200, 16–23.
- Czechowska-Biskup, R., Rokita, B., Lotfy, S., Ułanski, P., & Rosiak, J. M. (2005). Degradation of chitosan and starch by 360-kHz ultrasound. *Carbohydrate Polymers*, 60(2), 175–184.
- Donangelo, C. M., & Eggum, B. O. (1985). Comparative effects of wheat bran and barley husk on nutrient utilization in rats. I. Protein and energy. *British Journal of Nutrition*, 54(3), 741–751.
- Duclairoir, C., Orecchioni, A. M., Depraetere, P., Osterstock, F., & Nakache, E. (2003). Evaluation of gliadins nanoparticles as drug delivery systems: A study of three different drugs. *International Journal of Pharmaceutics*, 253(1–2), 133–144.
- Fiorucci, S., & Zacharias, M. (2010). Prediction of protein-protein interaction sites using electrostatic desolvation profiles. *Biophysical Journal*, 98(9), 1921–1930.
- Foegeding, E. A., & Davis, J. P. (2011). Food protein functionality: A comprehensive approach. *Food Hydrocolloids*, 25(8), 1853–1864.
- Gazulla, M. F., Rodrigo, M., Blasco, E., & Orduña, M. (2013). Nitrogen determination by SEM-EDS and elemental analysis. *X-Ray Spectrometry*, 42(5), 394–401.
- Grundas, S., & Wrigley, C. (2004). WHEAT/Ultrastructure of the grain, flour, and dough. In C. Wrigley, H. Corke, & C. Walker (Eds.), *Encyclopedia of grain science* (Vol. 3, pp. 391–400). New York: Academic Press.
- Gülseren, İ., Fang, Y., & Corredig, M. (2012). Whey protein nanoparticles prepared with desolvation with ethanol: Characterization, thermal stability and interfacial behavior. *Food Hydrocolloids*, 29(2), 258–264.
- Hollmann, J., Elbegzaya, N., Pawelzik, E., & Lindhauer, M. G. (2009). Isolation and characterization of glucuronarabinoxylans from wheat bran obtained by classical and ultrasound-assisted extraction methods. *Quality Assurance and Safety of Crops & Foods*, 1(4), 231–239.
- Hongsprabhas, P., & Barbut, S. (1997). Protein and salt effects on Ca<sup>2+</sup>-induced cold gelation of whey protein isolate. *Journal of Food Science*, 62(2), 382–385.
- Hurkman, W. J., & Tanaka, C. K. (2007). Extraction of wheat endosperm proteins for proteome analysis. *Journal of Chromatography B*, 849(1–2), 344–350.
- Idris, W. H., Babiker, E. E., & El. Tinay, A. H. (2003). Fractionation, solubility and functional properties of wheat bran proteins as influenced by pH and/or salt concentration. *Nahrung*, 47(6), 425–429.
- Jerkovic, A., Kriegl, A., Bradner, J., Atwell, B., Roberts, T., & Willows, R. (2010). Strategic distribution of protective proteins within bran layers of wheat protects the nutrient-rich endosperm. *Plant Physiology*, 152, 1459–1470.
- Jones, B., & Gersdorff, C. (1923). Proteins of wheat bran: I. Isolation and elementary analyses of a globulin, albumin; and prolamine. *Journal of Biological Chemistry*, 58(1), 117–131.
- Joye, I. J., Nelis, V. A., & McClements, D. J. (2015). Gliadin-based nanoparticles: Stabilization by post-production polysaccharide coating. *Food Hydrocolloids*, 43, 236–242.
- Ju, Z. Y., & Kilara, A. (1998). Effects of preheating on properties of aggregates and of cold-set gels of whey protein isolate. *Journal of Agricultural and Food Chemistry*, 46(9), 3604–3608.
- Khare, A. R., & Vasisht, N. (2014). Chapter 14-Nanoencapsulation in the food Industry: Technology of the future. In A. G. Gaonkar, N. Vasisht, A. R. Khare, & R. Sobel (Eds.), *Microencapsulation in the food industry* (pp. 151–155). San Diego: Academic Press.
- Kratz, F. (2014). A clinical update of using albumin as a drug vehicle — A commentary. *Journal of Controlled Release*, 190, 331–336.
- Lohcharoenkal, W., Wang, L., Chen, Y. C., & Rojanasakul, Y. (2014). Protein nanoparticles as drug delivery carriers for Cancer therapy. *BioMed Research International*, 2014, 12.
- Lott, J. N. A., & Spitzer, E. (1980). X-ray analysis studies of elements stored in protein body globoid crystals of *Triticum* grains. *Plant Physiology*, 66(3), 494–499.
- Maes, C., & Delcour, J. A. (2002). Structural characterisation of water-extractable and water-unextractable arabinoxylans in wheat bran. *Journal of Cereal Science*, 35, 315–326.
- Nelson, D., & Cox, M. (2008). *Lehninger principles of biochemistry* (5th ed.). NY: WH Freeman.
- Pace, C. N., Treviño, S., Prabhakaran, E., & Scholtz, J. M. (2004). Protein structure, stability and solubility in water and other solvents. *Philosophical Transactions of the Royal Society B: Biological Sciences*, 359(1448), 1225–1235.
- Robert, P., Marquis, M., Barron, C., Guillon, F., & Saulnier, L. (2005). FT-IR investigation of cell wall polysaccharides from cereal grains. Arabinoxylan infrared assignment. *Journal of Agricultural and Food Chemistry*, 53(18), 7014–7018.
- Rohiwal, S. S., Satvekar, R. K., Tiwari, A. P., Raut, A. V., Kumbhar, S. G., & Pawar, S. H. (2015). Investigating the influence of effective parameters on molecular characteristics of bovine serum albumin nanoparticles. *Applied Surface Science*, 334, 157–164.
- Sadeghi, S., Madadlou, A., & Yarmand, M. (2014). Microemulsification–cold gelation of whey proteins for nanoencapsulation of date palm pit extract. *Food Hydrocolloids*, 35, 590–596.
- Saulnier, L., Sado, P.-E., Branlard, G., Charmet, G., & Guillon, F. (2007). Wheat arabinoxylans: Exploiting variation in amount and composition to develop enhanced varieties. *Journal of Cereal Science*, 46, 261–281.
- Saunders, R. (1978). Wheat Bran: Composition and digestibility. In G. Spiller (Ed.), *Topics in dietary fiber research* (pp. 43–58). US: Springer.
- Sağlam, D., Venema, P., van der Linden, E., & de Vries, R. (2014). Design, properties, and applications of protein micro- and nanoparticles. *Current Opinion in Colloid & Interface Science*, 19(5), 428–437.
- Shewry, P. R., D'Ovidio, R., Lafiandra, D., Jenkins, J. A., Mills, E. N. C., & Békés, F. (2009). Wheat grain proteins. In K. Khan, & P. R. Shewry (Eds.), *Wheat: Chemistry and technology* (4th ed., pp. 223–298). St. Paul Minnesota: AACC International, Inc.
- Sweeting, L. M. (1998). Organic structural spectroscopy (Lambert, Joseph B.; Shurvell, Herbert F.; Lightner, David A.; Cooks, R. Graham). *Journal of Chemical Education*, 75(10), 1218.
- Talbot, M. J., & White, R. G. (2013). Cell surface and cell outline imaging in plant tissues using the backscattered electron detector in a variable pressure scanning electron microscope. *Plant Methods*, 9(40).
- Thakur, G., Prashanthi, K., & Thundat, T. (2013). Directed self-assembly of proteins into discrete radial patterns. *Scientific Reports*, 3, 1923.
- USDA. (2014). *National nutrient database for standard reference release 26* (Vol. 2014). Agricultural Research Service United States Department of Agriculture.
- Vázquez-Ortiz, F. A., Caire, G., Higuera-Ciapara, I., & Hernández, G. (1995). High performance liquid chromatographic determination of free amino acids in shrimp. *Journal of Liquid Chromatography*, 18(10), 2059–2068.
- Yedomon, B., Fessi, H., & Charcosset, C. (2013). Preparation of bovine serum albumin (BSA) nanoparticles by desolvation using a membrane contactor: A new tool for large scale production. *European Journal of Pharmaceutics and Biopharmaceutics*, 85(3, Part A), 398–405.
- Zhang, J., Liang, L., Tian, Z., Chen, L., & Subirade, M. (2012). Preparation and in vitro evaluation of calcium-induced soy protein isolate nanoparticles and their formation mechanism study. *Food Chemistry*, 133(2), 390–399.

## **ARTÍCULO 2**

### **Nanoparticle formation after mild thermal conditioning of proteins in a wheat bran extract fractioned by size exclusion chromatography**

J.G. Luna-Valdez, R.R. Balandrán-Quintana, J.A. Azamar-Barrios, G. Ramos-Clamont Montfort, A.M. Mendoza-Wilson, J.N. Mercado-Ruiz, T.J. Madera-Santana, A. Rascón-Chu, G. Guadalupe Chaquilla-Quilca

(2017)

Artículo en revision en:

Biomacromolecules

## **Nanoparticle Formation after mild thermal conditioning of proteins in a wheat bran extract fractionated by size exclusion chromatography**

### **Authors:**

Jesús G. Luna-Valdez<sup>a</sup>

René R. Balandrán-Quintana<sup>a\*</sup>

José A. Azamar-Barrios<sup>b</sup>

Gabriela Ramos-Clamont Montfort<sup>c</sup>

Ana M. Mendoza-Wilson<sup>a</sup>

Jorge N. Mercado-Ruiz<sup>a</sup>

Tomás J. Madera-Santana<sup>a</sup>

Agustín Rascón-Chu<sup>a</sup>

Guadalupe Chaquilla-Quilca<sup>d</sup>

<sup>a</sup>Centro de Investigación en Alimentación y Desarrollo, A.C. Coordinación de Tecnología de Alimentos de Origen Vegetal. Carretera a La Victoria km 0.6. 83304. Hermosillo, Sonora, México.

<sup>b</sup>Centro de Investigación y de Estudios Avanzados del IPN, Unidad Mérida. Departamento de Física aplicada. Carretera antigua a Progreso Km. 6. 97310. Mérida, Yucatán. México.

<sup>c</sup>Centro de Investigación en Alimentación y Desarrollo, A.C. Coordinación de Ciencia de Los Alimentos. Carretera a La Victoria km 0.6. 83304. Hermosillo, Sonora, México.

\*Corresponding author: René Renato Balandrán-Quintana. Centro de Investigación en Alimentación y Desarrollo, A.C. Coordinación de Tecnología de Alimentos de Origen Vegetal. Carretera a La Victoria km 0.6. 83304. Hermosillo, Sonora, México. Tel. +52 662 2892400x354. e-mail: [rbalandran@ciad.mx](mailto:rbalandran@ciad.mx)

## **ABSTRACT**

Spherical nanoparticles from protein-rich aqueous extracts of wheat bran have been previously obtained through adaptations to the cold gelation/desolvation method. Presumably, nanoparticles were formed by proteins, stabilized by calcium bridges and immersed into a matrix of polysaccharides, but it was not demonstrated. In the present work, cold gelation/desolvation experiments were performed with fractions resulting from the separation of the wheat bran extracts by size exclusion chromatography. Desolvated or undesolvated fractions were characterized by dispersive energy spectroscopy, scanning electron microscopy, SDS-PAGE electrophoresis and infrared spectroscopy. Nanoparticles of spherical shape with diameters between 190 and 250 nm were formed from a protein fraction whose relative molecular masses were between 20 and 43 kDa. The protein nature of the nanospheres was demonstrated, but new evidence suggests that calcium does not participate in their formation, but rather these are formed by effect of mild heat treatment before the addition of  $\text{CaCl}_2$ .

**Keywords:** nanostructures; cold gelation; preparative chromatography; cereal technology; protein nanotechnology.

## 1. INTRODUCTION

The development of protein nanoparticles is a growing field with applications in the pharmaceutical and food industries.<sup>1</sup> Proteins are GRAS (generally recognized as safe) substances and their functional properties of emulsion, foaming and gelling capacities, permit their incorporation into food and pharmaceuticals.<sup>2</sup> The chemical diversity of proteins favors a variety of molecular interactions such as hydrophobic, electrostatic, hydrogen bonding, van der Waals, steric repulsion and disulfide bridges. The latter govern protein conformation and aggregation but also drive the self-assembly to fabricate nanoparticles with uniform shape and size.<sup>3</sup>

Among the methods used to make protein nanoparticles are emulsification<sup>4</sup> and heat-induced gelation.<sup>5</sup> In the former, the protein is emulsified in oil by applying vigorous shearing force and the nanoparticles are formed at the oil/water interface. Surfactants are used to stabilize the emulsion and a cross-linker agent is added to control the size of the nanoparticles.<sup>6</sup> Heat-induced gelation is a multistep mechanism based on the disruption of the native structure of proteins when are exposed to temperatures higher than that necessary for denaturation<sup>7</sup>. In heat-induced gelation the gel structure is driven by polymerization of the denatured proteins, which leads to an increase in viscosity. As the aggregation process continues, it becomes necessary to apply mechanical shear force to limit the growth of large agglomerates.<sup>8</sup>

Another strategy to fabricate protein nanoparticles, not commonly employed, is the adaptation of the cold gelation/desolvation method.<sup>9</sup> In this process, a protein solution is heated at temperatures below that of denaturation, followed by cooling to room temperature and adjustment of pH to basicity. Finally, the protein solution is subjected to desolvation through addition of divalent ions, usually  $\text{Ca}^{2+}$ .<sup>10</sup> Heat treatment and basic

pH make proteins to expose their negatively charged groups, favoring formation of intra- and intermolecular  $\text{Ca}^{2+}$  bridges by electrostatic interactions. Thus, the repulsion forces between proteins are eliminated and subsequent aggregation occurs.<sup>2,11</sup> At a fixed pH value, particle size can be controlled via the concentration of  $\text{Ca}^{2+}$ .<sup>1</sup> The advantages of this method, compared to those of emulsification and heat-induced gelation, is that the use of organic solvents and shear forces are avoided.<sup>5,12</sup>

Most of the reports on obtaining protein nanoparticles by the heat-induced gelation, emulsification, and desolvation methods involve proteins derived from whey.<sup>13-14</sup> Few efforts have been directed to develop nanoparticles based on plant proteins, even though these are more affordable and acceptable to consumers. Among the few examples are the soy protein isolates,<sup>11,15</sup> wheat flour gluten,<sup>16-17</sup> zein<sup>18</sup> and wheat bran (WB) proteins.<sup>9</sup> In this context, spherical nanoparticles after cold gelation/desolvation of an aqueous extract of WB have been reported.<sup>9</sup> The nanospheres had diameters between 20 and 100 nm and were embedded within a matrix, so their composition and mechanism of formation were difficult to discern. Nanoparticle formation and stabilization was attributed to proteins and  $\text{Ca}^{2+}$ , respectively, but the complex nature of the WB extracts raises the question of whether other components were involved. In the present study, size exclusion chromatography (SEC) was used to purify the proteins of aqueous WB extracts. Then, cold gelation/desolvation assays were conducted with the SEC fractions to elucidate if proteins were involved in nanoparticle formation.

## **2. MATERIALS AND METHODS**

### **2.1. Materials**

The WB (*Triticum aestivum* L.) was purchased at a commercial mill in Hermosillo, Sonora, México. All chemicals, unless otherwise noted, were from Sigma-Aldrich (Sigma-Aldrich, St. Louis, MO, USA). Washing and extraction of WB, as well as reagent preparations, were performed with deionized water (18 M $\Omega$ ) obtained from a Milli-System (Bedford, MA, USA).

### **2.2. Aqueous extraction of WB**

Prior to aqueous extraction, WB was rapidly washed by immersion in cold water and then dried at 40 °C as previously described.<sup>19</sup> Aqueous extraction was performed according to the procedure reported in literature.<sup>9</sup> Briefly, WB was mixed with water (1:10 w/v) and extracted for 3 h at 4 °C. The extracts were filtered and the resulting filtrate was centrifuged for 20 min; supernatant was frozen at -40 °C and lyophilized (Labconco®, Kansas, MO, USA). The lyophilized powder was labeled as aqueous extract of WB (AEWB) and stored at -40 °C until subsequent treatments or analysis.

### **2.3. Size exclusion chromatography (SEC)**

#### ***2.3.1. Column preparation***

The AEWB was subject to further purification by SEC using a XK 16/70 preparative column, packed with 140 ml of Superdex 75 pg (GE Healthcare Bio-Sciences AB, Uppsala, Sweden). The column was equilibrated by passing 7.7 bed volumes of a buffer

prepared with 50 mM sodium phosphate plus 150 mM NaCl, pH 7.2. Flow rate was maintained at 8 ml/min, using a peristaltic pump FH 100 (Thermo Fisher Scientific Inc., Waltham, MA, USA). Column efficiency was tested according to instructions of the fabricant by eluting 0.7 ml of 1% acetone and collecting fractions of 0.75 ml; absorbance at 280 nm of each fraction was measured in a UV-Vis Cary 60 spectrophotometer (Agilent Technologies Inc, Headquarters, Santa Clara, CA, USA). By plotting  $Abs_{280\text{ nm}}$  vs. elution volume, a peak with a symmetric factor of 1.23 was obtained, which was within the range of optimal efficiency. The zero volume of the column ( $V_0$ ) was 42.75 ml and was determined with Dextran blue 2000 (GE Healthcare Biosciences AB, Uppsala, Sweden).

### ***2.3.2. Preparation and separation of the AEWB by SEC***

AEWB was dissolved (1:10 w/v ratio) in 50 mM sodium phosphate, 150 mM NaCl buffer, pH 7.2, sonicated for 15 min and centrifuged at 3,000xg for 5 min. The supernatant was vacuum filtered (0.45  $\mu\text{m}$ ). Then, soluble protein content of filtrate was estimated by the Bradford method (1976) and adjusted to 3 mg/ml by dilution with the phosphate buffer. Thus, the sample was ready to be injected into the column. The maximum sample volume to be injected in order to obtain the highest possible yield without compromising efficiency was 2.1 ml (1.5% of the column geometric volume). For injections, a 3 ml syringe was used, avoiding the formation of air bubbles.

A typical SEC run consisted in injecting the AEWB and eluting with 50 mM sodium phosphate, 150 mM NaCl buffer, pH 7.2, 1 ml/min elution rate. Volumes of 0.75 ml were collected and the absorbance of each one was measured at 280 nm in the Cary 60 spectrophotometer. Each peak obtained in the chromatogram of elution volume versus



$Abs_{280\text{ nm}}$ , was considered a SEC fraction. The relative molecular weight of each SEC fraction was calculated by using a standard curve constructed with proteins of known molecular weight (GE Healthcare Bio-Sciences AB, Uppsala, Sweden). Twenty highly reproducible SEC runs were performed and the eluates corresponding to each SEC fraction were collected, pooled out and labeled according to their elution order as pk-1...pk-n. The pooled SEC fractions were dialyzed in cellulose membranes (14 kDa MWCO) immersed in deionized water ( $18\text{ M}\Omega\text{ cm}^{-1}$ ) for 24 h with three exchanges. The dialysis process was done to eliminate salts from the buffer and was monitored by measuring electrical conductivity and pH. SEC fractions were lyophilized and stored at  $-40\text{ }^{\circ}\text{C}$  after taking a sample of each one for UV spectroscopy (section 2.6).

#### **2.4. Desolvation experiments with $\text{CaCl}_2$**

Lyophilized SEC fractions were individually dissolved in deionized water (4% w/v). Solutions were adjusted to pH 8.0 with 1 M NaOH and then centrifuged at  $5,000\times g$  for 5 min at  $4\text{ }^{\circ}\text{C}$ . Supernatants were recovered and their soluble protein content was estimated.<sup>20</sup> Subsequently, supernatants were heated for 3 h in a water bath at  $68.5\text{ }^{\circ}\text{C}$  and cooled under a stream of water to  $25\text{ }^{\circ}\text{C}$ . A volume of 0.25 ml of each solution was individually desolvated using the necessary volume of 0.25 M  $\text{CaCl}_2$  to reach a 0.00353 mmol  $\text{CaCl}_2/\text{mg}$  protein ratio (Table 1). When two phases (supernatant and precipitate) were formed after the addition of  $\text{CaCl}_2$ , these were best separated and recovered after centrifugation at  $5,000\times g$ . Then both were frozen out, lyophilized and stored at  $-40\text{ }^{\circ}\text{C}$  until further analysis. Control samples of each fraction with no addition of  $\text{CaCl}_2$  were also run. When precipitation occurred in some control fractions after the thermal

treatment, the supernatant was recovered by centrifugation at 3,000xg for 3 min, analyzed by SDS-PAGE as described in section 2.5 and subjected to desolvation.

## **2.5. Molecular mass profile (SDS-PAGE)**

Proteins from AEWB and SEC fractions were resolved in 12% SDS-PAGE polyacrylamide gel electrophoresis under reducing conditions.<sup>21</sup> Samples containing 15 µg of protein were loaded to gels in a Mini-Protean Tetra Cell (Bio Rad Laboratories Inc., Hercules, CA, USA) at constant voltage of 80 V and 14 mA. Gels were stained with Coomassie Brilliant Blue (G-250). Broad range markers (Bio Rad Laboratories Inc., Hercules, CA, USA) included myosin (200 kDa), β-galactosidase (116.2 kDa), phosphorylase *b* (97.4 kDa), bovine serum albumin (66.2 kDa), ovalbumin (45 kDa), carbonic anhydrase (31 kDa), trypsin inhibitor (21.5 kDa), lysozyme (14.4 kDa) and aprotinin (6.5 kDa). The protein migration patterns were compared with the broad range molecular weight standards from Bio-Rad and analyzed using the Image Lab program (Bio-Rad, Hercules, CA, USA) of the Molecular Imager Gel Doc XR+.

## **2.6. UV spectroscopy of SEC fractions and Fourier Transform Infrared Spectrometry (FTIR) of desolvated SEC fractions**

In order to assist in the identification of proteins and polysaccharides in SEC fractions and desolvated samples, UV spectroscopy and FTIR spectrometry were carried out. Before lyophilizing, samples of the SEC fractions were scanned in the UV spectral region in the Cary 60 spectrophotometer in order to identify characteristics absorbances.

Additionally, lyophilized precipitates and supernatants of desolvated samples were analyzed by FTIR. The latter was made with 50 mg of powder and data were collected in the range of 4,000–400  $\text{cm}^{-1}$  with a resolution of 2  $\text{cm}^{-1}$ ; each spectrum was the result of 32 scans. A Nicolet FT-IR iS50 spectrophotometer (Thermo Fisher Scientific Inc., Waltham, MA, USA) was used.

### **2.7. Elemental composition**

Elemental composition of desolvated SEC fractions was analyzed by X-ray dispersive energy spectroscopy (EDS).<sup>9</sup> Analysis was made in a JEOL JSM-7600F electron microscope (JEOL Ltd., Tokyo, Japan), equipped with a low-angle backscattered electron detector. Measurements were performed at 80 s with average scanned areas of 39,600  $\mu\text{m}^2$ . Data were reported as atomic %.

### **2.8. Morphology and particle size**

Morphology and particle size of lyophilized supernatants and precipitates of treatment and control samples were visualized by scanning electron microscopy (SEM). Each sample was placed on the sample holder and then coated with palladium-gold in a Q150R ES rotary pump ion-jet coater (Quorum Technologies Ltd., USA). SEM was performed on a JEOL JSM-7600F electron microscope (JEOL Ltd., Tokyo, Japan) at 2.0 kV.

### 3. RESULTS AND DISCUSSION

#### 3.1. Size exclusion chromatography

Six fractions were obtained from the SEC purification of AEWB (Figure 1A). Peaks on the chromatogram were identified according to their elution order as pk-1, pk-Int, pk-2, pk-3, pk-4 and pk-5. The soluble protein content of the lyophilized and reconstituted SEC fractions (4% w/v) ranged 0.04–12.6 mg/ml, with relative molecular masses 0.4–94 kDa as seen in Table 2. The pk-Int fraction (Figure 1A) was considered as an independent fraction because of the significant amounts of protein detected (4.78 mg/ml) in the reconstituted lyophilisate.

Absorbance at 280 nm in the SEC fractions could be due not only to proteins, which is more evident in fractions with low or no protein content, like pk-4 and pk-5 (Table 2). Phenolic acids, from which ferulic acid is the most abundant in WB, are found in the external layers<sup>22,23</sup> frequently esterified with hemicelluloses, mainly arabinoxylans.<sup>24</sup> To discriminate between protein and phenolic compounds, UV spectroscopy is used.<sup>25</sup> Typical shapes of esterified ferulic acid in the 320–340 nm region are seen in the pk-1 and pk-4 UV spectra (Figure 1B), whereas the single peak centered at 280 nm in the other SEC fractions is assigned to protein or free phenolic compounds; in absence of protein, the strong absorbance at 280 nm in pk-5 may be assigned to free ferulic acid.<sup>25</sup> It is worth to note that there could also be phenolic compounds in pk-3, besides proteins, since the more intense absorbance at 280 nm compared to that of pk-2 does not match its protein content (Table 2). Thus, according to literature reports, protein determination and UV spectral analysis, it is suggested that pk-Int and pk-2 are composed of protein, although the presence of carbohydrates is not ruled out; pk-1 and pk-4 are a mix of

esterified ferulic acid and protein; pk-3 is protein plus free phenolic compounds and pk-5 may be composed of free ferulic acid.<sup>25</sup>

### **3.2. Desolvation experiment with the SEC fractions**

Figure 2A shows the aspect of prepared SEC samples prior the thermal treatment; in all cases clear solutions were seen. Within the first 2 min of thermal conditioning (Figure 2B) both pk-2 and its control became white and gelatinous. This observation was interesting because the temperature was not enough to favor gelation in comparison to that reported for WB proteins<sup>26</sup> so it was considered worth to investigate it. To do this, the experiment was repeated with a fresh sample of pk-2 (control) and after the thermal treatment at 68.5 °C the formation of a white precipitate occurred again, which was separated from the supernatant by centrifuging at 3,000xg for 3 min and was identified as pk-2CP. The supernatant was identified as pk-2CS and a sample of it was taken and identified as pk-2CS (2) in order to be desolvated as the rest of the SEC fractions. Aliquots of both pk-2CP and pk-2CS were subjected to SDS-PAGE as described in section 2.5 and the remainders were lyophilized and characterized like the precipitates of all samples. The aspect of the rest of samples was unaltered by effect of the thermal treatment and it was maintained during the following 3 h in all cases, except pk-3 and its control, which presented a very small fraction of precipitate with the same color and consistency as pk-2.

After the addition of 0.25 M CaCl<sub>2</sub> two discernible phases were quickly detected in pk-2 and pk-3 (Figure 2C) but not in pk-1, pk-Int, pk-4 or pk-5. The pk-2CS (2) sample also formed two discernible phases after addition of CaCl<sub>2</sub> (not shown), which were

identified pk-2S2 and pk-2P2 (i.e. supernatant and precipitate) and were lyophilized and characterized like the rest of samples.

### 3.3. SDS-PAGE of AEWB and SEC fractions

A typical SDS-PAGE gel of AEWB and SEC fractions is shown in [Figure 3A](#). The molecular mass profile of AEWB was in the range 5–94 kDa, which matches well that obtained by SEC. The sum of the bands of pk-1, pk-Int, pk-2 and pk-3 equals that of the AEWB. No bands arose in pk-5 lane whereas two <14 kDa faint lines were observed in pk-4, which is in accordance with the results of protein analysis ([Table 2](#)). The most intense bands in pk-2 are between 20–30 kDa, while in pk-3 the most intense ones are between 6–11 kDa. By the other hand, pk-Int had a range of molecular masses between 5–78 kDa.

[Figure 3B](#) shows the SDS-PAGE gels of the pk-2 fraction, the supernatant pk-2CS and the precipitate pk-2CP. An extra lane was loaded with AEWB in order to show reproducibility in the mass profile. If comparing the intensity of bands in pk-2, pk-2CS and pk-2CP, it is evident that the precipitated proteins after the thermal treatment were those of 20–43 kDa, contained in pk-2, since bands lower than 21 kDa remained in the supernatant (pk-2CS).

### 3.4. FTIR

In [Figure S1](#) and [Figure S2](#) ([Supporting Information](#)), IR spectra of supernatants and precipitates after desolvation of pk-1, pk-Int, pk-2 and pk-3 are shown. Those of pk-4 and pk-5 are seen in [Figure S3](#). Spectra showed characteristic bands of proteins and polysaccharides in the 1700–1500 cm<sup>-1</sup> and 1200–800 cm<sup>-1</sup> regions, respectively,<sup>27,28</sup>

which supports that discussed in the UV spectral analysis (section 3.1). The band centered at  $1050\text{ cm}^{-1}$  and those around  $1165\text{ cm}^{-1}$  and  $895\text{ cm}^{-1}$  are assigned to C-OH bending, glycosidic linkages and  $\beta$ -(1 $\rightarrow$ 4) linkages, respectively, and are characteristic of arabinoxylans; it is not easy to distinguish ferulic acid from proteins by FTIR as both components absorb in the same region.<sup>28</sup> The most evident difference between IR spectra of supernatants and precipitates is the change in shape of the  $1050\text{ cm}^{-1}$  band and its shift to  $1017\text{ cm}^{-1}$ . The latter can be attributed to the formation of carbohydrate-protein complexes through intermolecular interactions or cross-linking through ferulic acid substituents, as it is reported.<sup>29</sup> All these components are present in the SEC fractions (section 3.1) so the addition of  $\text{Ca}^{+2}$  ions could have been resulted in carbohydrate-protein complexes through electrostatic interactions, which were reflected in shifts of the band assigned to polysaccharides.

### **3.5. Particle morphology and size**

In order to observe nanoparticle formation, lyophilized supernatants and precipitates of desolvated SEC fractions were analyzed. Figure 4 shows SEM micrographs of supernatants and precipitates of pk-1, pk-Int and pk-3 obtained after desolvation with calcium, as well as their non-solvated controls. The pk-1 control (Figure 4A) had a rough surface, that of supernatant was smooth (Figure 4B) and the precipitate presented a coralloid morphology (Figure 4C).

Morphologies of control, supernatant and precipitate of pk-Int (Figure 4D-F) and pk-3 (Figure 4G-I) showed a similar pattern to that of pk-1, excepting that spherical and ovoid shapes with sizes between 210 and 470 nm can be seen in the pk-3 control (Figure

4G). The formation of these nanostructures may be due to proteins of molecular mass between 20-31 kDa (Figure 3A). Proteins of the same mass are present in pk-2CP, which formed the nanoparticles obtained. The shape of these nanostructures may be due to the low concentration of these proteins<sup>30</sup> present in this fraction.

Figure 5 shows the particle morphology of supernatants and precipitates of pk-2, pk-2 control, and pk-2CS (2). The formation of rock-like particles with dimensions ranging 51–500 nm is observed in the supernatant of pk-2 (Figure 5A) whereas in the precipitate (Figure 5B) spherical structures with diameters ranging 190–250 nm are seen, besides some coral-like structures at the right of the image. In the precipitate of pk-2 control (pk-2CP) spherical structures (Figure 5D) identical to those in the pk-2 precipitate (Figure 5B) were formed, but not the coralloid structures observed at the right of Figure 5B. Since pk-2CP comes from a control sample it is suggested that the nanoparticles were formed prior the addition of CaCl<sub>2</sub> and that the thermal conditioning was responsible for their formation. The latter is corroborated with the images shown in Figure 5E and Figure 5F which correspond to the supernatant (pk-2S2) and precipitate (pk-2P2) of the pk-2CS (2) sample, respectively (section 3.2). It can be seen in the precipitate (Figure 5F) a coral-like morphology very similar to that of precipitates of all the evaluated fractions, excepting pk-2CP (Figure 5D). This confirms that added calcium is not involved in the formation of nanoparticles but rather in the precipitation of coralloid structures, which indeed could be crystals.<sup>9</sup>

### 3.6. Elemental composition of desolvated SEC fractions

The elemental composition of supernatants and precipitates of SEC fractions subject to desolvation with CaCl<sub>2</sub> are presented in Table S1, Table S2 and Table S3 (Supporting



Information). Because of the organic origin of the samples, C and O were the most abundant elements. The presence of N is due to the protein content.

The N content of pk-3 was higher than that of pk-1 or pk-Int in both, control, supernatant or precipitate (Table S1 of Supporting Information). This result does not agree with the lowest protein concentration in pk-3, according to the Bradford analysis (Table 2). However, since EDS is a surface-analyzing method, penetration of x-rays is of just a few nanometers<sup>31</sup> so it is suggested that proteins in pk-3 are in the surface and hence more exposed to x-rays than in pk-1 or pk-Int. It is also interesting that in pk-1, pk-Int or pk-3 the N content was not very different between their respective supernatants and precipitates, which suggest that proteins in these fractions are not involved in particle formation as was evident in Figure 4.

The absence of Ca in supernatants of pk-1, pk-Int and pk-3 (Table S1) confirms its involvement in the precipitates formed after desolvation in these fractions. Na and P are probably due in part to remainders of phosphate buffer used in the SEC separation, whereas P could also come from phytates present in the WB. The presence of S may correspond to amino acid residues such as cysteine, whereas Cl in supernatants and precipitates surely comes from CaCl<sub>2</sub> (the desolvation agent) since it was not detected in controls.

Elemental composition of supernatant and precipitate of pk-2 control after thermal treatment, as well as that of pk-2 and pk-2 (2) after desolvation, is shown in Table S2 (Supporting Information). Within a same sample it is observed that the highest N content was in the precipitate and the supernatant of the pk-2 control, in which the formation of spherical particles apparently free of coralloid structures was observed by SEM (Figure 5D). If comparing the composition of the precipitates from pk-2 control and pk-2, an

evident difference in Na, P, Cl and Ca contents is seen. That is, the nanoparticles in the pk-2 control precipitate are formed mainly by proteins, unlike those obtained in the precipitate of desolvated pk-2, where the presence of coralloid structures was observed in addition to nanoparticles (Figure 5B). A higher content of S is also seen, which supports the presence of protein. The absence of Ca in the precipitate of the control sample corroborates that Ca does not participate in the formation of nanoparticles. Meanwhile, the elemental composition of pk-2P2 shows a higher content of Na, P and Ca.

It is also observed in Table S2 that after desolvation and further precipitation protein is still dissolved in the supernatant of pk-2 as suggested by the N content. However, the latter is much higher in the pk-2 precipitate, which indicates that the nanoparticles seen by SEM in Figure 5B are largely made up of protein. The contents of P and Ca in pk-2 and pk-2 (2) precipitates indicate that the coral-like structures seen at the right of Figure 5B and those in Figure 5F could be a form of calcium phosphate precipitated by saturation of precursor ions once the addition of  $\text{CaCl}_2$ .

## CONCLUSIONS

Nanoparticles of spherical shape with sizes between 190 and 250 nm were obtained after thermal conditioning of a SEC fraction which contained proteins with molecular mass between 20–43 kDa estimated by SDS-PAGE. The evidence suggests that Ca did not participate in the formation of nanoparticles, because these were formed prior to the addition of  $\text{CaCl}_2$  by effect of the heat treatment. Further research is required to establish the mechanism by which the nanoparticles were formed.

## **SUPPORTING INFORMATION**

In supporting information file are the FTIR spectra of the desolvated SEC fractions as well tables describing their elemental composition.

## **ACKNOWLEDGMENTS**

To Consejo Nacional de Ciencia y Tecnología (CONACYT), Mexico, for financing the project CB2011-169839 and the scholarship for the doctoral studies of the author Luna-Valdez. It is acknowledged the support of the staff of the different departments of CIAD. Thanks to the Laboratorio de Química de Materiales CINVESTAV-IPN Unidad Mérida Yucatán and the Laboratorio Nacional de Nano y Biomateriales (LANNBIO), projects FOMIX-YUCATAN 2008-108160 and CONACYT LAB-2009-01 N° 123913. Special thanks to Dora Huerta-Quintana, Ana Ruth Cristobal Ramos and M.C. Daniel Aguilar Treviño from CINVESTAV-IPN Unidad Mérida, for their technical assistance in SEM and EDX analysis.

## REFERENCES

- (1) Sağlam, D.; Venema, P.; van der Linden, E.; de Vries, R. *Curr. Opin. Colloid Interface Sci.* **2014**, *19*, 428–437.
- (2) Bryant, C. M.; McClements, D. (1998). *Food Sci. Technol.* **1998**, *9*, 143–151.
- (3) Zhang, S. *Nat. Biotechnol.* **2003**, *21*, 1171–1178.
- (4) Arroyo-Maya, I.; Rodiles-López, O.; Cornejo-Mazón, M.; Gutiérrez-Lopez, F.; Hernández-Arana, A.; Barbosa-Cánovas, G. V.; Flores-Flores, J. O.; Hernández-Sánchez, H. *Am Dairy Sci Assoc* **2012**, *95*, 6204–6214.
- (5) Moakes, R. J. A.; Sullo, A.; Norton, I.T. *Food Hydrocolloids.* **2015**, *45*, 227–235.
- (6) Mishra, V.; Mahor, S.; Rawat, A.; Gupta, P. N.; Dubey, P.; Khatri, K.; Vyas, S. *P. J. Drug Target.* **2006**, *14*, 45–53.
- (7) Bauer, R.; Hansen, S.; Øgendal, L. *Int. Dairy J.* **1998**, *8*, 105–112.
- (8) Chung, C.; Degner, B.; McClements, D. J. *Food Res. Int.* **2014**, *56*, 136–145.
- (9) Luna-Valdez, J. G.; Balandrán-Quintana, R. R.; Azamar-Barrios, J. A.; Clamont-Montfort, G. R.; Mendoza-Wilson, A. M.; Mercado-Ruiz, J. N.; Madera-Santana, T. J.; Rascón-Chu, A.; Chaquilla-Quilca, G. (2017). *Food Hydrocolloids.* **2017**, *62*, 165–173.
- (10) Chen, L.; Subirade, M. *Biomacromolecules* **2009**, *10*, 3327–3334.
- (11) Zhang, J.; Liang, L.; Tian, Z.; Chen, L.; Subidare, M. *Food Chem.* **2012**, *133*, 390–399.
- (12) Arroyo-Maya, I. J.; Hernández-Sánchez, H.; Jiménez-Cruz, E.; Camarillo-Cadena, M.; Hernández-Arana, A. *Biophys. Chem.* **2014**, *193-194*, 27-34.

- (13) Lohcharoenkal, W.; Wang, L.; Chen, Y. C.; Rojanasakul, Y. *Biomed Res. Int.* **2014**, 1–12.
- (14) Weber, C.; Kreuter, J.; Lager, K. *Int. J. Pharmaceut.* **2000**, 196, 197–200.
- (15) Renkema, J. M. S.; Knabben, J. H. M.; van Vliet, T. *Food Hydrocolloids.* **2001**, 15, 407–414.
- (16) Duclairoir, C.; Orecchioni, A.-M.; Depraetere, P.; Osterstock, F.; Nakache, E. *Int. J. Pharm.* **2003**, 253, 133–144.
- (17) Joye, I. J.; Nelis, V. A.; McClements, D. J. *Food Hydrocolloids.* **2015**, 43, 236–242.
- (18) Gomez-Estaca, J.; Balaguer, M. P.; Gavara, R.; Hernandez-Munoz, P. *Food Hydrocolloids.* **2012**, 28, 82–91.
- (19) Campas-Ríos, M. J.; Mercado-Ruiz, J. N.; Valdéz-Covarrubias, M. A.; Islas-Rubio, A. R.; Mendoza-Wilson, A. M.; Balandrán-Quintana, R. R. *J. Food Biochem.* **2012**, 36, 470–478.
- (20) Bradford, M. M. *Anal. Biochem.* **1976**, 72:248–254.
- (21) Laemmli, U. K. *Nature* **1970**, 227:680–685.
- (22) Vaher, M.; Matso, K.; Levandi, T.; Helmja, K.; Kaljurand, M. *Procedia Chem* **2010**, 2, 76–82.
- (23) De Brier, N.; Gomand, S. V.; Donner, E.; Paterson, D.; Delcour, J. A.; Lombi, E.; Smolders, E. *J. Agr. Food Chem.* **2015**, 63, 1276–1285.
- (24) Saulnier, L.; Vigouroux, J.; Thibault, J. *Carbohydr. Res.* **1995**, 272, 241–53.
- (25) Hromádková, Z.; Paulsen, B. S.; Polovka, M.; Košťálová, Z.; Ebringerová A. *Carbohydr. Polym.* **2013**, 93, 22–30.
- (26) Idris, W. H.; Babiker, E. E.; El-Tinay, A. H. *Nahrung* **2003**, 47, 425–429.

Pelton, J. T.; McLean, L. R. *Anal. Biochem.* **2000**, *277*, 167–176.

(27) Robert, P.; Marquis, M.; Barron, C.; Guillon, F.; Saulnier, L. *J. Agr. Food Chem.* **2005**, *53*, 7014–7018.

(28) Lapierre, C.; Pollet, B.; Ralet, M. -C.; Saulnier, L. *Phytochemistry* **2001**, *57*, 765–772.

(29) Ge, J.; Lei, J.; Zare R. N. *Nano Lett.* **2011**, *11*, 2551–2554.

(30) Gazulla, M. F.; Rodrigo, M.; Blasco, E.; Orduña, M. *X-Ray Spectrom.* **2013**, *42*, 394–401.

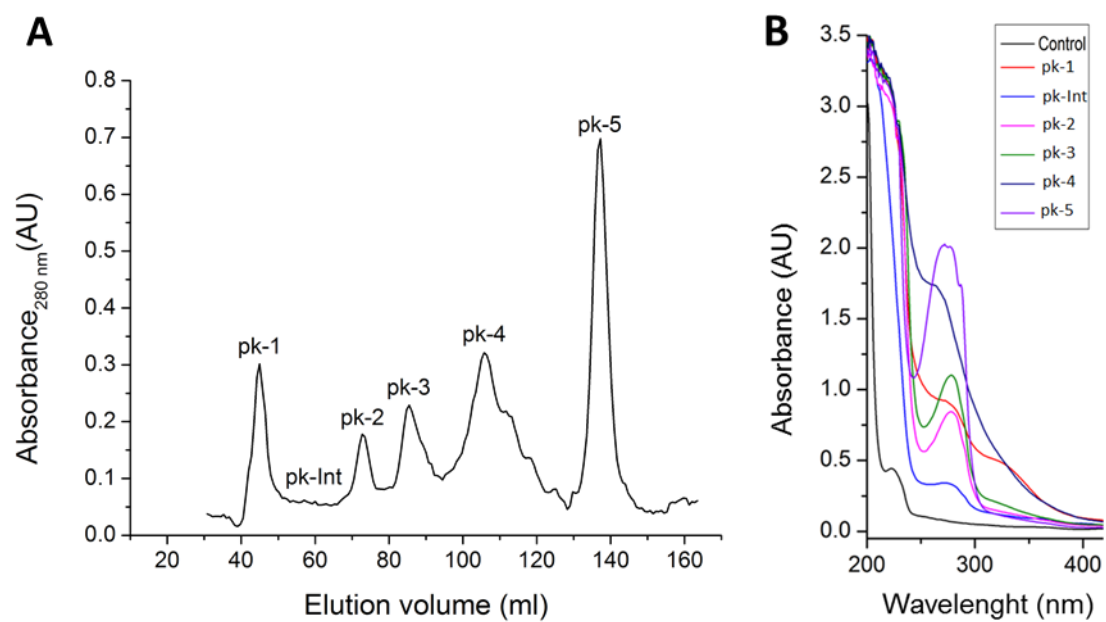


**Figure 1.** Size exclusion chromatography (SEC) of an aqueous extract of wheat bran (AEWB) through a column packed with Superdex 70. Protein load: 6.3 mg; flow-rate: 1 ml/min (A); UV spectra of each SEC fraction (B).

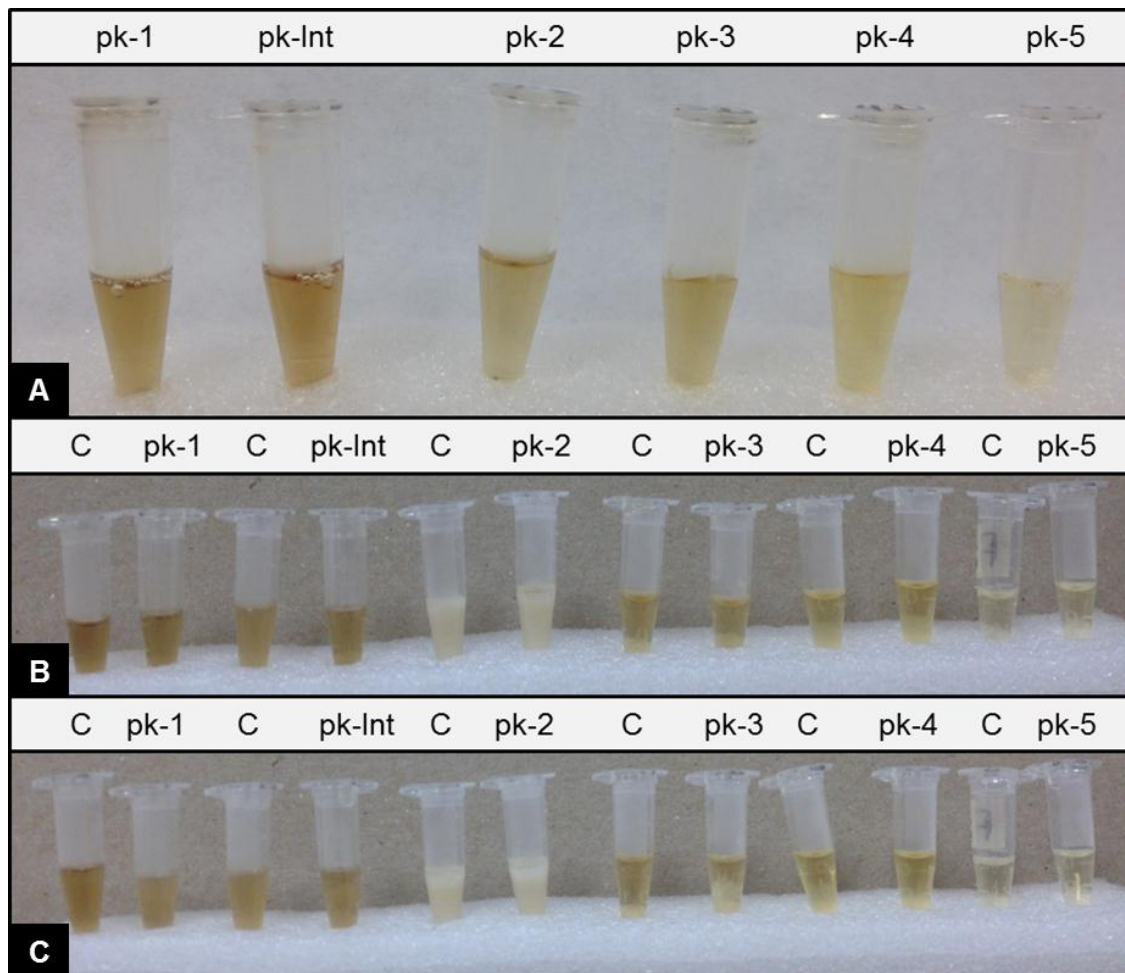


**Figure 2.** Images of the AEWB SEC fractions solutions and their respective controls. Before thermal treatment (A); after thermal treatment (B); after desolvation with  $\text{CaCl}_2$  (C).



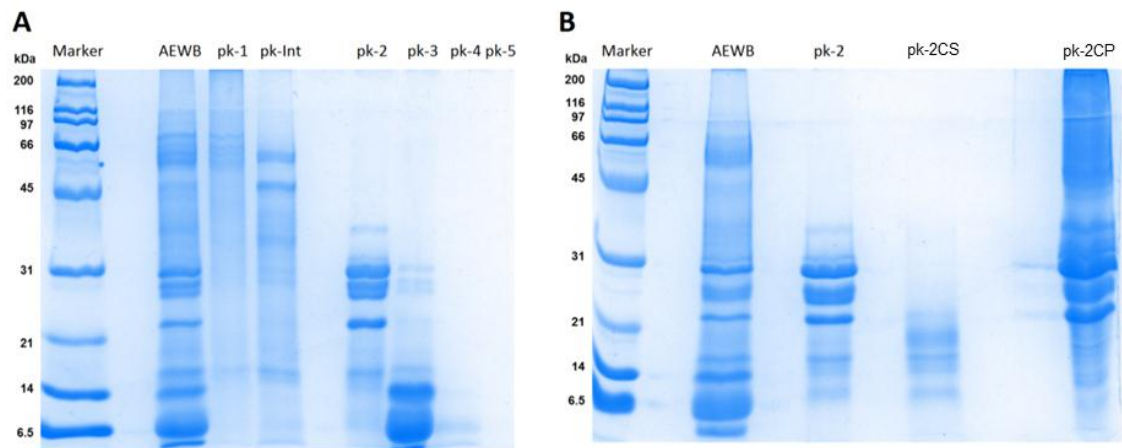


**Figure 3.** SDS-PAGE, under denaturing and reducing conditions of: AEWB and fractions (A); AEWB, pk-2 fraction, pk-2CS and pk-2CP (B).

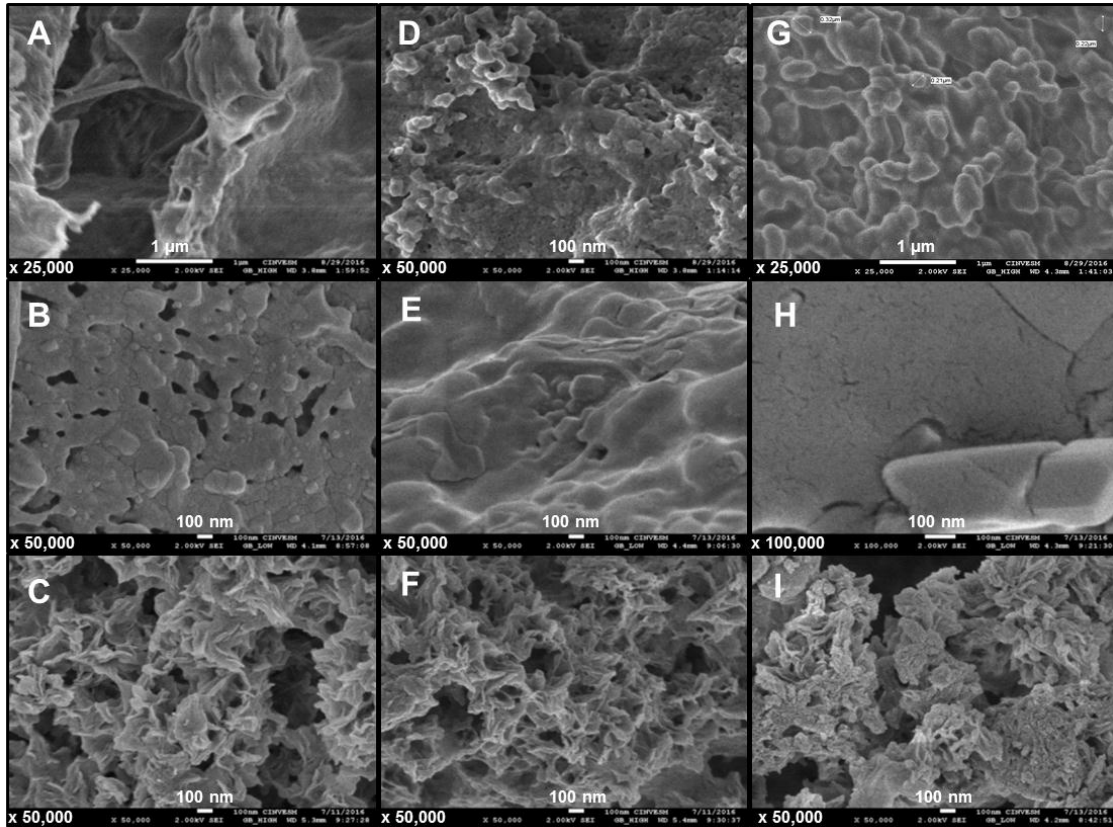


**Figure 4.** SEM images of the structures obtained after subjecting the pk-1, pk-Int and pk-3 SEC fractions of AEWB to desolvation with CaCl<sub>2</sub>. pk-1 [control (A), supernatant (B), precipitate (C)]; pk-Int [control (D), supernatant (E), precipitate (F)]; pk-3 [control (G), supernatant (H), precipitate (I)].

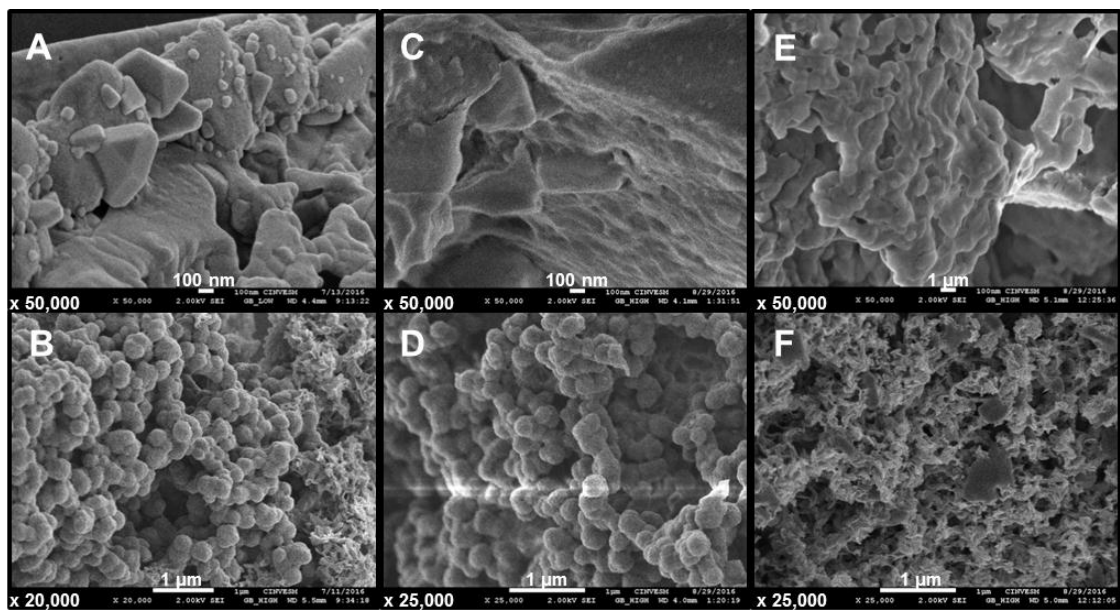


**Figure 5.** SEM images of the morphology of supernatants and precipitates after thermal conditioning and subjecting the p-k2 SEC fraction to desolvation with CaCl<sub>2</sub>. pk-2 desolvated with CaCl<sub>2</sub> (A-B); pk-2CS (C); pk-2CP (D); pk-2S2 and pk-2P2 (E-F).

**Table 1.** Protein to CaCl<sub>2</sub> ratios in each SEC fraction of AEWB subjected to desolvation.

SEC fraction and controls	Volume (ml)	Soluble protein (mg/ml)	CaCl <sub>2</sub> (mmoles)	mmol CaCl <sub>2</sub> /mg protein
pk-1 control	0.250	7.74	0	0
pk-1	0.250	7.74	0.00683	0.00353
pk-Int control	0.250	4.78	0	0
pk-Int	0.250	4.78	0.00422	0.00353
pk-2 control	0.250	7.08	0	0
pk-2	0.250	7.08	0.00625	0.00353
pk-3 control	0.250	3.54	0	0
pk-3	0.250	3.54	0.00312	0.00353

**Table 2.** Molecular weight distribution of the aqueous extract of wheat bran (AEWB), fractionated by size exclusion chromatography (SEC).

Peak label	Peak start (ml)	Peak end (ml)	Elution volume (ml)	Protein (mg/ml)	Relative molecular mass (kDa)
pk-1	41.25	49.5	45	7.74	117–73
pk-2	69.75	75.75	72.75	12.6	22–16
pk-Int	51	64.5	57.75	4.78	67-30
pk-3	82.5	90.75	85.5	3.54	11–7
pk-4	96.75	120	105.75	0.04	5-1
pk-5	129.75	144.75	137.25	nd <sup>a</sup>	<1

<sup>a</sup> nd = no detected

## Supporting information

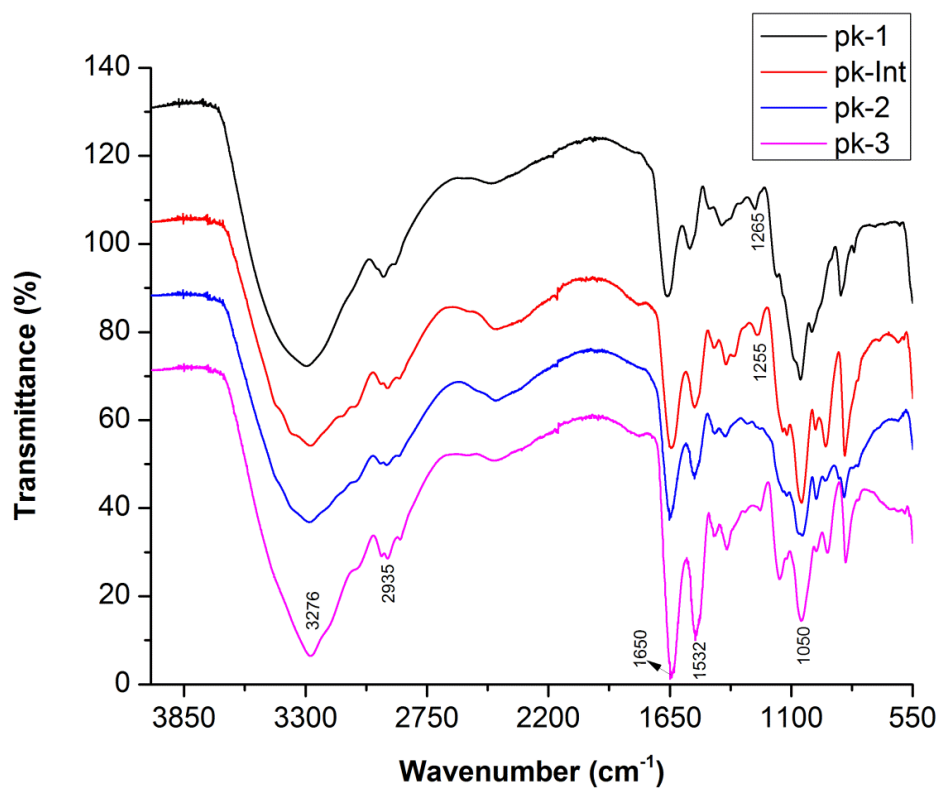


**Figure S1.** FTIR spectra of supernatants after cold gelation/desolvation of the AEWB SEC fractions with 0.25 M CaCl<sub>2</sub>.

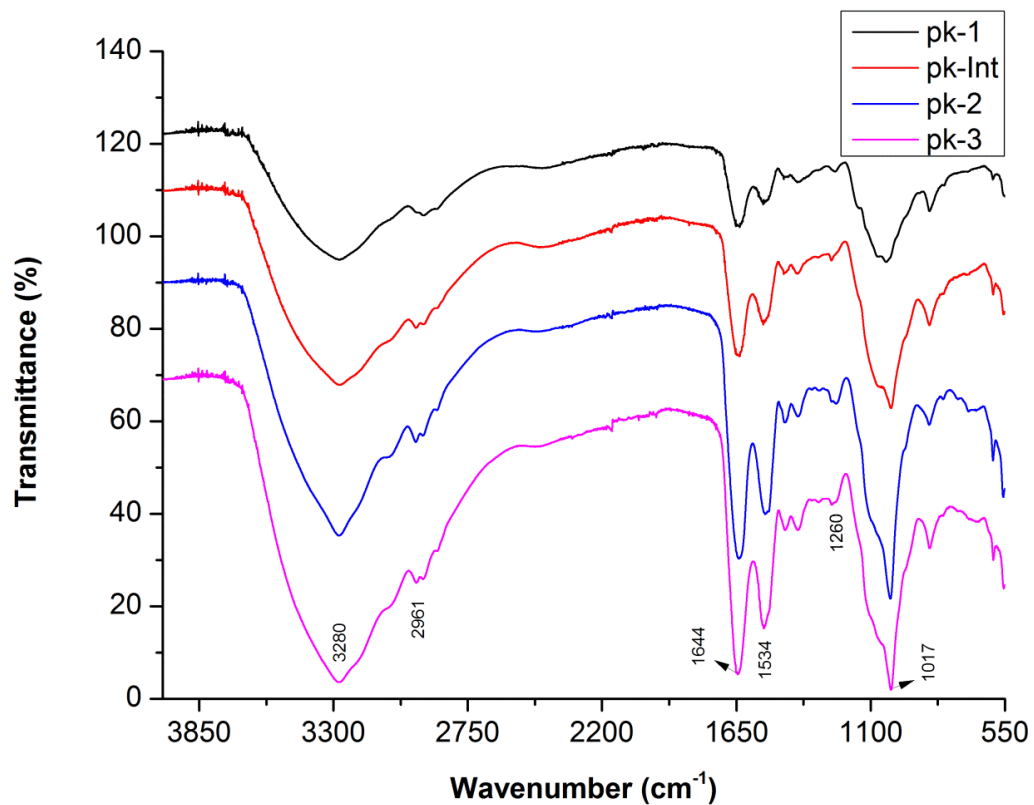


**Figure S2.** FTIR spectra of precipitates after cold gelation/desolvation of the AEWB SEC fractions with 0.25 M CaCl<sub>2</sub>.

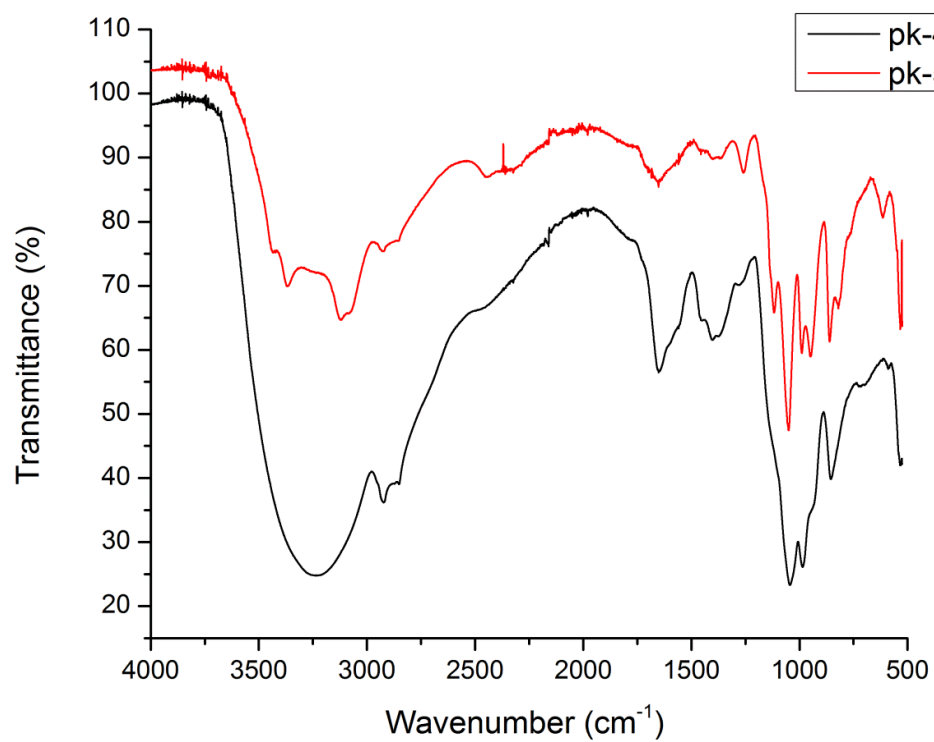


**Figure S3.** FTIR spectra of pk-4 and pk-5 SEC fractions after cold gelation/desolvation with 0.25 M CaCl<sub>2</sub>.



**Table S1.** Elemental composition (atomic %) of supernatants and precipitates of the SEC fractions pk-1, pk-Int, and pk-3 subject to desolvation with CaCl<sub>2</sub> after thermal conditioning.

Element	Controls <sup>a</sup>			Supernatants			Precipitates		
	pk-1	pk-Int	pk-3	pk-1	pk-Int	pk-3	pk-1	pk-Int	pk-3
<b>C</b>	58.4	50.1	53.2	44.9	55.8	51.6	67.0	38.2	43.3
<b>N</b>	5.6	11	19.5	4.23	7.1	10.9	1.2	5.3	10.8
<b>O</b>	32.2	31.0	23.8	39.6	29.4	30.0	16.2	41.9	35.8
<b>Na</b>	2.4	4.1	1.4	7.29	4.4	4.1	1.1	4.7	3.1
<b>P</b>	1.1	2.7	1.0	2.53	1.6	1.7	5.7	4.4	3.4
<b>S</b>	0.0	0.1	0.8	nd <sup>b</sup>	nd	0.3	Nd	nd	0.2
<b>Cl</b>	nd	nd	Nd	1.2	1.4	1.1	1.1	1.1	0.4
<b>Ca</b>	nd	0.5	0.1	nd	nd	nd	8.6	3.6	2.6

<sup>a</sup> pk-1, pk-Int, and pk-3 controls did not form two phases after thermal treatment

**Table S2.** Elemental composition (atomic %) of supernatants and precipitates of the pk-2 SEC fraction of AEWB and pk-2 (2) after desolvation with CaCl<sub>2</sub>.

Element	pk-2 control		pk-2		pk-2 (2) <sup>a</sup>	
	Supernatant	Precipitate	Supernatant	Precipitate	pk-2S2	pk-2P2
C	49.0	52.8	59.1	47.4	53.2	38.5
N	9.1	19.0	3.9	14.1	4.5	nd
O	33.4	25.5	28.6	27.0	30.9	41.4
Na	5.1	1.5	5.3	2.2	6.3	4.98
P	2.8	0.7	1.7	3.8	3.2	7.32
S	0.2	0.4	nd <sup>b</sup>	nd	nd	nd
Cl	nd	Nd	1.3	1.2	1.6	1.1
Ca	nd	nd	nd	3.9	nd	6.6

<sup>a</sup> pk-2 to which the precipitate formed after thermal treatment was removed (section 2.4)

<sup>b</sup> nd = no detected

**Table S3.** Elemental composition of pk-4 and pk-5 SEC fractions after preconditioning at 68.5 °C and desolvated or not (controls) with CaCl<sub>2</sub>.

Element	pk-4		pk-5	
	Control	Desolvated <sup>a</sup>	Control	Desolvated
C	44.51	40.81	21.38	27.73
N	1.4	3.02	nd <sup>b</sup>	nd
O	44.2	46.33	54.28	50.41
Na	5.89	5.92	15.3	16.25
Mg	0.37	0.45	nd	nd
P	3.55	3.27	9.04	8.6
S	nd <sup>b</sup>	0.1	nd	nd
Cl	nd	Nd	nd	nd
Ca	nd	0.1	nd	nd

<sup>a</sup> Two phases were no formed in pk-4 and pk-5 after adding CaCl<sub>2</sub> so the analysis was performed in the lyophilisate.

<sup>b</sup> nd = no detected

### ARTÍCULO 3

**FTIR analysis of thermally-induced nanoparticles from a fraction of water soluble wheat bran proteins, to elucidate the formation mechanism.**

J.G. Luna-Valdez, R.R. Balandrán-Quintana, J.A. Azamar-Barrios, G. Ramos-Clamont Montfort, A.M. Mendoza-Wilson, J.N. Mercado-Ruiz, T.J. Madera-Santana, A. Rascón-Chu, G.

(2017)

Artículo en revisión en:

Spectrochimica Acta Part A: Molecular and Biomolecular Spectroscopy

**FTIR analysis of thermally-induced nanoparticles from a fraction of water soluble wheat bran proteins, to elucidate the formation mechanism.**

**Authors:**

Luna-Valdez, J.G.<sup>a</sup>

Balandrán-Quintana, R.R.<sup>a\*</sup>

Azamar-Barrios, J.A.<sup>b</sup>

Ramos-Clamont Montfort, G.<sup>c</sup>

Mendoza-Wilson, A.M.<sup>a</sup>

Mercado-Ruiz, J.N.<sup>a</sup>

Madera-Santana, T.J.<sup>a</sup>

Rascón-Chu, A.<sup>a</sup>

<sup>a</sup>Centro de Investigación en Alimentación y Desarrollo, A.C. Coordinación de Tecnología de Alimentos de Origen Vegetal. Carretera a La Victoria km 0.6. 83304. Hermosillo, Sonora, México.

<sup>b</sup>Centro de Investigación y de Estudios Avanzados del IPN, Unidad Mérida. Departamento de Física aplicada. Carretera antigua a Progreso Km. 6. 97310. Mérida, Yucatán. México.

<sup>c</sup>Centro de Investigación en Alimentación y Desarrollo, A.C. Coordinación de Ciencias de Los Alimentos. Carretera a La Victoria km 0.6. 83304. Hermosillo, Sonora, México.

\*Corresponding author: René Renato Balandrán-Quintana. Centro de Investigación en Alimentación y Desarrollo, A.C. Coordinación de Tecnología de Alimentos de Origen Vegetal. Carretera a La Victoria km 0.6. 83304. Hermosillo, Sonora, México. Tel. +52 662 2892400x354. E-mail: [rbalandran@ciad.mx](mailto:rbalandran@ciad.mx)

## **ABSTRACT**

Thermal treatment of a protein-rich fraction of wheat bran resulted in the formation of 195–250 nm diameter spheres, which were the result of the aggregation of smaller nanospheres (30 nm). The elemental analysis revealed that the nanoparticles are formed by C, O, and N, whose elements constitute 97% while the S represented 0.45%. FTIR spectra confirmed the protein nature of nanoparticles and the second-derivative analysis of the Amide I band indicated that  $\beta$ -sheet structure of proteins was reduced from 46% to 20% after exposure to the thermal treatment, whereas that corresponding to  $\beta$ -sheet intermolecular aggregates increased from 5% to 38%. The overall analysis indicated that temperature made individual proteins to exposure both thiol groups and  $\beta$ -sheets, favoring intermolecular interactions through disulfide bridges and  $\beta$ -sheet aggregates which resulted in nanospheres. Further agglomeration of nanospheres is drive by non-specific intermolecular interactions. For first time is demonstrated that a brief thermal treatment of proteins leads to nanospheres formation.

## 1. INTRODUCTION

Protein nanoparticles (PNPs) are of great interest to industry. In processed foods PNPs can be used to improve nutritional value by encapsulating nutrients and bioactive compounds labile to process conditions or even to enhance sensorial characteristics (Foegeding & Davis, 2011; Saglam, Venema, de Vries, Sagis, & van der Linden, 2011), whereas in pharmaceutical industry have potential as drug carriers (Boulaiz et al., 2011). Because of their origin, the PNPs are biocompatible and biodegradable besides to have the advantage of binding to a large number of compounds in a relatively non-specific way (Yedomon, Fessi, & Charcosset, 2013). For example, in the manufacture of protein-rich beverages, one of the most recurrent problems is agglomeration, which arises from the heat treatment of foods rich in protein, which affects the texture, taste, and appearance of these products. It is for this reason that the use of microparticles has been proposed, with which better characteristics can be obtained. However, current knowledge about the undesirable aggregation of proteins by effect of temperature in concentrated systems of these macromolecules and the ways of control and prevention is very limited, which hinders the development of products with high protein concentration (Saglam, Venema, De Vries, Sagis, & van der Linden, 2011).

In this sense, the formation of spherical nanoparticles after cold gel/desolvation of aqueous extracts from wheat bran has been reported (Luna-Valdez et al., 2017). These extracts contain low molecular weight proteins (20-43 kDa) have been shown to have the ability to form nanoparticles without the need to use reagents for their preparation, only exposing it to a heat treatment for a very short time (Luna-Valdez et al., manuscript in revision). These nanoparticles, being of protein sources are biocompatible,

biodegradable and non-antigenic, even have the peculiarity of binding to a large number of compounds in a relatively non-specific way (Yedomon, Fessi, & Charcosset, 2013), characteristics that are required for be used in the areas mentioned above. In addition, they have the advantage that in these there is no possibility of toxic residues because no organic solvents are used or cross-linking for their elaboration, as in nanoparticles made with proteins already reported (Konan, Gurny, & Allémann, 2002; Langer et al., 2003; Gülseren, Fang, & Corredig, 2013; Yedomon, Fessi, & Charcosset, 2013), however the formation mechanism remained to be elucidated.

The formation of spherical nanoparticles after cold gel/desolvation of aqueous extracts from wheat bran has been reported (Luna-Valdez et al., 2017) and demonstrated their protein nature (Luna-Valdez et al., manuscript in revision), however the formation mechanism remained to be elucidated.

Because the secondary structure of proteins is determinant for the way in that they are self-assembled, a first approach to investigate the formation mechanisms of PNPs is studying the protein conformational changes in response to process conditions. Circular dichroism is the most used method for such a task, however the purity of proteins is fundamental to obtain reliable results so is not appropriate for complex systems, besides that proteins must be in solution, which excludes its use in the solid state (Kelly et al., 2005). Other available options are x-ray crystallography and nuclear magnetic resonance (NMR) spectroscopy, which are the most powerful techniques to analyze protein-protein interactions and to obtain a complete three-dimensional landscape. However, these techniques have several drawbacks. Crystallography studies require high quality monocrystals, which are not available for most proteins, besides the procedure is very slow. NMR spectroscopy has better flexibility but the interpretation of the NMR



spectrum of large proteins is very complex, so the technique is limited to small proteins (30 kDa) (Haris & Severcan, 1999; Haris, 2013).

Another method through which is possible to monitor subtle changes in the polypeptide backbone conformation is Fourier Transform Infrared Spectroscopy (FTIR). This tool is very sensitive to changes in hydrogen bonds, so it is useful to analyze modifications in the secondary structure of proteins caused by effect of temperature (van Stokkum et al., 1995; Natalello, Ami, Brocca, Lotti, & Doglia, 2005) or pH (Vicent, Steer & Levin, 1984). In fact FTIR is successfully used in protein stability and aggregation analyses (Carbonaro & Nucara, 2010; Miller, Bourassa, & Smith, 2013). Data on the secondary structure of proteins predicted by FTIR is in good agreement with that obtained by X-ray crystallography (Dong, Huang, & Caughey, 1990; Natalello, Ami, Brocca, Lotti, & Doglia, 2005; Kong & Yu, 2007).

FTIR is based on the vibrations of atoms in a molecule. The FTIR spectrum results from the absorption energy produced by the vibration of chemical bonds (stretching and bending movements). Such absorption arises from the transitions between the vibrational and rotational states of the molecule and is generated when the transition causes a change in the dipole moment (Barth, 2007). Characteristic groups of atoms give rise to vibrational bands centered at typical frequencies in the spectrum, regardless of the molecule in which they are found. Because these resonant frequencies are determined by the shape of the molecular potential energy surfaces, the atomic mass and the associated vibronic coupling, the technique can be used for the structural and chemical characterization of very complex mixtures (Carbonaro & Nucara, 2010).

For the quantitative estimation of different protein secondary structures ( $\alpha$ -helix,  $\beta$ -sheets,  $\beta$ -turns, random), the Amide I region ( $1700\text{--}1600\text{ cm}^{-1}$ ) of the FTIR spectrum is

subjected to deconvolution or second-derivative to identify the frequency peaks of its structural components. Then a multi-peak adjustment through a Gaussian or Lorentzian function is made and, finally, the relative amounts of different types of secondary structure are calculated from the areas of the plotted peaks (Dong et al., 1992; Carbonaro & Nucara, 2010).

FTIR spectroscopy has important advantages. The spectrum of almost any biological material can be obtained in a wide variety of environments, so is possible to analyze the structure of proteins either in solution (aqueous and non-aqueous), suspension (membranes and aggregates) or solid state (glass, thin films and powder), besides that a small amount of sample is required (10 µg) regardless of protein size (Haris & Severcan, 1999; van de Weert, Haris, Hennink, & Crommelin, 2001; Carbonaro & Nucara, 2010).

In the present work, FTIR spectroscopy was used in combination with scanning electron microscopy to investigate the formation mechanism of spherical particles that are formed after thermal treatment of a protein fraction of wheat bran obtained by size exclusion chromatography (SEC).

## **2. MATERIALS AND METHODS**

### **2.1. Materials and nanoparticle production**

Wheat bran extraction was performed according to Luna-Valdez et al. (2017) and the aqueous extracts were further fractionated by size exclusion chromatography (SEC). Nanoparticles were produced from an aqueous solution of the SEC fraction identified as that containing the wheat bran proteins involved in the formation of nanoparticles

reported by Luna-Valdez et al. (2017). Details on SEC and nanoparticle production methodologies are reported by Luna-Valdez et al. (manuscript in revision in the journal *Biomacromolecules*). Unless otherwise noted, all reagents were purchased from Sigma (Sigma-Aldrich, St. Louis, MO, USA).

## **2.2. Elemental composition**

The elemental composition of the nanostructures was quantified by energy dispersive X-ray spectroscopy (EDS) using a JEOL JSM-7600F electron microscope (JEOL Ltd., Tokyo, Japan) equipped with a low angle backscattered electron detector. Measurements were performed at 80 s and the average scanned areas were  $39,600 \mu\text{m}^2$  at each sample. The results were reported as atomic percentage.

## **2.3. Morphology and size**

Morphology and size of synthesized nanoparticles were visualized by scanning electron microscopy (SEM) in a JEOL JSM-7600F electron microscope (JEOL Ltd., Tokyo, Japan) at 2.0 kV. Samples were individually placed in the sample holder of the equipment and coated with palladium-gold in a Q150R ES rotary pump ion-jet coater (Quorum Technologies Ltd., USA). In addition, a portion of the powder nanoparticle (50 mg) was resuspended in 1 mL of water and sonicated for 5 min at 25 °C. Then 15  $\mu\text{L}$  of this suspension was taken out and placed on the sample holder where it was allowed to dry at room temperature (25 °C). Finally, the sample was analyzed by SEM under the conditions mentioned above.

## **2.4. Functional group analysis (FTIR)**

Functional group analysis of control sample and nanoparticles was performed using Fourier Transform Infrared Spectrometry (FTIR). FTIR absorption spectra in the 4000–400  $\text{cm}^{-1}$  range were collected in transmittance mode using a Thermo Nicolet Nexus 670 FTIR spectrometer (Thermo Nicolet Analytical Instruments, Madison, WI). Fifty mg of each sample were analyzed, collecting a total of 32 scans with a 2  $\text{cm}^{-1}$  resolution.

## **2.5. FTIR data analysis**

The 1700–1600  $\text{cm}^{-1}$  spectral region was selected for the Amide I analysis. Each spectrum was smoothed with an 11-point Savitzky-Golay smoothing function (Natalello, Ami, Brocca, Lotti, & Doglia, 2005; Liu et al., 2009). The overlapping of bands was enhanced using second-derivative calculation. The secondary structure composition was determined by second-derivative using the OMNIC software (Liu et al., 2009) whereas second-derivative inverted spectra were obtained multiplying by -1. Then the Gaussian functions of the OriginPro 8.6 (OriginLab Corp., MA, USA) software were used for multi-peak fitting. Initial band positions were taken directly from the second-derivative spectra and then were applied to calculate the area of each component representing a type of secondary structure. During the curve-fitting process, heights, widths and positions of all bands were varied simultaneously, with only the peak wavenumber as restriction (Dong et al., 1992; Murayama & Tomida, 2004).

### 3. RESULTS AND DISCUSSION

#### 3.1. Particle morphology and size

The protein nanoparticles obtained are shown in Figure 1A. The formation of spherical structures with diameters ranging between 190–250 nm is observed which agree as it was reported previously (Luna-Valdez et al., 2017). Upon suspending the powder in water and sonicate for 5 min, both size and morphology of the structures were maintained (Figure 1B) but the presence of smaller particles is also noted, which are better observed at higher magnification in Figure 1C. At an even greater magnification (Figure 1D) is observed that the smaller particles were in fact nanospheres with diameter  $\approx 30$  nm which are assembled to form the larger spheres. It is possible that the 190–250 nm spheres were joined by weak intermolecular interactions which were disrupted by ultrasound exposing thus the 30 nm nanospheres. Luna-Valdez et al. (2017) reported the effect of ultrasound on making visible spherical particles formed after cold gelation/desolvation of an aqueous extract of wheat bran.

Formation of aggregates by effect of temperature has been widely reported for proteins such as bovine serum albumin (BSA),  $\beta$ -lactoglobulin, ovalbumin and whey proteins isolates (Doi, 1993; Aymard, Gimel, Nicolai, & Durand, 1996; Ikeda & Morris, 2002; Veerman, Sagis & Linden, 2003; Bolder, Hendrickx, Sagis & Linden, 2006; Lovedey, Wang, Rao, Anema, Creamer & Singh, 2010; Oboroceanu, Wang, Brodkorb, Magner, & Auty, 2010; Lovedey, Su, Rao, Anema, & Singh, 2012).

The morphology of those aggregates consisted of fine strands with diameters less than 10 nm, which differs from the obtained in the present work, possibly due to the differences in process conditions since those experiments were run at pH 2, 80 °C with a thermal induction time of 1–20 h. In most studies protein solutions had an ionic strength in the 10–100 mM range, some using NaCl and/or CaCl<sub>2</sub>. Oboroceanu et al. (2010) and Bolder et al. (2006) did not use salts during the thermal incubation of proteins, but even so, fine strands aggregates were obtained. Loveday et al. (2010) and Borzova et al., (2016) reported the presence of a small number of spherical aggregates (15–25 nm) intercalated within the fine strands. Unlike Loveday et al. (2010), Borzova et al., (2016) dissolved the protein in phosphate buffer pH 7 and run the experiment at 65 °C, but in both studies the formation of spherical nanoparticles required a thermal incubation between 330 and 360 min, which is a very long time by comparison to the present work. It is worth to note that although thermal treatment was 180 min, only 2 min of exposure is enough to observe the presence of a white precipitate from which the nanoparticles are visualized (Luna-Valdez et al., manuscript in revision).

### **3.2. Determination of functional groups**

Figure 2A and 2B show the IR spectrum of control sample and nanoparticles obtained by heat treatment, respectively; in both spectra, characteristic bands of proteins (1700–1600 cm<sup>-1</sup>) and polysaccharides (1200–800 cm<sup>-1</sup>) are observed (Pelton & McLean, 2000). The Amide I absorption occurs in the 1600–1700 cm<sup>-1</sup> region and arises mainly from the C=O stretching vibration of the peptide group (Haris & Severcan, 1999). The peak at

1600–1500  $\text{cm}^{-1}$  is assigned to Amide II, which corresponds primarily to N-H bending with a contribution from C-N stretching vibrations. In addition, one band very weak in the region 1200-1300  $\text{cm}^{-1}$  is assigned to Amide III, which is due to a complex mix of N-H bending and C-H stretching along with deformation vibrations of C-H and N-H (Haris & Severcan, 1999; Barth, 2007). The broad band in the 3000–3600  $\text{cm}^{-1}$  region is assigned to the O-H stretching bonds groups (Elisa, Puhl, Kadla, & Khan, 2006) and the C-H stretch bonds appear around 2900  $\text{cm}^{-1}$  (Maréchal, 2003).

When analyzing the region 1200–800  $\text{cm}^{-1}$  a maximum absorption band centered at 1050  $\text{cm}^{-1}$  was found, which might be assigned to the characteristic C-OH bending of arabinoxylans, in addition to two bands at 988 and 946  $\text{cm}^{-1}$  that are related to the degree of substitution of arabinoxylans (Robert, Marquis, Barron, Guillon, & Saulnier, 2005).

In the nanoparticles spectrum (Figure 2B) a greater intensity and definition of the Amide I, II and III bands was observed in comparison to the control sample. It is also observed a decrease in the intensity of bands in the region 1200–800  $\text{cm}^{-1}$ , suggesting a lower presence of carbohydrates in the nanoparticles. In addition, in this same spectra at 560  $\text{cm}^{-1}$ , a new band was observed, which can be assigned to S-S stretching (Sadeghi et al., 2014). At the same time a decrease in intensity of the band assigned to S-H stretching (2600-2520  $\text{cm}^{-1}$ ) of cysteine residues (Fabian & Mäntele, 2002) was observed, suggesting the formation of disulfide bonds in the nanoparticles.

The possibility of an overlap between the Amide bands I and II can be ruled out since they are well defined and intense. Water vapor bands, which are easily identified as very thin bands at 1600 and 3700  $\text{cm}^{-1}$ , are not seen in this spectrum (Maréchal, 2003). In addition, sodium phosphate buffer was used as solvent for protein separation before

making nanoparticles, which is one of the accepted salts when analysis in the infrared spectrum is going to be performed, since does not contain carboxylic acid groups overlapping those of the main chain of proteins (Fabian & Vogel, 2002).

### **3.3. Second-derivate and estimation of protein secondary structure**

Analysis of Amide I band allows detecting small conformational changes in the structure of proteins. However, the IR bands corresponding to each conformation are very close to each other so that they overlap. To solve individual components of each conformation, the second-derivative method was used, which is one of the two most popularly employed for secondary structure analysis (Kong & Yu, 2007); it is more sensitive than deconvolution (Carbonaro & Nucara, 2010).

Figure 3 shows the second-derivative spectra of the 1700–1600  $\text{cm}^{-1}$  region of both control and nanoparticles. In the second-derivative of control (Figure 3A), 10 bands were observed. Bands appearing in the 1680–1668  $\text{cm}^{-1}$  region can be assigned to  $\beta$ -turn conformations, while the bands at 1659  $\text{cm}^{-1}$  and 1646  $\text{cm}^{-1}$  can be attributed to  $\alpha$ -helix and random structures, respectively. The components at 1691  $\text{cm}^{-1}$ , 1638  $\text{cm}^{-1}$  and 1628  $\text{cm}^{-1}$  can be assigned to  $\beta$ -sheet structures. The band of low intensity at 1620  $\text{cm}^{-1}$  can instead be assigned to aggregates (Dong, Caughey, Caughey, Bhat & Coe, 1999; Dong, Huang, & Caughey, 1992).

In the second-derivative spectrum of nanoparticles (Figure 3B), a decrease in the intensity of peaks in the 1690–1670  $\text{cm}^{-1}$  region, which correspond to  $\beta$ -turn conformations, was observed. One band at 1664  $\text{cm}^{-1}$  (not seen in the control) is also



observed, which is assigned to  $3_{10}$ -helix structures. The bands at  $1657\text{ cm}^{-1}$  and  $1647\text{ cm}^{-1}$  are assigned to  $\alpha$ -helical and random conformations, respectively, whereas the bands at  $1695\text{ cm}^{-1}$  and  $1633\text{ cm}^{-1}$  are assigned to  $\beta$ -sheet structures. In addition, a band of great amplitude and intensity at  $1619\text{ cm}^{-1}$  is assigned to intermolecular  $\beta$ -sheets aggregates (Dong, Huang, & Caughey, 1992; Dong, Caughey, Caughey, Bhat, & Coe, 1999).

Quantitative information on the secondary structure of proteins in both the control and nanoparticles was obtained through a curve fitting analysis of the Amide I band and performed as a linear combination of the components identified in the second derivative spectrum. It is assumed that the sums of the areas of conformations of the Amide I band are related to the total of a given protein (Byler & Susi, 1986; Kong & Yu, 2007). Figure 4 and Figure 5 show the decomposition of the Amide I band of control and nanoparticles, respectively, in Gaussian components. The results show that the secondary structure of proteins in control is dominated by  $\beta$ -sheet conformations, representing 46%. In addition, 18%  $\beta$ -turn, 14%  $\alpha$ -helix, 16% random and 5% aggregates, was calculated.

Figure 5 shows that proteins underwent a change in their structure after being heated since the percentage of  $\beta$ -sheet conformation decreased up to 21%. This result is in good agreement with that obtained by Natalello *et al.* (2005), who reported a 50% decrease in  $\beta$ -sheet conformations after subjecting the *Candida rugosa lipase* protein to  $64\text{ }^{\circ}\text{C}$ , besides a simultaneous decrease in  $\alpha$ -helix conformations. Unlike them, in the present work, the  $\alpha$ -helix remained constant

Meanwhile, the  $\beta$ -turn conformations accounted for 11%, which means a decrease in that structure compared to the control proteins. By the other hand, the random conformations remained unchanged. Also, the loss of  $\beta$ -sheets was accompanied by a band of great amplitude and intensity at  $1619\text{ cm}^{-1}$ , which is represented by 38% and is due to the formation of aggregates by intermolecular  $\beta$ -sheets of proteins induced by the heat treatment (Haris & Severcan 1999; Seshadri, Khurana, & Fink, 1999; Yan, Wang, He, & Zhou, 2004; Natalello, Ami, Brocca, Lotti, & Doglia, 2005).

The formation of aggregates by intermolecular  $\beta$ -sheets may be due to the experiment was performed at pH 8. That is, when a  $\text{pH} > \text{pI}$  of the proteins is used, aggregation proceeds through the formation of relatively small ordered aggregates (oligomers) that are characterized by a sizeable amount of intermolecular  $\beta$ -sheets, as revealed by FTIR spectroscopy for the BSA (Militello et al., 2004).

It must be considered that the results obtained on the conformational changes of the proteins can not only be due to the effect of the temperature but also to the loss of the hydration layer after the lyophilization process. That is, during this process dehydration-induced alterations in the absorption characteristics of the amide bond can be produced. Even the predicted values may not only be related to changes in secondary structure but also to the absence or presence of protein-protein contacts and changes in hydrogen-bonding characteristic. However, this does not exclude the use of FTIR to determine the effect of lyophilization on protein stability (van de Weert, Haris, Hennink & Crommelin, 2001). In addition, the presence of carbohydrates in nanoparticles (Figure 2) might protect dried proteins because these solutes bind to the dried protein, thus serving as a water substitute, when the hydration shell of the protein is removed (Carpenter & Crowe, 1988; Carpenter & Crowe, 1989)

However, the possible changes that could have been generated in the structure of proteins by the effect of lyophilization should have been minimal, since the morphology of the nanoparticles was not apparently affected, as can be observed when comparing Figure 1A and Figure 1B, which correspond to lyophilized nanoparticles and to nanoparticles that were resuspended in water and further sonicated, respectively (section 2.4).

Several investigation suggests that heating proteins above their denaturation temperature results is aggregation, because temperature causes a molecular unfolding that favors protein-protein intermolecular interactions, such as dipole and electrostatic as well as thiol/disulfide exchanges (Mulvihill & Donovan, 1987; Mulvihill, Rector, & Kinsella, 1991; Anker, Standing, & Hermansson, 1999). These interactions favor the aggregation of proteins as long as conditions of pH and temperature as well as the salt and protein concentration are controlled. In the salt absence, the unfolded proteins can remain separated due to the strong electrostatic repulsion, however as the salt concentration increases the electrostatic repulsion between the charged molecules decreases. At low salt levels, most of the surface of the protein molecules is unable to form bonds with other proteins due to residual electrostatic repulsion between them. However, some interactions may occur between non-polar regions of the protein whereas other domains can be involved in hydrophobic interactions. It is suggested that these interactions form filament structures, arguing that they bind at fixed sites at opposite ends of the molecule (Doi, 1993). In this regard, whey proteins and  $\beta$ -lactoglobulin have been reported to form gels with different structures, depending on the type and amount of salt present during thermally induced gelation. That is, a fine stranded matrix is formed when protein suspensions contain monovalent cation ( $\text{Li}^+$ ,  $\text{K}^+$ ,  $\text{Rb}^+$ ,  $\text{Cs}^+$ ) chlorides, sodium sulfate or

sodium phosphate at ionic strengths  $\leq 0.1$  M (Foegeding, Bowland & Hardin, 1995). These morphologies have been reported by other authors (Aymard, Gimel, Nicolai, & Durand, 1996; Ikeda & Morris, 2002; Veerman, Sagis & Linden, 2003; Lovedey, Wang, Rao, Anema, Creamer & Singh, 2010; Lovedey, Su, Rao, Anema, & Singh, 2012). In our case, the possibility of formation of this type of structures is unlikely, since the proteins used for the experiments were previously dialyzed.

In cases where the salt concentration in the protein solution is high, electrostatic repulsion between proteins is minimal, so they can form bonds at any point on their surface. This leads to the formation of large spherical aggregates (Kitabatake & Doi, 1993). For example, when ionic strength is greater than 0.1 M, the resulting matrix is composed of fine strands and spherical aggregates (Foegeding, Bowland & Hardin, 1995; Borzova, Markossian, Chebotareva, & Kleymenov, 2016). This possibility can also be ruled out, due to the low presence of salts in the nanoparticles formed (Table 1).

Nevertheless, there is also the possibility that the nanoparticles have been produced by disulfide bonds due to the appearance of a broad band at  $560\text{ cm}^{-1}$  in the infrared spectrum of nanoparticles, which display the formation of disulfide bonds (Sadeghi et al., 2014). To support this, the proteins (20-43 kDa) that were involved in the formation of nanoparticles are rich in cysteine, amino acid that can form these types of bonds between neighboring residues (Doi, 1993). These proteins (wheat bran albumin) have been previously identified by mass spectrometry by Chaquilla-Quilca et al. (2017) using the method reported by Huerta-Ocampo et al. (2014).

During the thermal aggregation process, the proteins undergo a partial unfolding of their native structure, which generates changes in the three-dimensional structure by disruption of hydrogen bonds and non-polar hydrophobic groups, this causes that

hydrophobic groups and free-SH groups became more exposed and could form intermolecular disulfide bond and hydrophobic interactions among the unfolded protein chains, resulting in the formation of aggregates (Shimada et al., 1989; Vetri, Librizzi, Leone, & Militello, 2007). It is known that the intermolecular disulfide bonds are dependent on both pH and temperature, so is possible that the formation of aggregates has been through this route since the experiment was run at pH 8 and 68.5 °C. Under these conditions, the propensity of proteins to undergo irreversible thermal denaturation increases as does the degree of thiol oxidation and subsequent polymerization (Monahan, German, & Kinsella, 1995). In that sense, Hoffmann et al. (1994) reported that  $\beta$ -lactoglobulin, dispersed in water at neutral pH and heated at 65 °C, formed aggregates by intermolecular disulfide cross-linking, noting that non-covalent interactions may be involved but only to a lesser extent. Similar results have been reported by other groups (Petruccelli, & Añón, 1995; Aymard, Gimel, Nicolai, & Durand, 1996; Bauer, Carrotta, Rischel, & Ogendal, 2000).

It is likely that the aggregation of the nanostructures obtained in the present work obeys to the two-step mechanism proposed by Aymard et al. (1996) for the thermal aggregation of  $\beta$ -lactoglobulin at pH 7. Such mechanism consists in the formation of aggregates of small particles (globules) by disulfide interchange, which arises from denatured monomers that are consequently associated in dimers, whose size does not seem to depend on the initial protein concentration, temperature, and ionic strength, under the range of conditions tested (step 1). In the second step, the globules are added to form fractal structures. Ikeda et al. (2002) also agreed on a two-step aggregation mechanism, reporting the formation of thermally induced aggregates (fine-strands) at pH

2 of  $\beta$ -lactoglobulin and whey protein isolates. While at pH 7, aggregates were composed of ellipsoidal particles.

By the other hand, Oboroceanu et al. (2010) reported the fibrillary aggregation of  $\beta$ -lactoglobulin at pH 2, concluding that the formation mechanism also consisted of two steps, but unlike Aymar et al. (1996) they concluded that  $\beta$ -lactoglobulin fibrils consist of polypeptide fragments bound by non-covalent intermolecular bonds and that are not formed from intact monomers. Recently, Borzova et al. (2016) also reported BSA, pH 7, formed aggregates by heat treatment, noting that protein unfolding resulted in the formation of two non-native protein forms with a different propensity to aggregation. The formation of primary aggregates occurred in a highly reactive unfolded form, while the secondary aggregates were formed by the unfolded forms of low reactivity. The hydrodynamic radius of the secondary aggregates was higher.

Based on the above mentioned and the morphology of the nanoparticles obtained in this work, it is possible to consider that the nanostructures were formed by a mechanism similar to the two-step aggregation mechanism. This mechanism coincides with that observed in SEM (Figure 1D), because apparently the spheres are formed by smaller aggregates (30 nm diameter), which could have been formed by disulfide bonds (globules) and in turn, these form aggregates of greater size by physical interactions such as van der Waals forces, hydrogen bonding, and hydrophobic or electrostatic interactions (Le Bon, Nicolai, & Durand, 1999). The presence of nanostructures of 30 nm after resuspending the nanoparticles in water and sonicated for 5 min, makes us to think that the aggregate-aggregate interactions effectively correspond to physical interactions, since a part of these were disaggregated from the larger nanoparticles by effect of ultrasound, which are observed in the surroundings of these (Figures 1B, and

1C), unlike nanoparticles that were not treated with ultrasound. In support of this Hu et al. (2013) reported a decrease in no-covalent interactions of soy protein isolate in dispersion after ultrasonic treatment.

## **CONCLUSION**

Conformational changes experienced by wheat bran proteins involved in the formation of nanoparticles were seen through the analysis of Amide I. The results showed that these proteins form aggregates by intermolecular  $\beta$ -sheets by effect of temperature. These aggregates were possibly consequence of the formation of globules product of the intermolecular disulfide cross-linking. While the nanostructures seen in SEM, are possibly the result of the connection between the globules by nonspecific physical interactions.

## **ACKNOWLEDGMENTS**

To Consejo Nacional de Ciencia y Tecnología (CONACYT), Mexico, for financing the project CB2011-169839 and the scholarship for the doctoral studies of the author Luna-Valdez. It is acknowledged the support of the staff of the different departments of CIAD. Thanks to the Laboratorio de Química de Materiales CINVESTAV-IPN Unidad Mérida Yucatán and the Laboratorio Nacional de Nano y Biomateriales (LANNBIO), projects FOMIX-YUCATAN 2008-108160 and CONACYT LAB-2009-01 N° 123913 and Dora

Huerta Quintana, Ana Ruth Cristobal Ramos from CINVESTAV-IPN Unidad Mérida, for their technical assistance in the STEM, and SEM-EDX analysis, respectively.

## REFERENCES

- Anker, M., Stading, M., & Hermansson, AM. (1999). Effects of pH and the gel state on the mechanical properties, moisture contents and glass transition temperatures of whey protein films. *Journal Agricultural and Food Chemistry*, 47, 1878–1886.
- Aymard, P., Gimel, JC., Nicolai, T., & Durand, D. (1996). Experimental evidence for a two-step process in the aggregation of  $\beta$ -lactoglobulin at pH 7. *Journal de Chimie Physique*, 93, 987-997.
- Barth, A. (2007). Infrared spectroscopy of proteins. *Biochimica et Biophysica Acta*, 1767(9), 1073–1101.
- Bauer, R., Carrotta, R., Rischel, C., & Ogendal, L. (2000). Characterization and isolation of intermediates in  $\beta$ -lactoglobulin heat aggregation at high pH. *Biophysical Journal*, 79, 1030-1038.
- Borzova, V. A., Markossian, K. A., Chebotareva, N. A., & Kleymenov, S. Y. (2016). Kinetics of Thermal Denaturation and Aggregation of Bovine Serum Albumin. *Journal Pone*, 1-29.
- Boulaiz, H., Alvarez, P. J., Ramirez, A., Marchal, J. A., Prados, J., Rodríguez-Serrano, F., Perán, M., Melguizo, C., & Aranega, A. (2011). Nanomedicine: Application areas and development prospects. *Molecular Science*, 12, 3303-3321.



- Byler, D. M., & Susi, H. (1986). Examination of the Secondary Structure of Proteins by Deconvolved FTIR Spectra. *Biopolymers*, 25, 469-487.
- Carbonaro, M., & Nucara, A. (2010). Secondary structure of food proteins by Fourier transform spectroscopy in the mid-infrared region. *Amino Acids*. 38, 679-690.
- Carpenter, J. F., & Crowe, J. H. (1988). Modes of stabilization of a protein by organic solutes during desiccation. *Cryobiology*, 25, 459-470.
- Carpenter, J. F., & Crowe, J. H. (1989). An infrared spectroscopic study of the interactions of carbohydrates with dried proteins. *Biochemistry*, 28, 3916-3922.
- Chaquilla-Quilca G., Balandrán-Quintana R. R., Huerta-Ocampo J. G. Clamont-Montfort G. R., & Luna-Valdez J. G. (2017). Identification of proteins contained in aqueous extracts of wheat bran through a proteomic approach. *Journal of Cereal Science*. (in revision).
- Doi, E. (1993). Gels and Gelling of globular proteins. *Trends in Food Science & Technology*. 4, 1-5.
- Dong, A., Caughey, B., Caughey, WS., Bhat, KS., & Coe JE. (1992). Secondary structure of the pentraxin female protein in water determined by infrared spectroscopy: Effects of calcium and phosphorylcholine. *Biochemistry*, 31, 9364–9370.
- Dong, A., Huang, P., & Caughey WS. (1992). Redox-dependent changes in  $\beta$ -extended chain and turn structures of cytochrome c in water solution determined by second derivative amide I infrared spectra. *Biochemistry*, 31, 182–189.
- Dong, A., Huang, P., & Caughey, W. S. (1990). Protein secondary structure in water from second-derivative amide I infrared spectra. *Biochemistry*, 29, 3303-3308

- Elissa, A. S., Puhl, C., Kadla, J. F., & Khan, S. A. (2006). Enzymatic cross-linking of  $\beta$ -lactoglobulin: conformational properties using FTIR spectroscopy. *Biomacromolecules*, 7, 1707-1713.
- Fabian, H., & Mäntele, W. (2002). Infrared Spectroscopy of Proteins. Handbook of Vibrational Spectroscopy. ed. John Wiley & Sons, Chichester, 1–27 (2000).
- Fabian, H., & Vogel, H. J. (2002). Fourier Transform Infrared Spectroscopy of Calcium-Binding Proteins. In H. J. Vogel (Ed.), Calcium-Binding Protein Protocols: Volume 2: Methods and Techniques (pp. 57–74). Totowa, NJ: Springer New York.
- Foegeding, E. A., & Davis, J. P. (2011). Food protein functionality: A comprehensive approach. *Food Hydrocolloids*, 25, 1853-1864.
- Foegeding, E. A., Bowland, E. L., & Hardin C. C. (1995). Factors that determine the fracture properties and microstructure of globular protein gels. *Food Hydrocolloids*, 9, 237-249.
- Göllner, E. M., Blaschek, W., & Classen, B. (2010). Structural investigations on arabinogalactan-protein from wheat, isolated with yariv reagent. *Journal of Agricultural and Food Chemistry*, 58, 3621-3626.
- Gülseren, I., Fang, Y., & Corredig, M. (2012). Whey protein nanoparticles prepared with desolvation with ethanol: Characterization, thermal stability and interfacial behavior. *Food Hydrocolloids*, 29, 258-264.
- Haris, P. I. (2013). Probing protein–protein interaction in biomembranes using Fourier transform infrared spectroscopy. *Biochimica et Biophysic Acta*, 1828, 2265-2271.

- Haris, P. I., & Severcan, F. (1999). FTIR spectroscopic characterization of protein structure in aqueous and non-aqueous media. *Journal of Molecular Catalysis B: Enzymatic*, 7, 207–221.
- Hu, H., Wu, J., Li-Chan, E. C. Y., Zhu, L., Zhang, F., Xu, X., Fan, G., Wang, L., Huang, X., & Pan, S. (2013). Effects of ultrasound on structural and physical properties of soy protein isolate (SPI) dispersions. *Food Hydrocolloids*, 30, 647-655.
- Huerta-Ocampo J.A., Barrera-Pacheco A., Mendoza-Hernández C.S., Espitia-Rangel E., Mock H.P., & Barba de la Rosa A.P., 2014. Salt stress-induced alterations in the root proteome of *Amaranthus cruentus* L. *Journal of Proteome Research*. 13(8), 3607-3627.
- Ikeda, S., & Morris, V. J. (2002). Fine-stranded and particulate aggregates of heat-denatured whey proteins visualized by atomic force microscopy. *Biomacromolecules*, 3, 382-389.
- Kelly, S.M., Jess, T.T., & Price, N.C. (2005). How to study proteins by circular dichroism. *Biochimica et Biophysica Acta*. 1751, 119-139.
- Kitabatake, N., & Doi, E. (1993). Improvement of protein gel by physical and enzymatic treatment. *Food Reviews International*, 9, 445-471.
- Konan, Y. N., Gurny, R., & Allémann, E. (2002). Preparation and characterization of sterile and freeze-dried sub-200 nm nanoparticles. *International Journal of Pharmaceutics*, 233, 239-252.
- Kong, J., & Yu, S. (2007). Fourier transform infrared spectroscopic analysis of protein secondary structures. *Acta Biochimica et Biophysica Sinica*, 39 (8), 549-559.

- Langer, K., Balthasar, S., Vogel, V., Dinauer, N., Von Briesen, H., & Shubert, D. (2003). Optimization of the preparation process for human serum albumin (HAS) nanoparticles. *International Journal of Pharmaceutical*, 257, 169-180.
- Lapierre, C., Pollet, B., Ralet, M. -C., & Saulnier, L. (2001). The phenolic fraction of maize bran: evidence for lignin-heteroxylan association. *Phytochemistry*, 57, 765-772.
- Le Bon, C., Nicolai, T., & Durand, D. (1999). Kinetics of aggregation and gelation of globular proteins after heat-induced denaturation. *Macromolecules*, 32, 6120-6127.
- Liu, G., Li, J., Shi, K., Wang, S., Chen, J., Liu, Y., & Huang, Q. (2009). Composition, Secondary Structure, and Self-Assembly of Oat Protein Isolate. *Journal of Agricultural and Food Chemistry*, 57, 4552-4558.
- Maréchal, Y. (2003). Observing the water molecule in macromolecules and aqueous media using infrared spectrometry. *Journal of Molecular Structure*, 648, 27-47.
- Militello, V., Casarino, C., Emanuele, A., Giostra, A., Pullara, F., & Leone, M. (2004). Aggregation kinetics of bovine serum albumin studied by FTIR spectroscopy and light scattering. *Biophysical Chemistry*, 107, 175-187.
- Miller, L. M., Bourassa, M. W., & Smith, R. J. (2013). FTIR spectroscopic imaging of protein aggregation in living cells. *Biochimica et Biophysica Acta*, 1828, 2339-2346.
- Mulvihill, DM., & Donovan, M. (1987). Whey proteins and their thermal denaturation: a review. *Irish Journal of Food Science and Technology*, 11, 43-75.

- Mulvihill, DM., Rector, D., & Kinsella, JE. (1991). Mercaptoethanol, N-ethylmaleimide, propylene glycol and urea effects on rheological properties of thermally induced  $\beta$ -lactoglobulin gels at alkaline pH. *Journal of Food Science*, 56, 1338–1341.
- Murayama, K., & Tomida, M. (2004). Heat-induced secondary structure and conformation change of bovine serum albumin investigated by fourier infrared spectroscopy. *Biochemistry*, 43, 11526-11532.
- Natalello, A., Ami, D., Brocca, S., Lotti, M., & Doglia, S. M. (2005). Secondary structure, conformational stability and glycosylation of a recombinant *Candida rugosa* lipase studied by Fourier-transform infrared spectroscopy. *Biochemical Journal*, 385, 511-517.
- Pelton, J. T., & McLean, L. R. (2000). Spectroscopic methods for analysis of protein secondary structure. *Analytical Biochemistry*, 277, 167-176.
- Petrucelli, S., & Añón, M. C. (1995). Thermal aggregation of soy protein isolates. *Journal of Agricultural and Food Chemistry*, 43, 3035-3041.
- Robert, P., Marquis, M., Barron, C., Guillon, F., & Saulnier, L. (2005). FT-IR investigation of cell wall polysaccharides from cereal grains. Arabinoxylan infrared assignment. *Journal of Agricultural and Food Chemistry*, 53(18), 7014-7018.
- Sadeghi, S., Madadlou, A., & Yarmand, M. (2014). Microemulsification-cold of date palm pit extract. *Food Hydrocolloids*, 35, 590-596.
- Saglam, D., Venema, P., de Vries, R., Sagis, L. M.C., & van der Linden, E. (2011). Preparation of high protein micro-particles using two-step emulsification. *Food Hydrocolloids*, 25, 1139-1148.

- Seshadri, S., Khurana, R., & Fink, A. L. (1999). Fourier transform infrared spectroscopy in analysis of protein deposits. *Methods in Enzymology*, 309, 559–576.
- Shimada, K., & Cheftel, J. C. (1989). Sulfhydryl group/disulfide bond interchange reactions during heat-induced gelation of whey protein isolate. *Journal Agricultural Food Chemistry*, 37, 161-168.
- Surewicz, W. K., Mantsch, H. H., & Chapman, D. (1993). Determination of protein secondary structure by Fourier transform infrared spectroscopy: a critical assessment. *Biochemistry*, 32, 389-394.
- van de Weert, M., Haris, P.I., Hennink, W.E., & Crommelin, D.J.A. (2001). Fourier transform infrared spectrometric analysis of protein conformation: effect of sampling method and stress factors. *Analytical Biochemistry*, 297, 160–169.
- van Stokkum, I. H. M., Lindsell, H., Hadden, J. M., Haris, P. I., Chapman, D., & Bloemenda, M. (1995). Temperature-induced changes in protein structures studied by fourier transform infrared spectroscopy and global analysis. *Biochemistry*, 34, 10508-10518.
- Vicent, J. S., Steer, C. J., & Levin, I. w. (1984). Infrared spectroscopic study of the pH-dependent secondary structure of Brain Clathrin. *Biochemistry*, 23, 625-631.
- Yan, Y., Wang, Q., He, H., & Zhou H. (2004). Protein thermal aggregation involves distinct regions: sequential events in the heat-induced unfolding and aggregation of hemoglobin. *Biophysical Journal*, 86, 1682-1690.
- Yedomon, B., Fessi, H., & Charcosset, C. (2013). Preparation of Bovine Serum Albumin (BSA) nanoparticles by desolvation using a membrane contactor: A new tool for large scale production. *European Journal of Pharmaceutics and Biopharmaceutics*, 85, 398-405.

**Manuscript in revision:**

Luna-Valdez, J. G., Balandrán-Quintana, R. R., Azamar-Barrios, J. A., Clamont-Montfort, G. R., Mendoza-Wilson, A. M., Mercado-Ruiz, J. N., Madera-Santana, T. J., Rascón-Chu, A., & Chaquilla-Quilca, G. Nanoparticle formation after mild thermal conditioning of proteins contained in a wheat bran extract fractioned by size exclusion chromatography (in revision in journal *Biomacromolecules*).

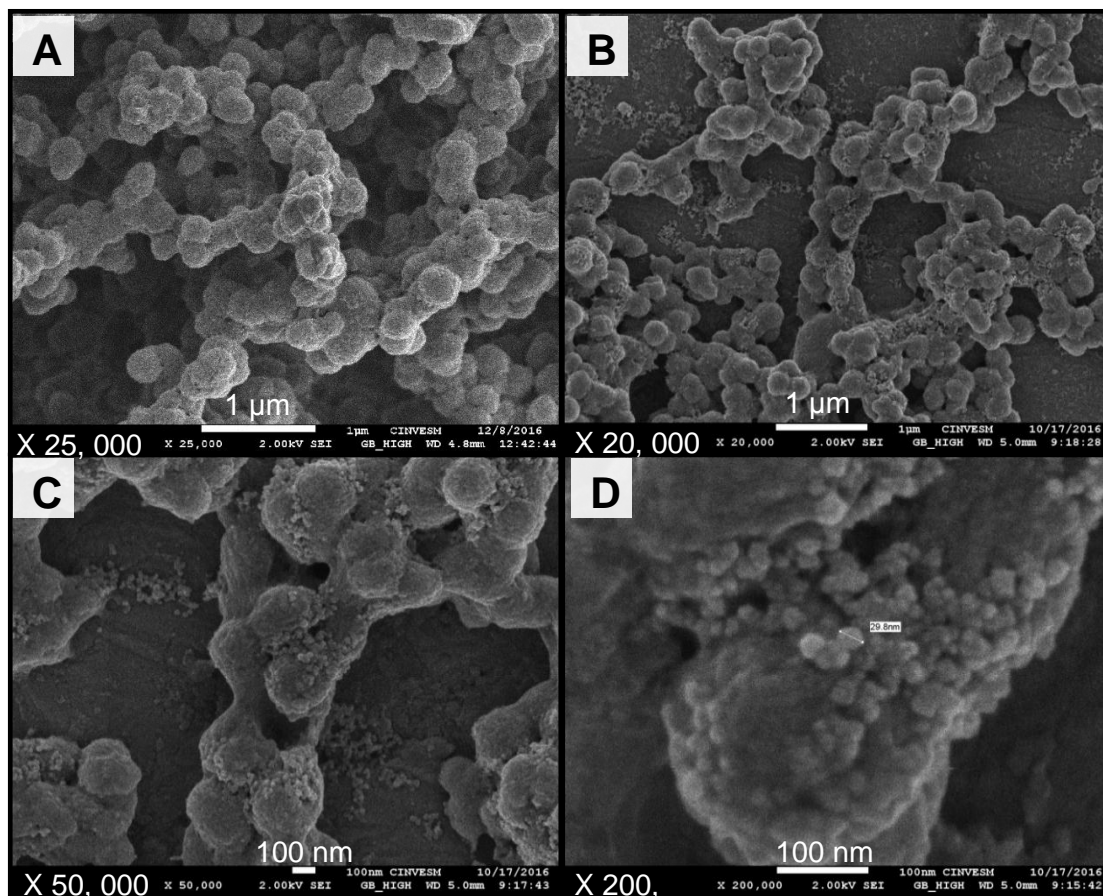


**Figure 1.** SEM images of nanoparticles formed from water soluble proteins of wheat bran after thermal treatment at 68.5 °C.



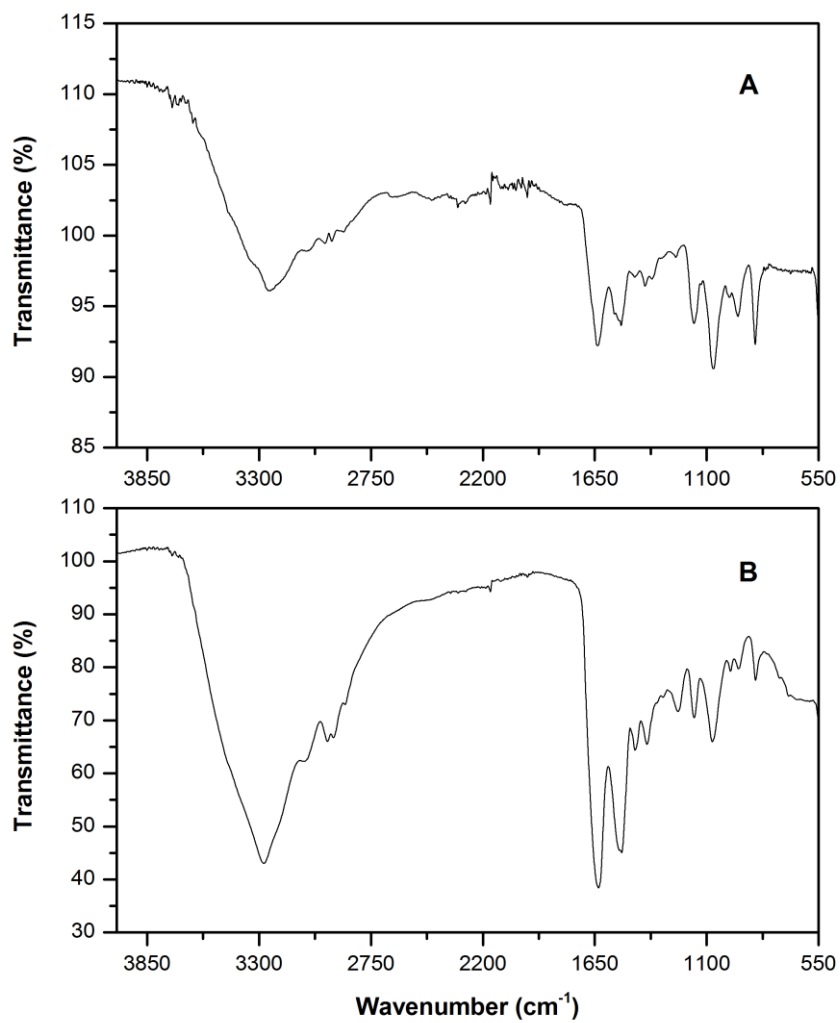


**Figure 2.** FTIR spectra of the control sample (A) and the nanoparticles obtained by thermal treatment of water soluble proteins from wheat bran (B).

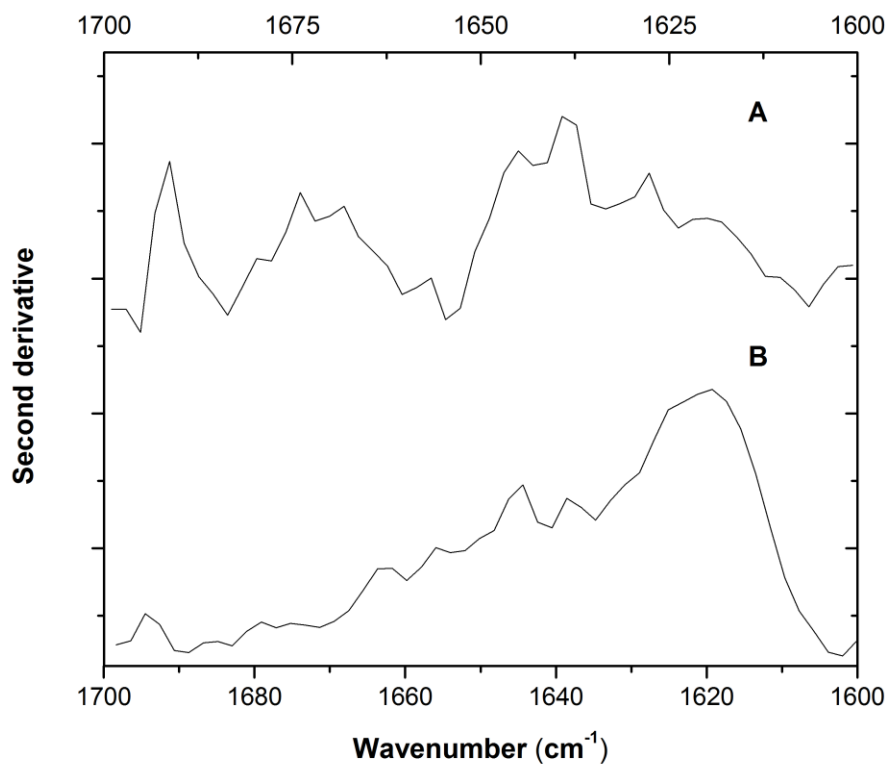


**Figure 3.** Second-derivative spectra of the Amide I region of control (A) and nanoparticles obtained after thermal treatment of water soluble wheat bran proteins (B).

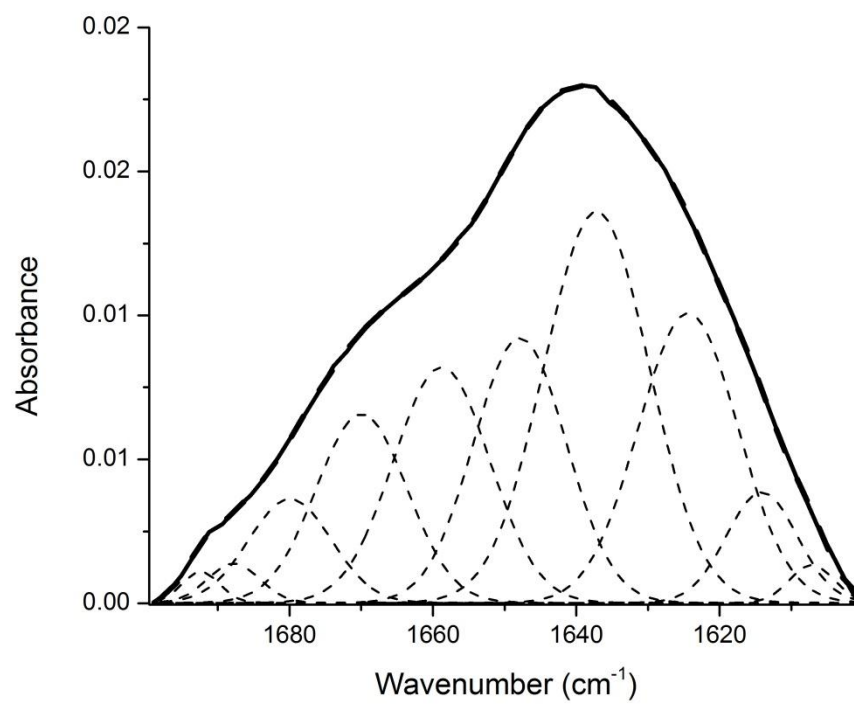


**Figure 4.** Decomposition of amide I band of the control proteins into Gaussian components.

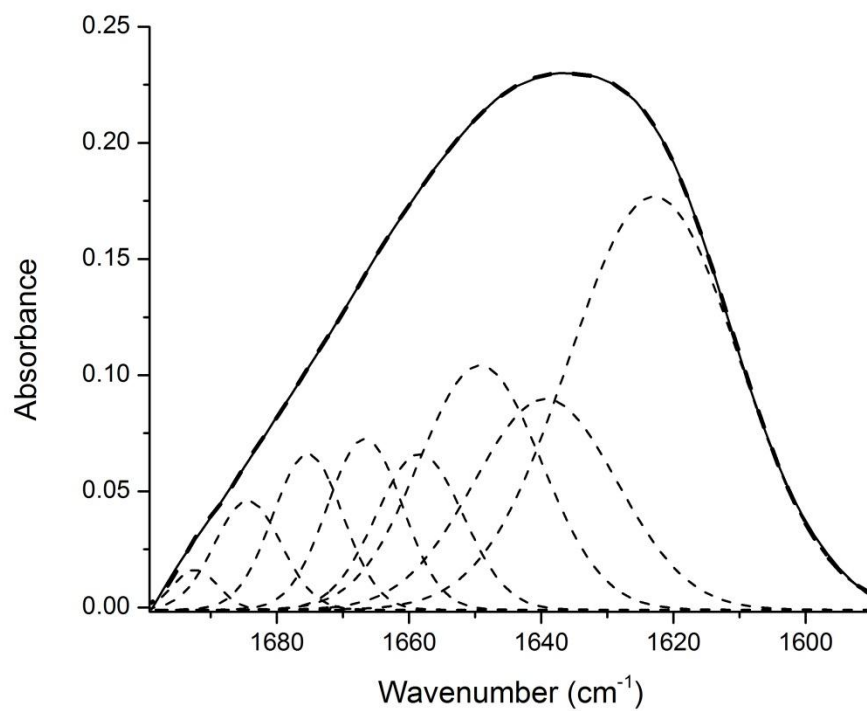


**Figure 5.** Decomposition of Amide I band of water soluble wheat bran proteins subject to heat treatment (68.5 °C) (nanoparticles), into Gaussian components.

**Table 1.** Elemental composition of nanoparticles.

Element	(atomic %)
C	53.76
N	18.22
O	25.37
Na	1.36
P	0.62
S	0.45

ANEXO

**Tabla 1.** Proteínas de la fracción de albúminas de salvado de trigo involucradas en la formación de nanopartículas .

Número de banda en el gel SDS-PAGE <sup>a</sup>	Proteína	Organismo	Número de acceso <sup>b</sup>	Experimental PM <sup>c</sup>	Peso molecular teórico (PM <sub>PI</sub> <sup>d</sup> )	Puntuación <sup>e</sup>	PC <sup>f</sup> /CS <sup>g</sup>	Porcentaje de cisteína
10	Aldosa reductasa	<i>Triticum urartu</i>	EMIS68426.1	43.5	35.95/6.87	169	6/24%	1.56
11	Proteína inhibidora de la xilanasasa I	<i>Triticum aestivum</i>	Q8L5C6.2	34	33.25/8.66	175	9/34%	1.6
12	Quitinasa clase II	<i>Triticum aestivum</i>	AA X83262.1	30	28.20/8.66	225	6/42%	2.69
13	Proteína hipotética F775_32839 (similar a la Taumatina)	<i>Aegilops tauschii</i>	EMT26984.1	26	17.74/6.52	171	7/59%	8.75
14	Inhibidor endógeno de alfa-amilasa/subtilisina	<i>Triticum aestivum</i>	P16347.1	20	19.62/6.77	467	12/78%	2.2

<sup>a</sup>Figura 3B(pk-2) artículo 3; <sup>b</sup>Números de acceso en la base de datos de proteínas NCBI; <sup>c</sup> peso molecular experimental (Datos obtenidos en este trabajo mediante SDS-PAGE); <sup>d</sup> peso molecular teórico y pI; <sup>e</sup> resultados de Mascot reportados después de buscar en el subconjunto *Viridiplantae* de la base de datos de proteínas NCBI (octubre 2016, secuencias \_4298025). Las puntuaciones de iones individuales > 44 indican identidad u homología extensa (p <0,05); <sup>f</sup> Péptidos que coinciden; <sup>g</sup> cobertura de secuencia. (Datos reportados por Chaquilla-Quila et al., 2017).

